Computational Radiology Laboratory
Harvard Medical School
www.crl.med.harvard.edu

Children's Hospital
Department of Radiology
Boston Massachusetts

Translation of neuroimaging technologies to advance clinical care

Simon K. Warfield, Ph.D.

Associate Professor of Radiology

Department of Radiology

Children's Hospital Boston

Children's Hospital Boston
The Hospital for Children

Outline

- Imaging of epilepsy patients
- Fetal MRI
- Image segmentation

Surgical Planning for Epilepsy

- Epilepsy
  - affects over 2.5 million Americans, approximately 1% of population across the world.
  - Annual health care cost of $12.5 billion per year in USA.
  - 75% of patients have their first seizure in childhood.
  - 20% of patients become candidates for surgery after a long period of partially effective medication that can have debilitating educational and sociological side effects.
  - Hetereogeneous causes and consequences of epilepsy in pediatric patients.

Pediatric Epilepsy Surgical Planning

- Objective: Enable an early and effective surgical intervention by accurate identification and localization of seizure foci.

- Imaging of epilepsy:
  - Structural : MRI, DTMRI.
  - Metabolic/function: PET,SPECT,MRS,fMRI.
  - Electrical imaging key to seizure focus localization: EEG, MEG.

Preoperative visualization

- Teenage girl with refractory seizures
- Suspected cortical dysplasia
- Aim to detect and visualize:
  – Region of dysplasia (MRI)
  – Connected white matter (DT-MRI)

Preoperative visualization

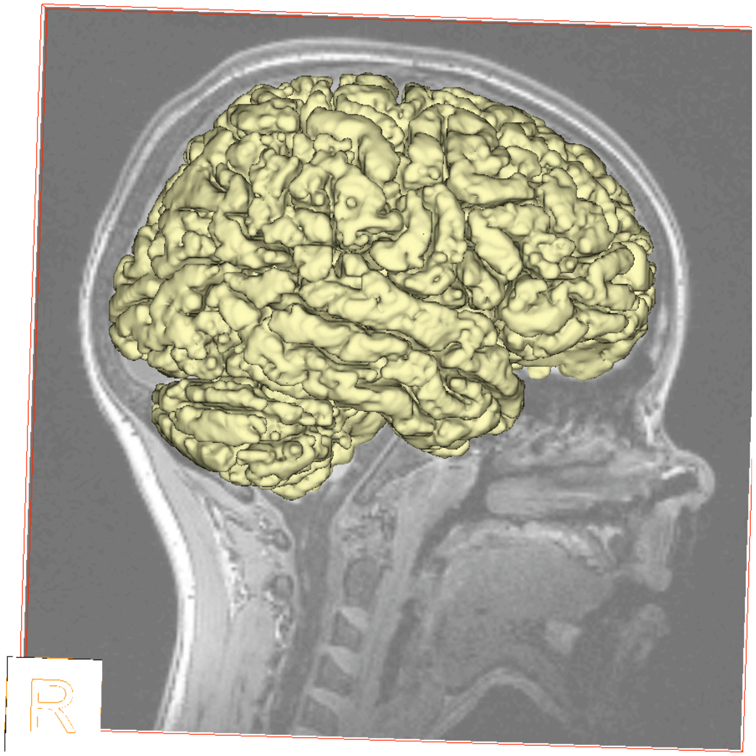

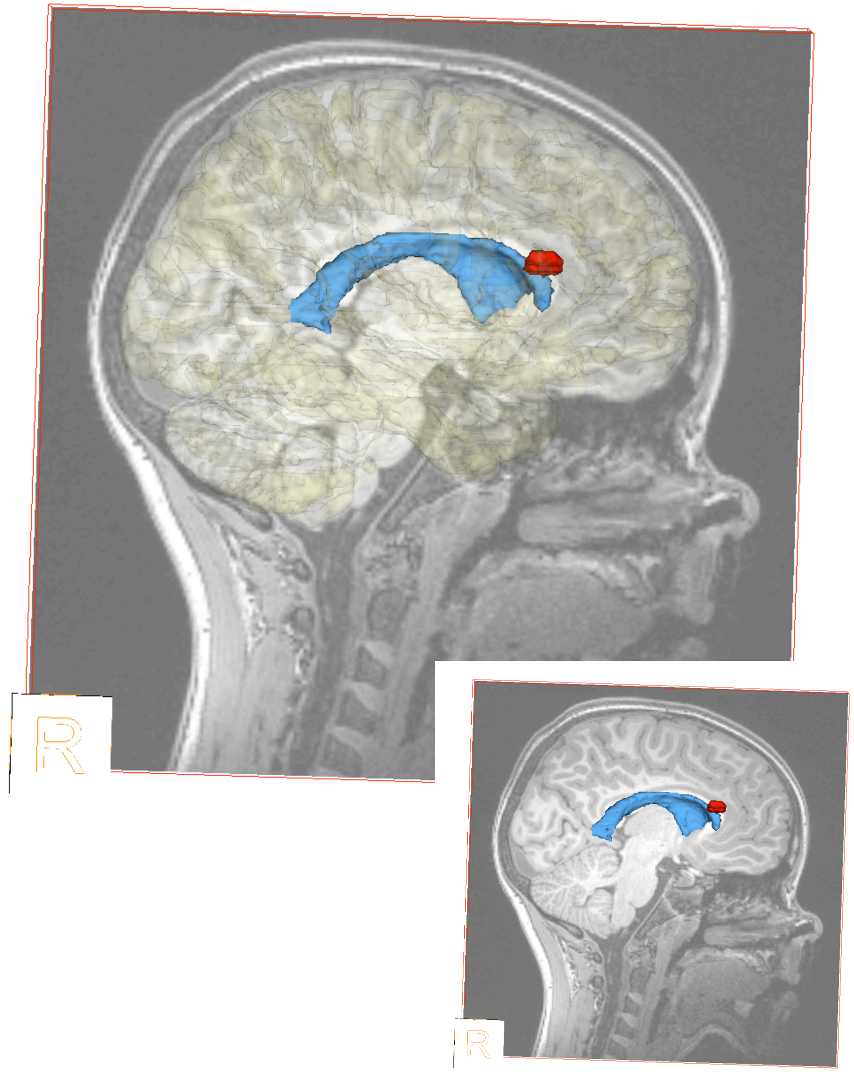

Automatic segmentation of the brain surface and ventricles. Focal dysplasia shown in red.

Preoperative visualization

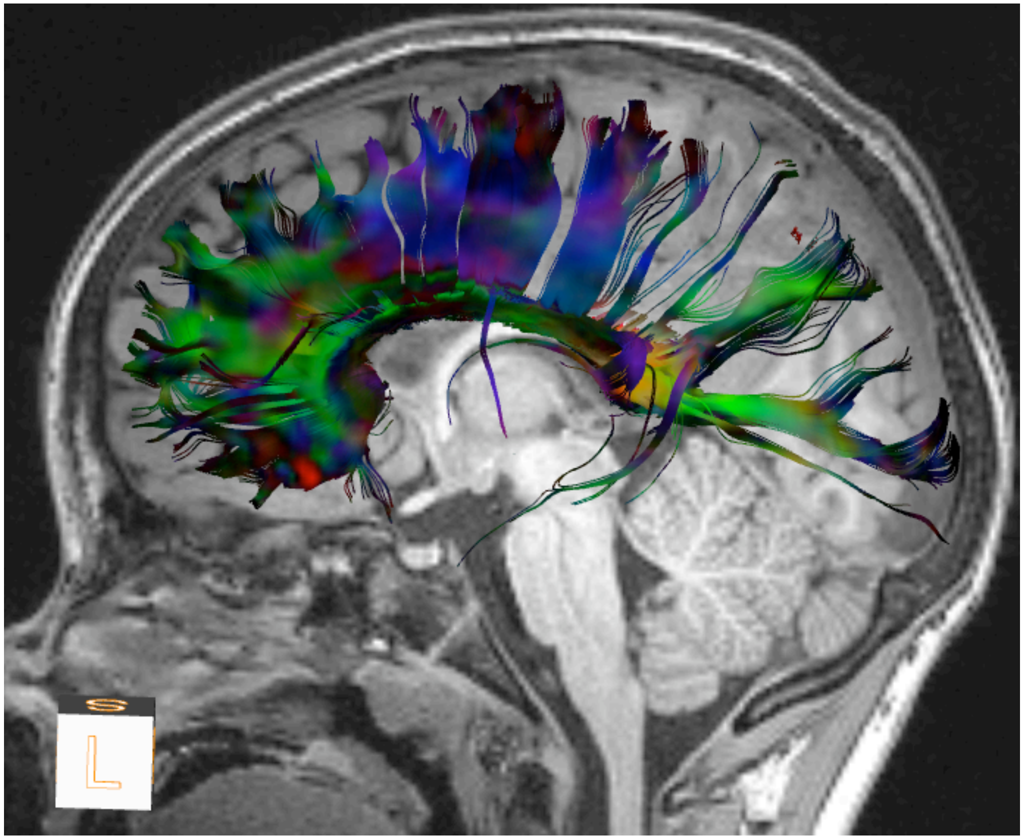

Projections through the corpus callosum.

Corticospinal tract

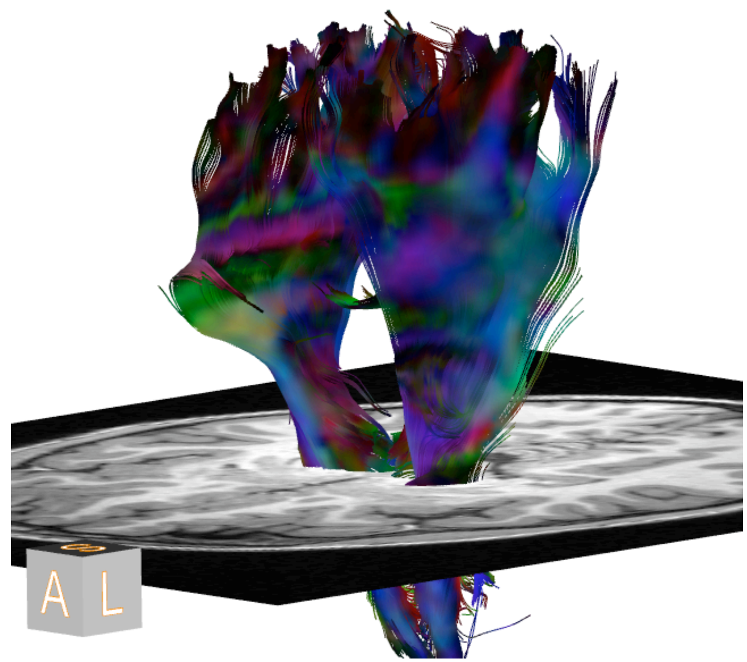

White matter near dysplasia

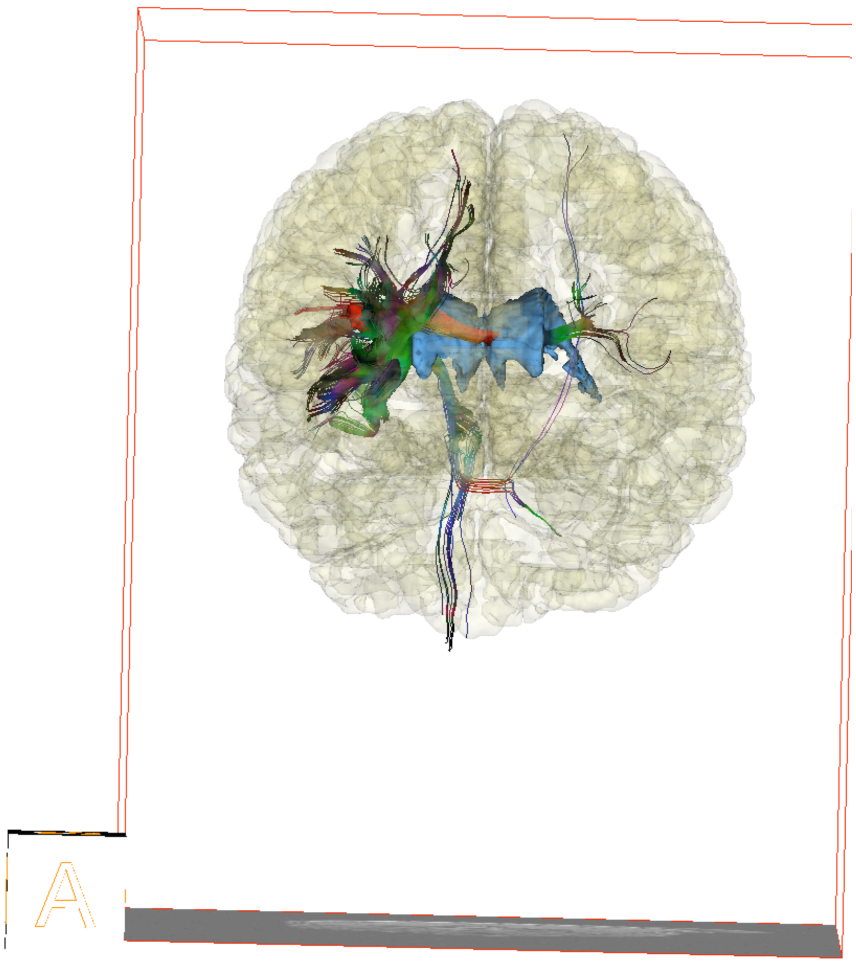

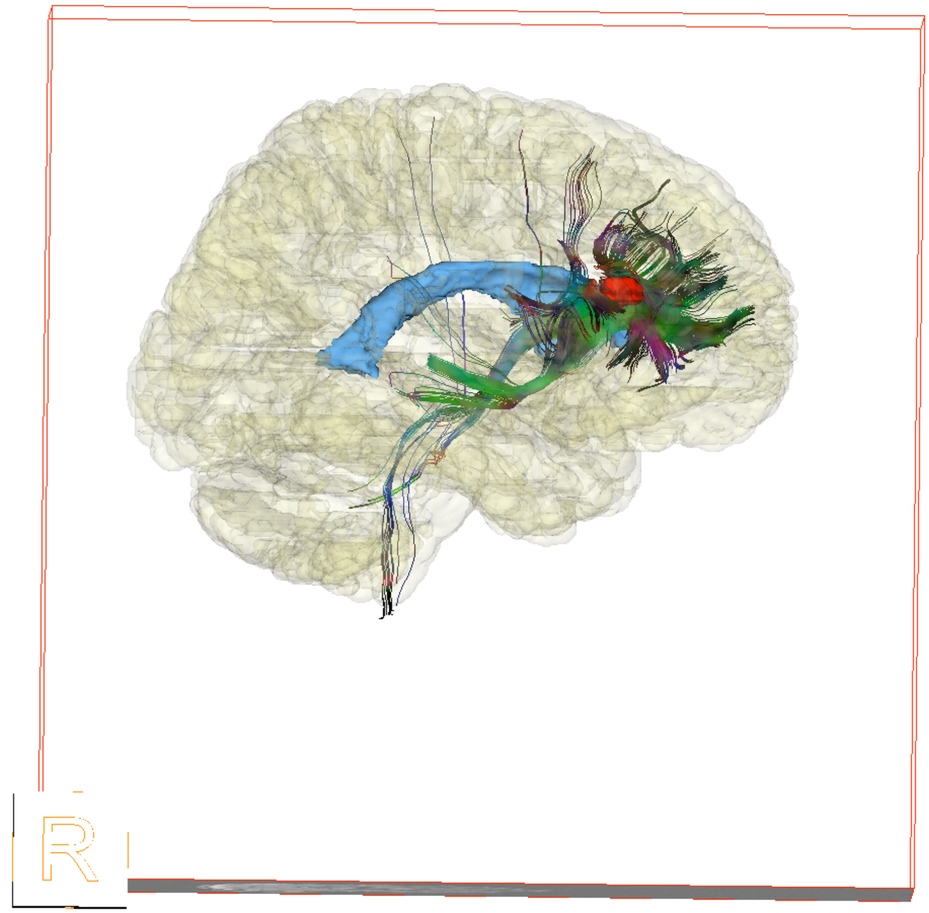

Preoperative visualization

Language localization in 7 year old boy.

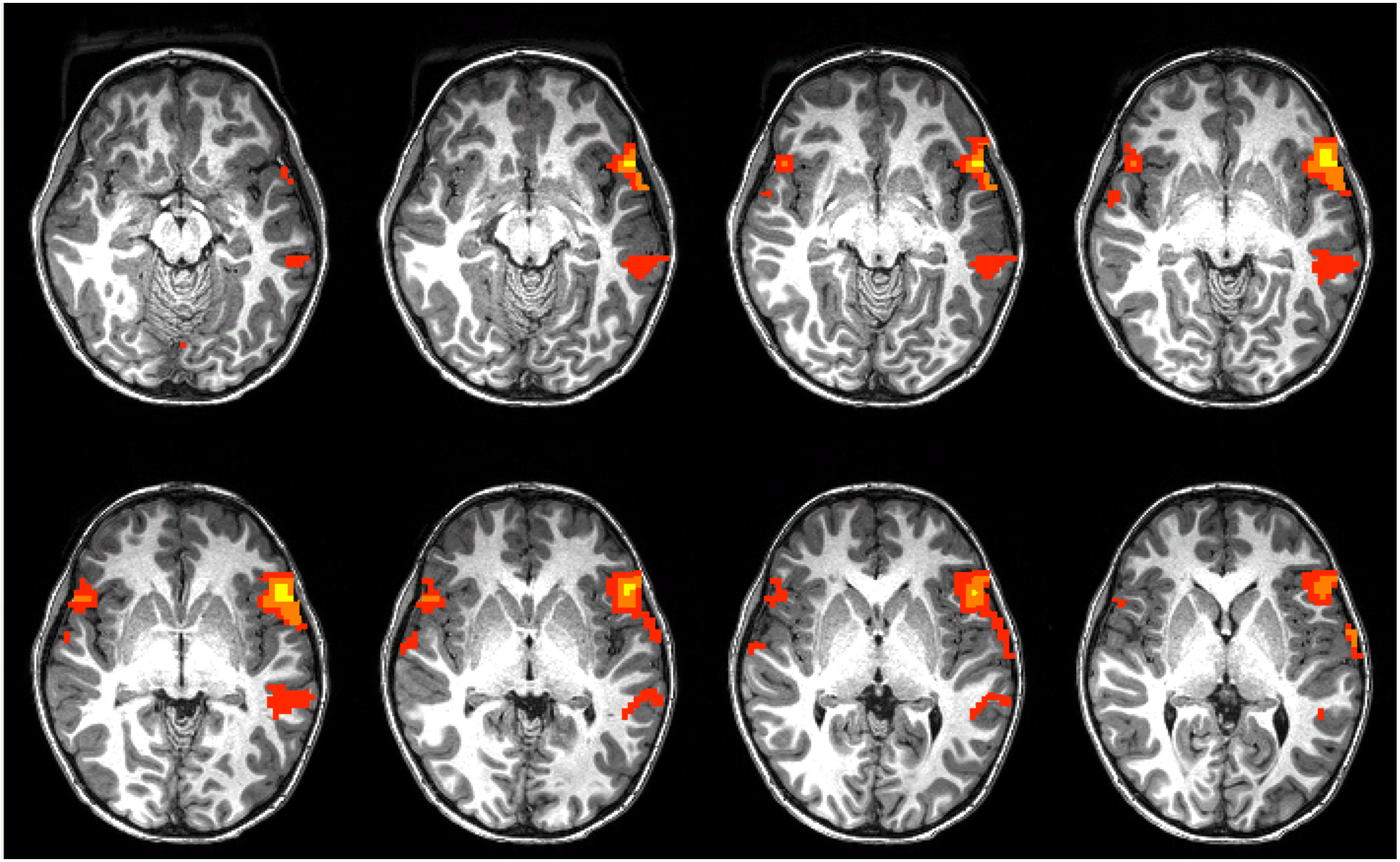

Preoperative visualization

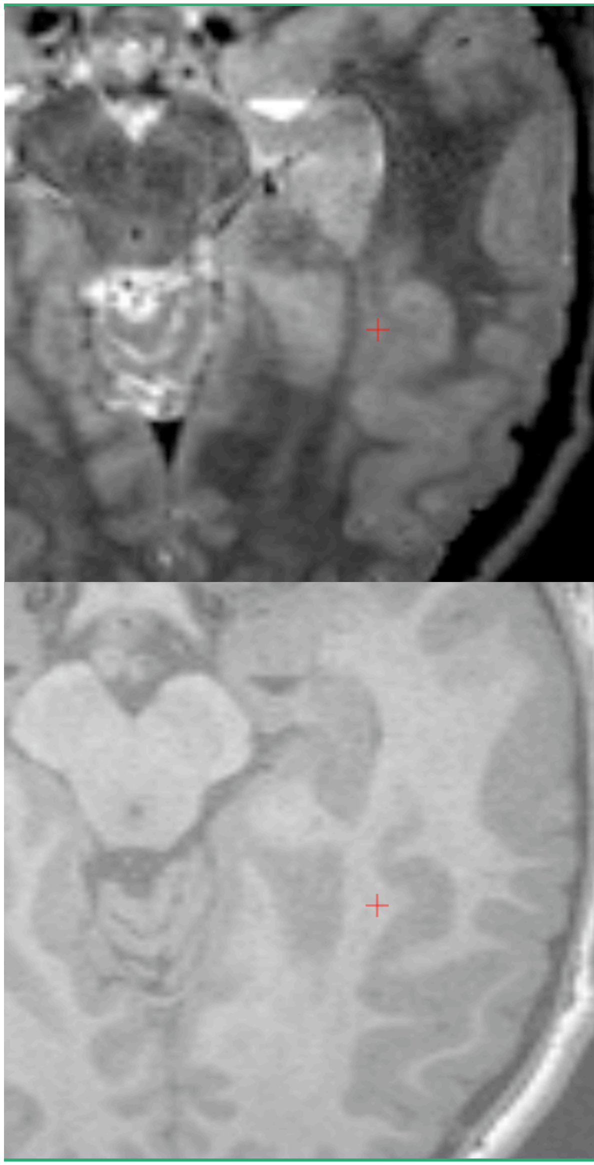

FLAIR cortical dysplasia with MRI, DTI

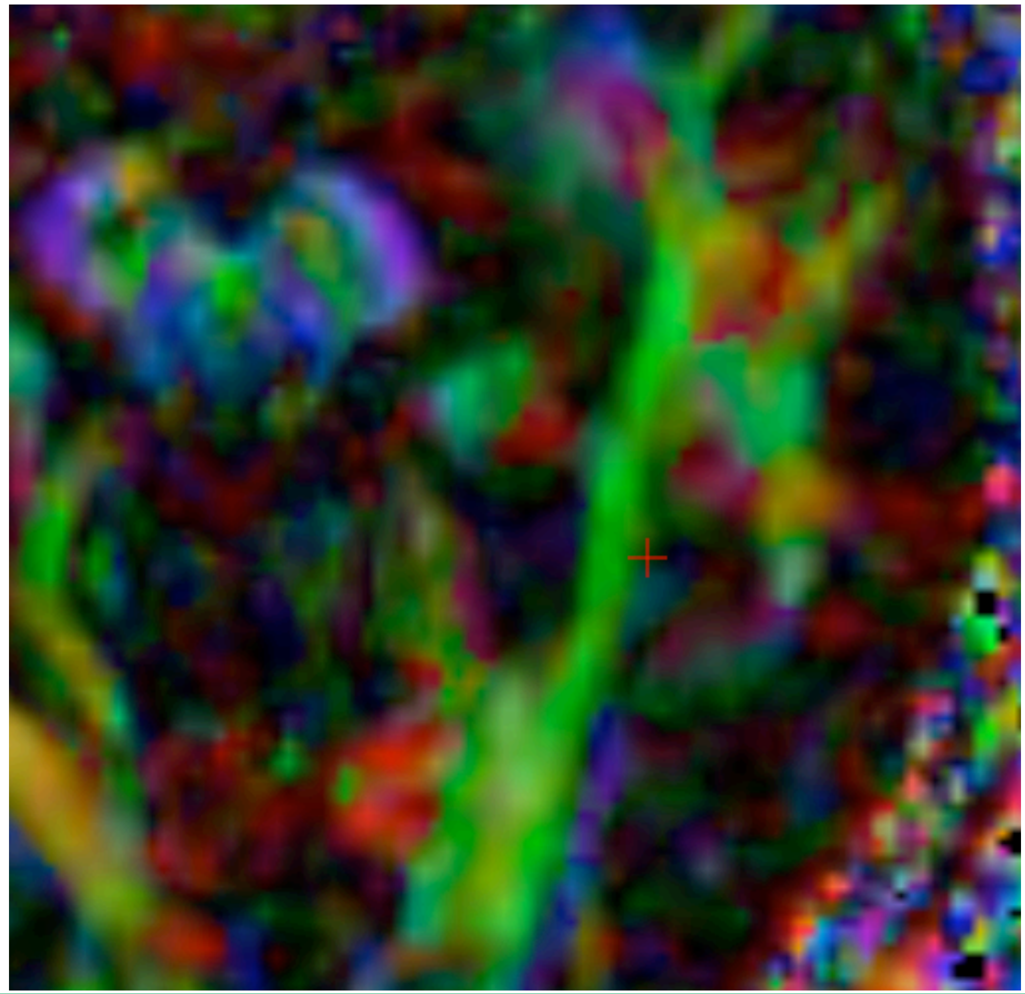

PET and MRI fusion

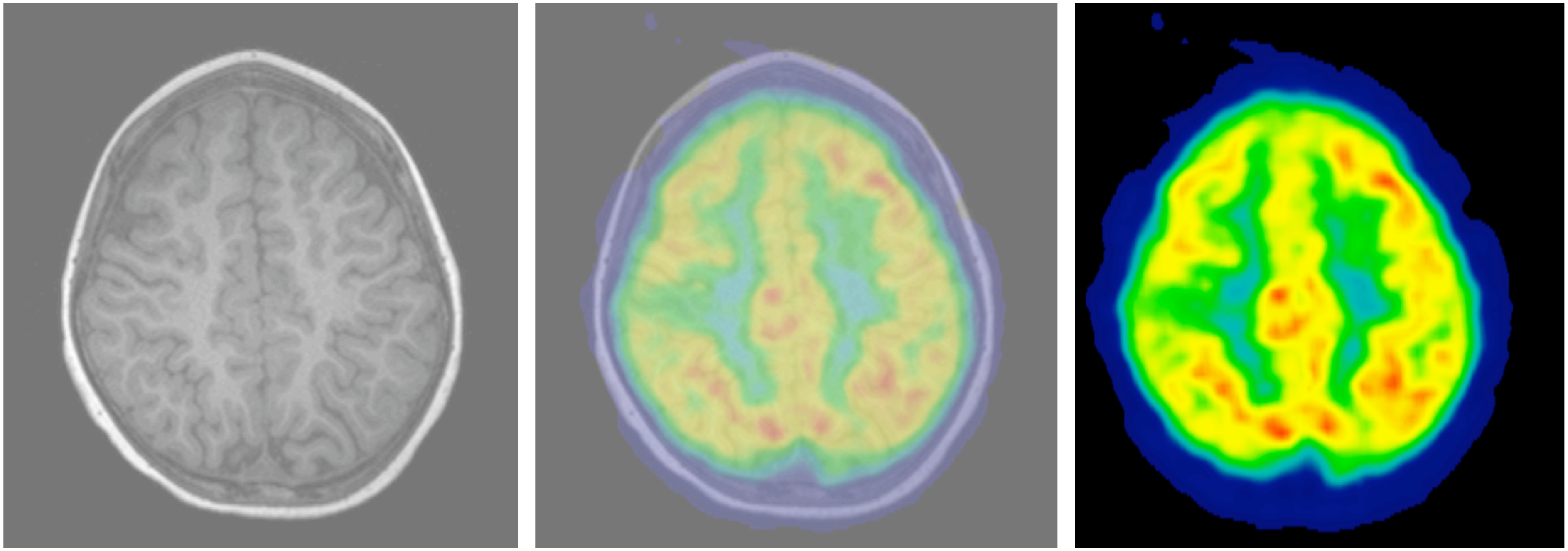

Localization of PET hypoperfusion with MRI.

Invasive Source Localization

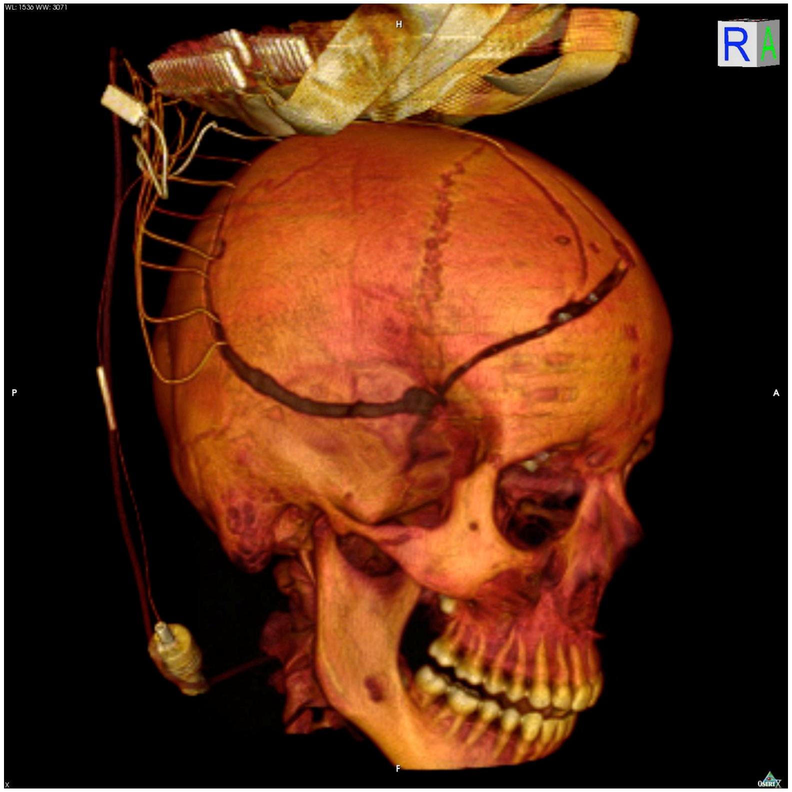

Visualization of CT with intracranial strips and grids allows precise determination of anatomical location of electrodes that detected seizures during long-term monitoring.

Invasive Source Localization

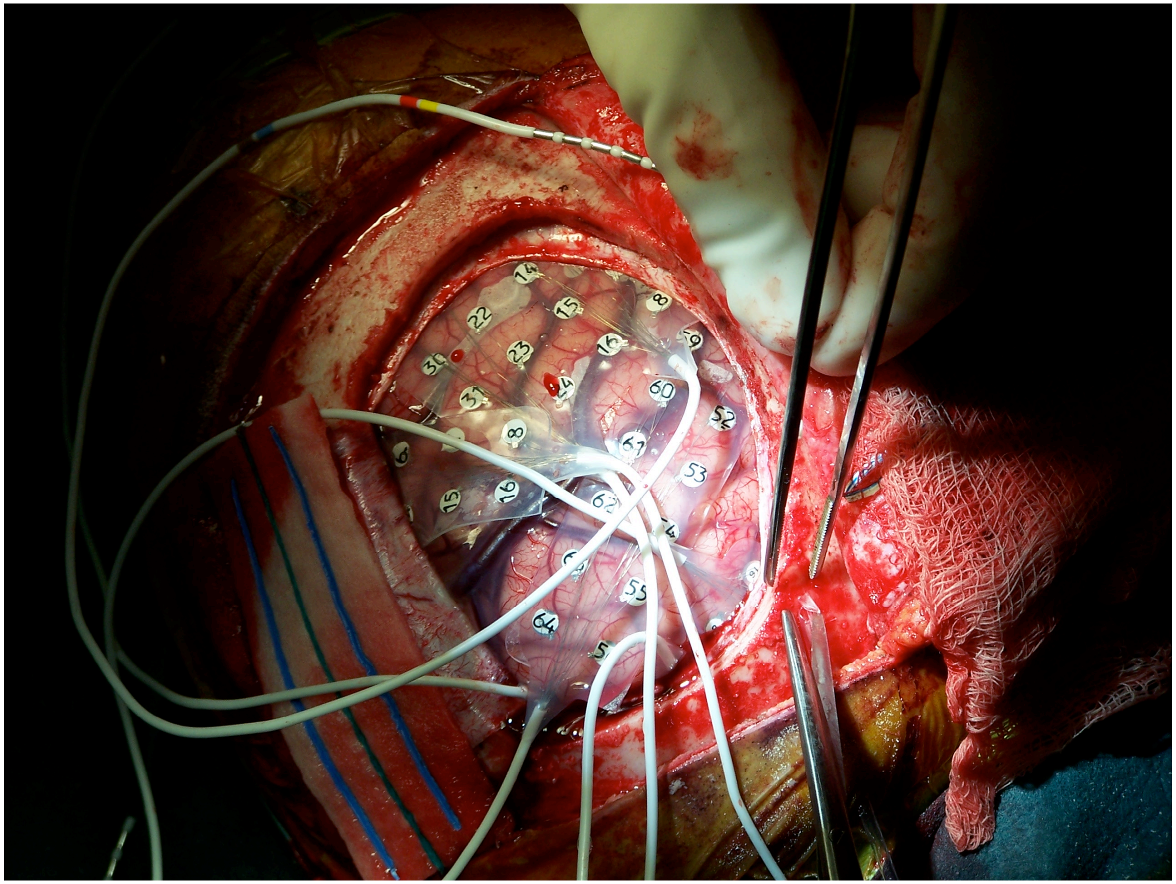

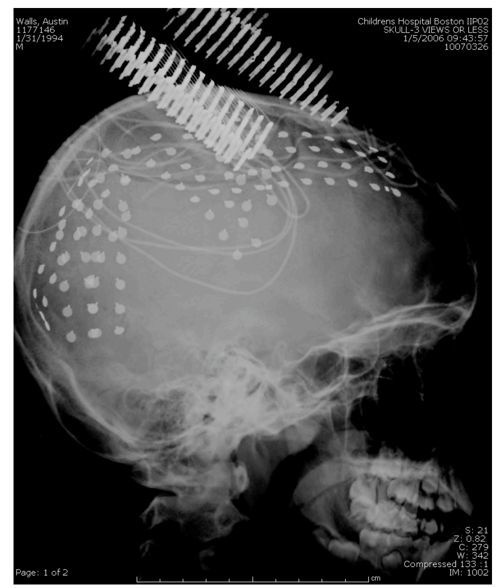

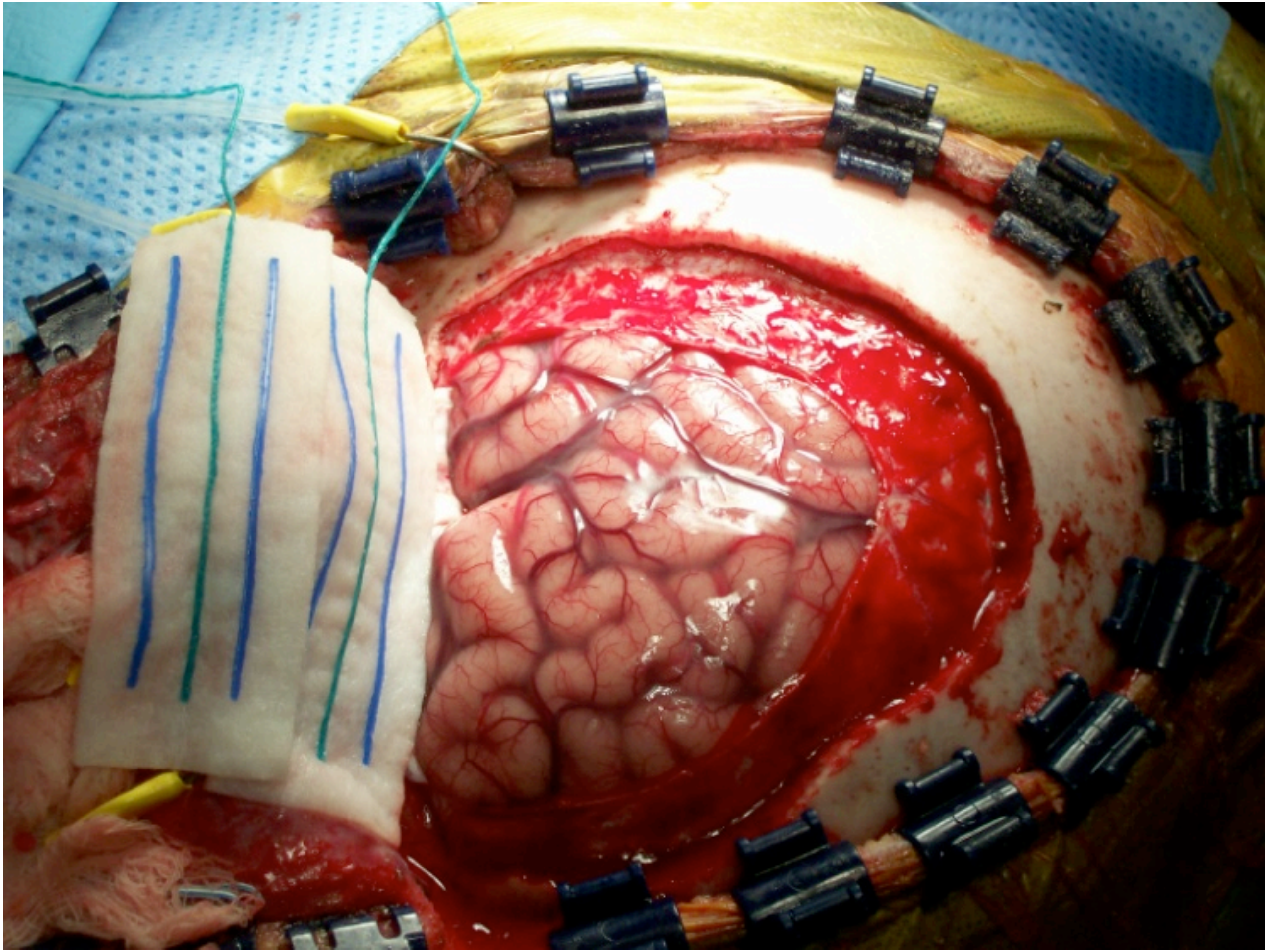

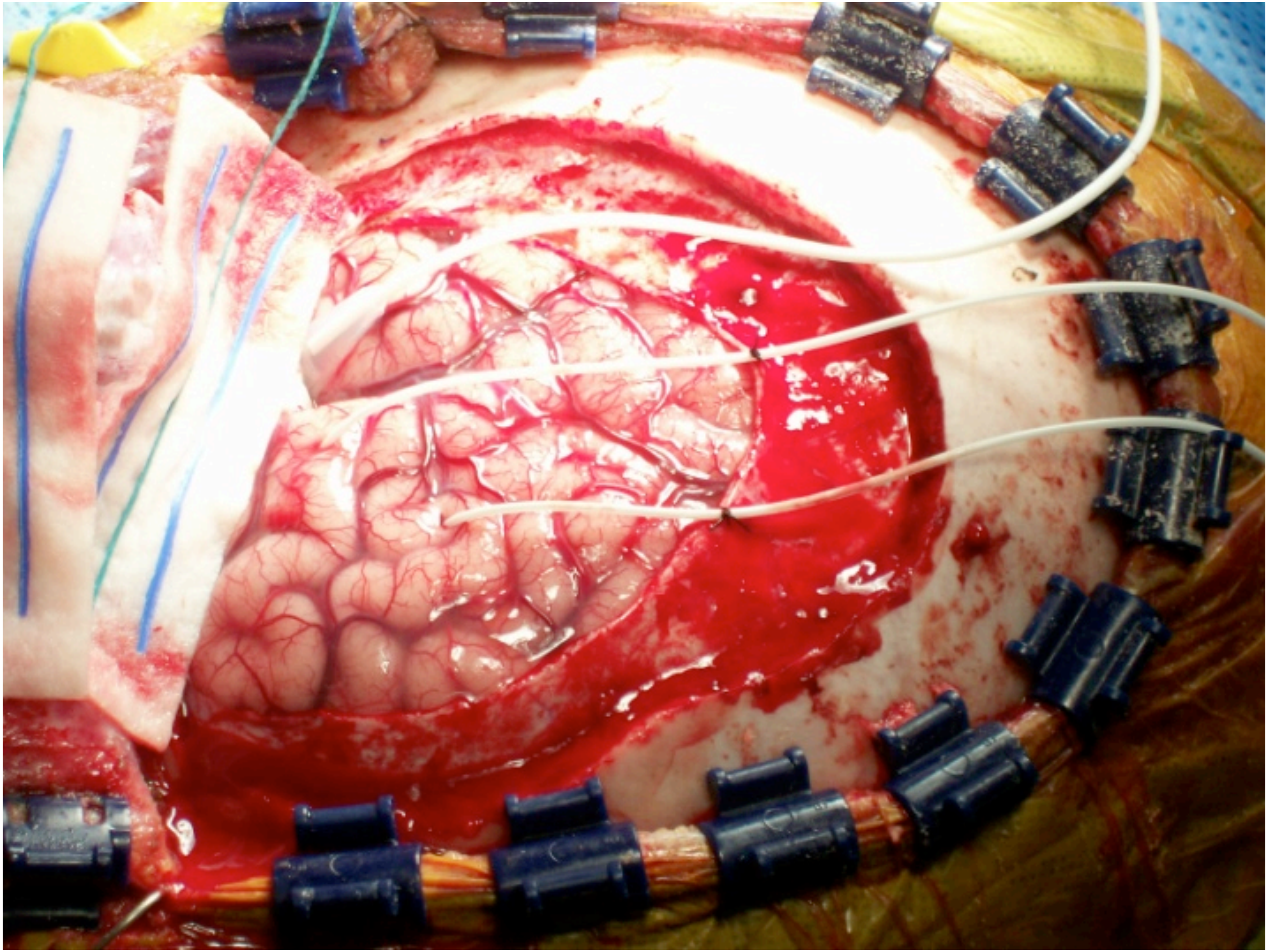

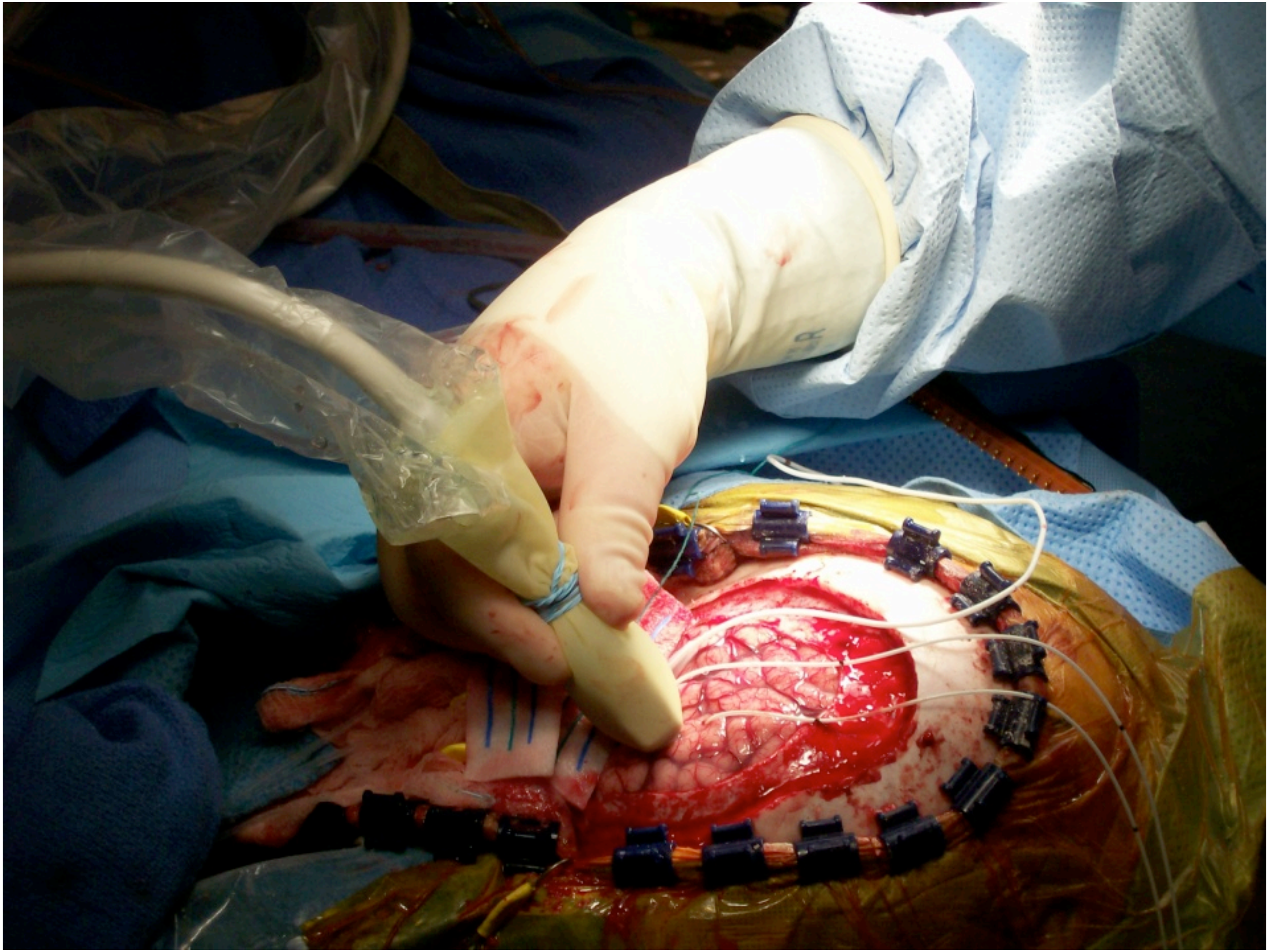

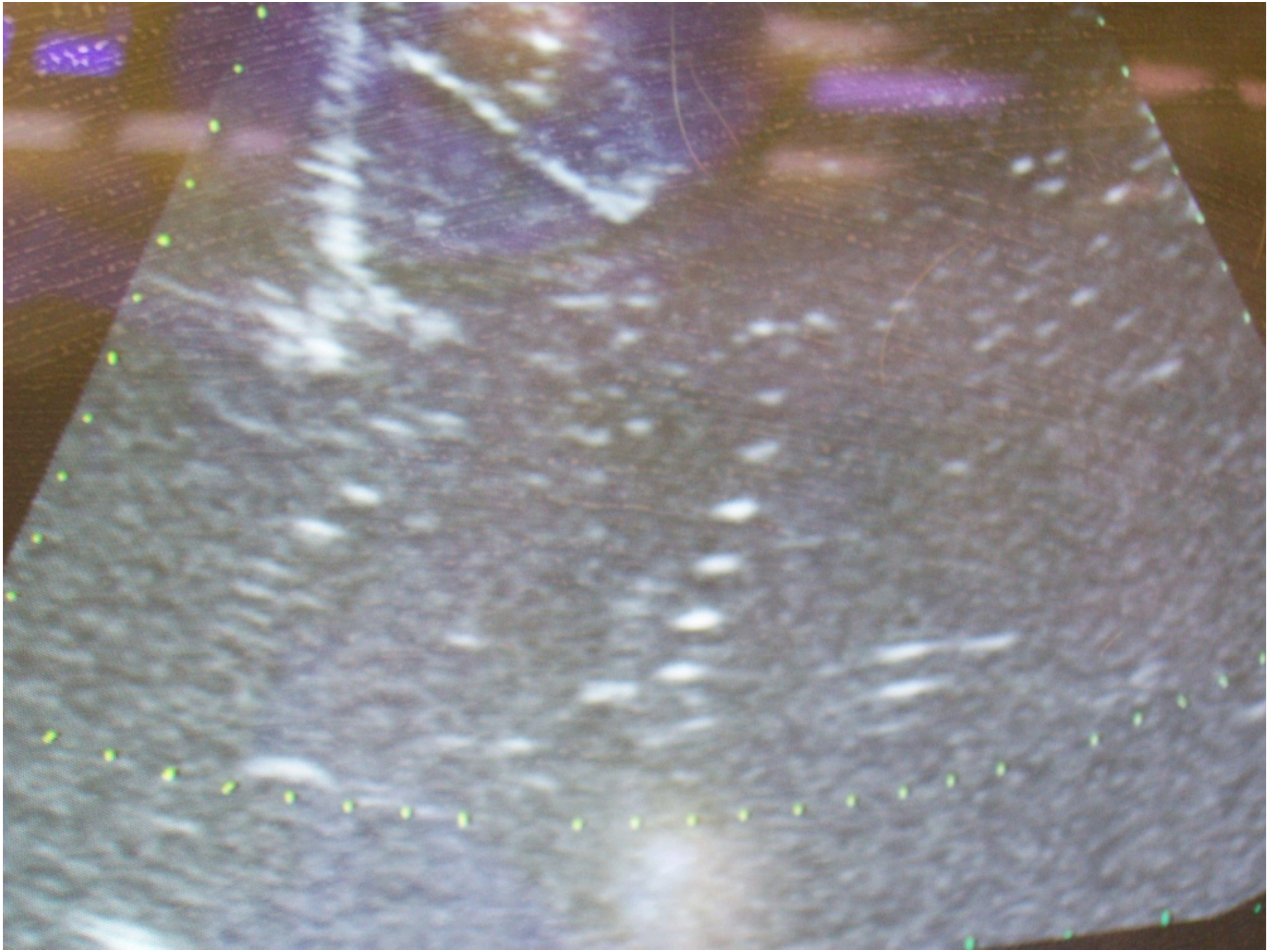

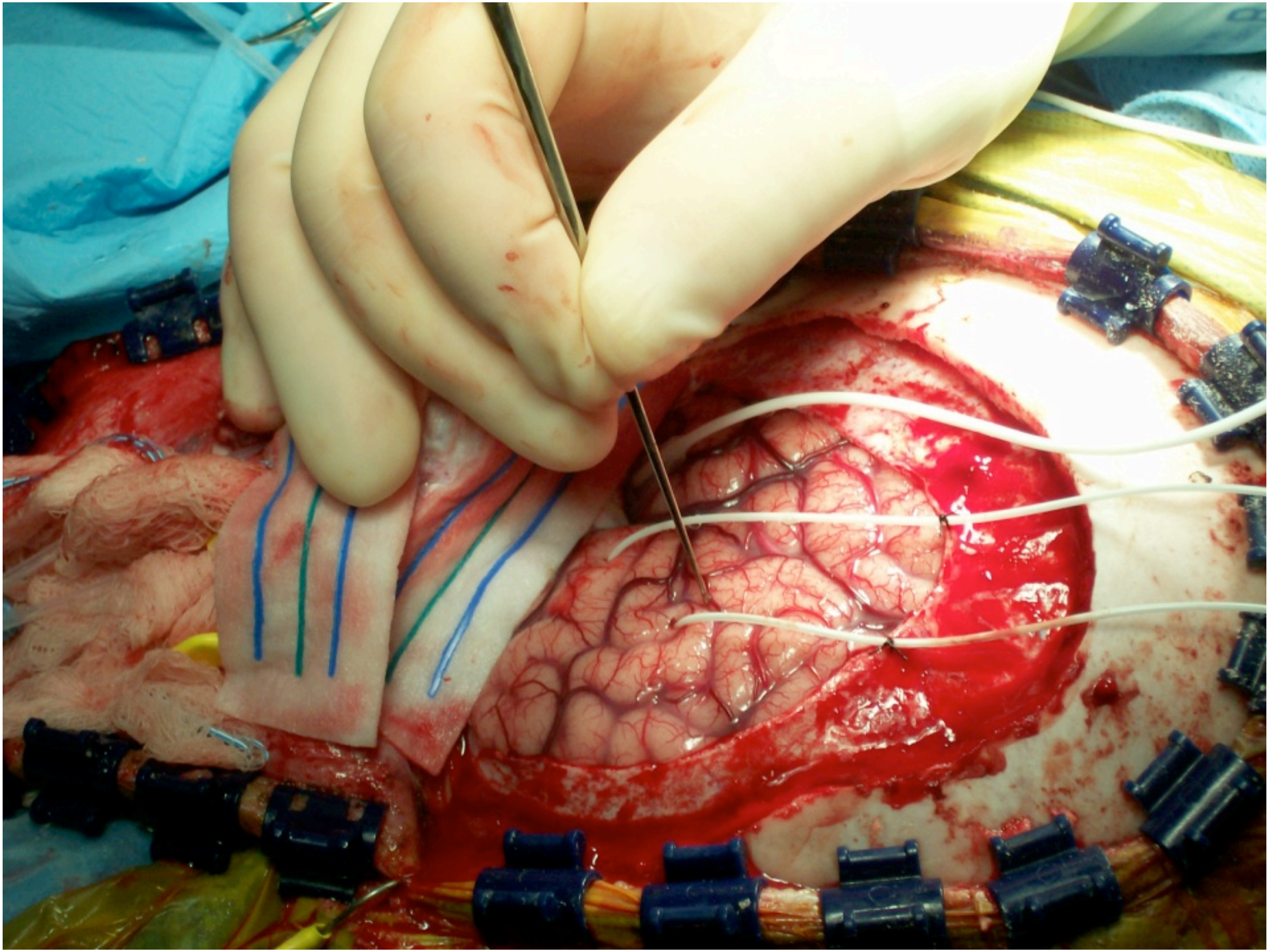

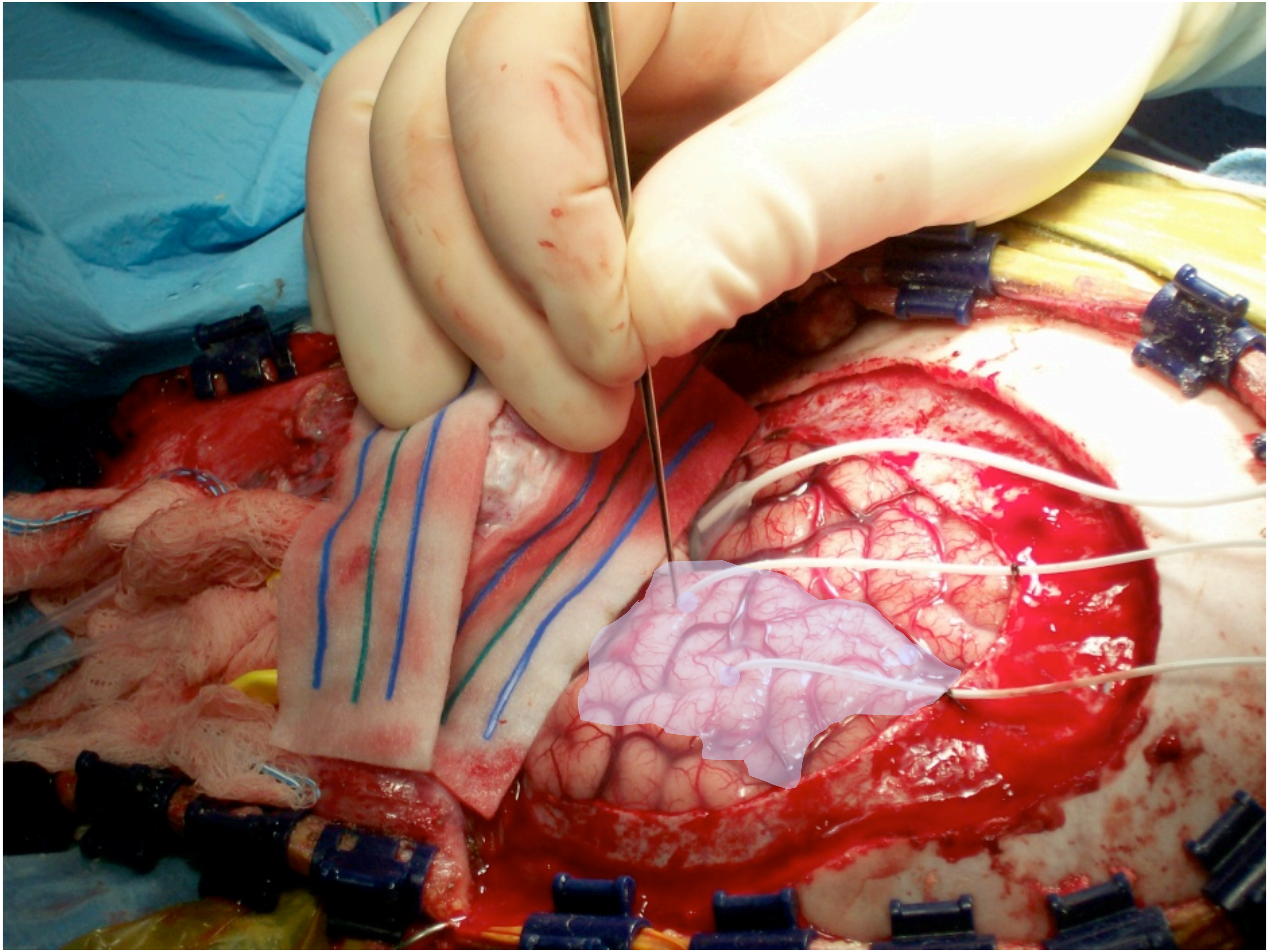

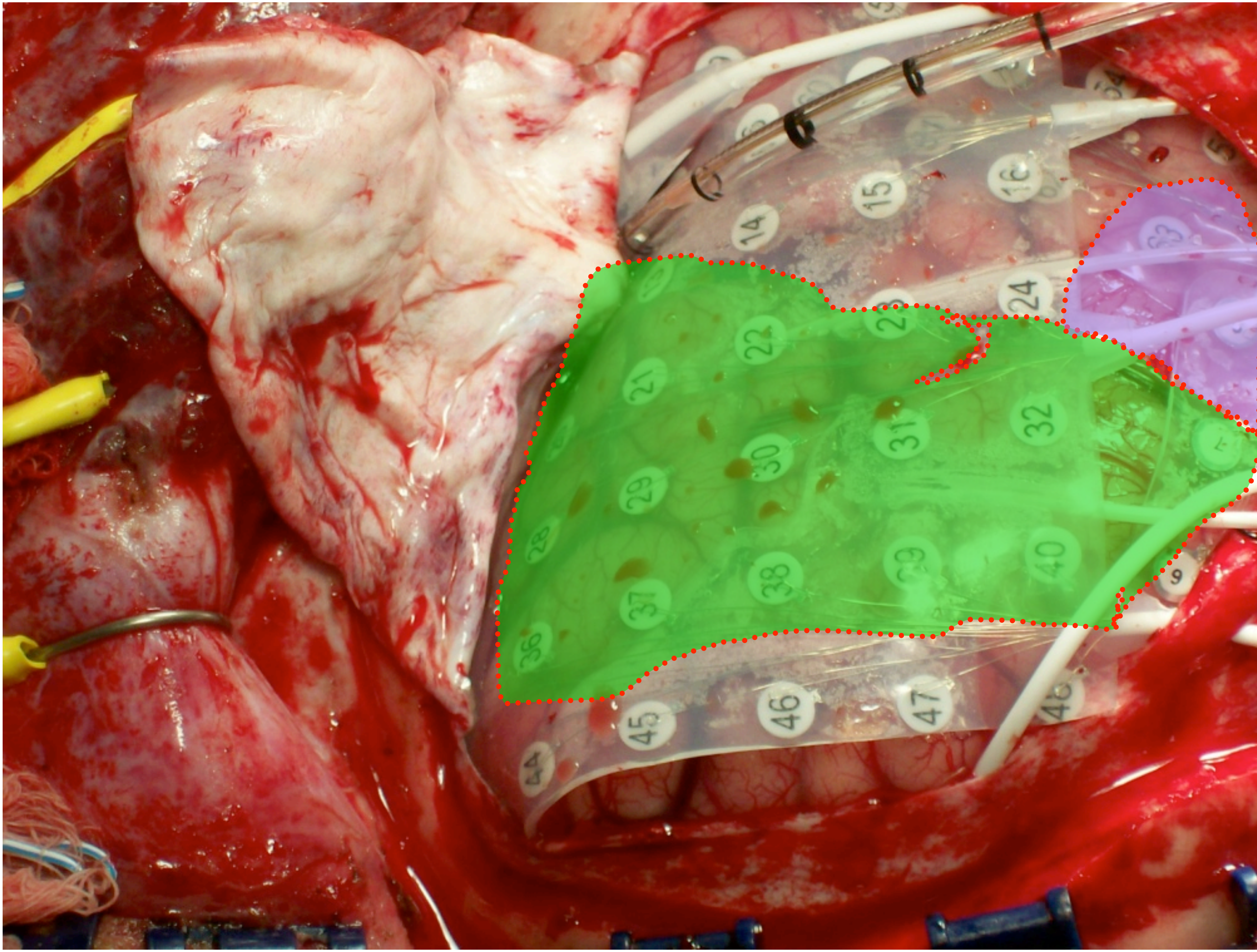

14
15
16
24
22
21
32
31
30
29
28
40
38
37
36
45
46
47
44

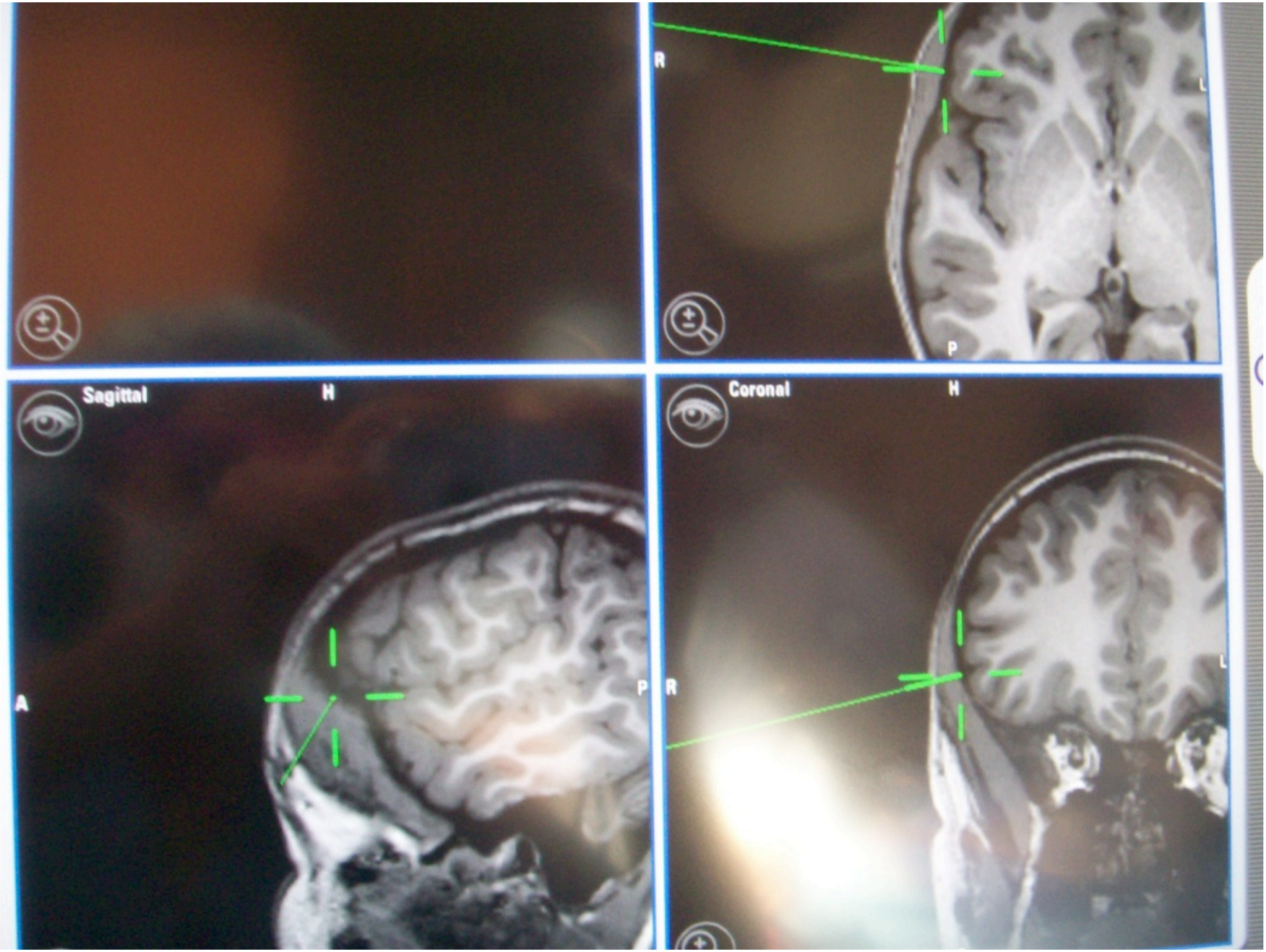

R
L
P
Sagittal
H
A
P
Coronal
H
R
L

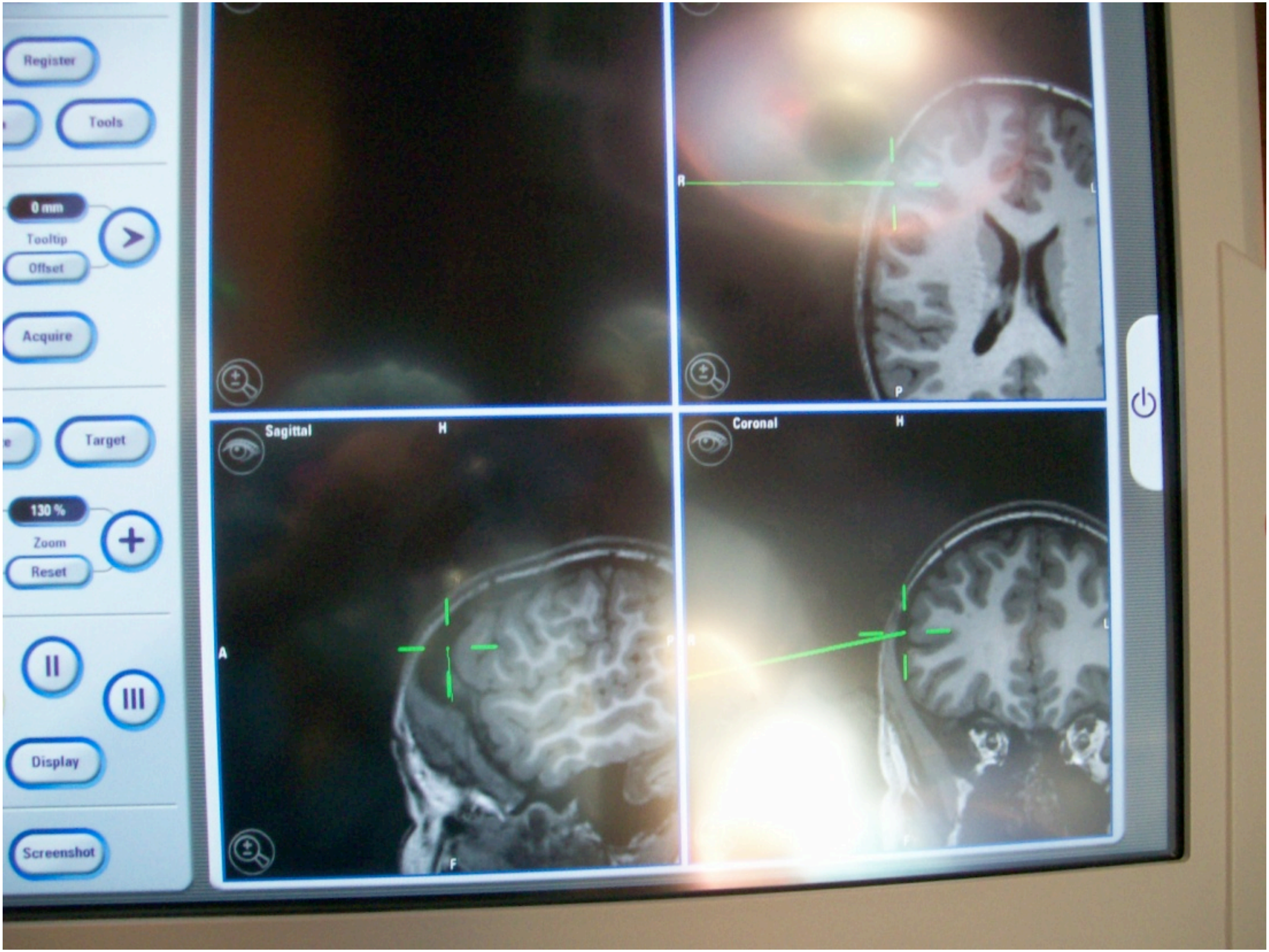
Register
Tools
0 mm
Tooltip
Offset
Acquire
Target
130 %
Zoom
Reset
Display
Screenshot
Sagittal
H
A
F
Coronal
H
R
P

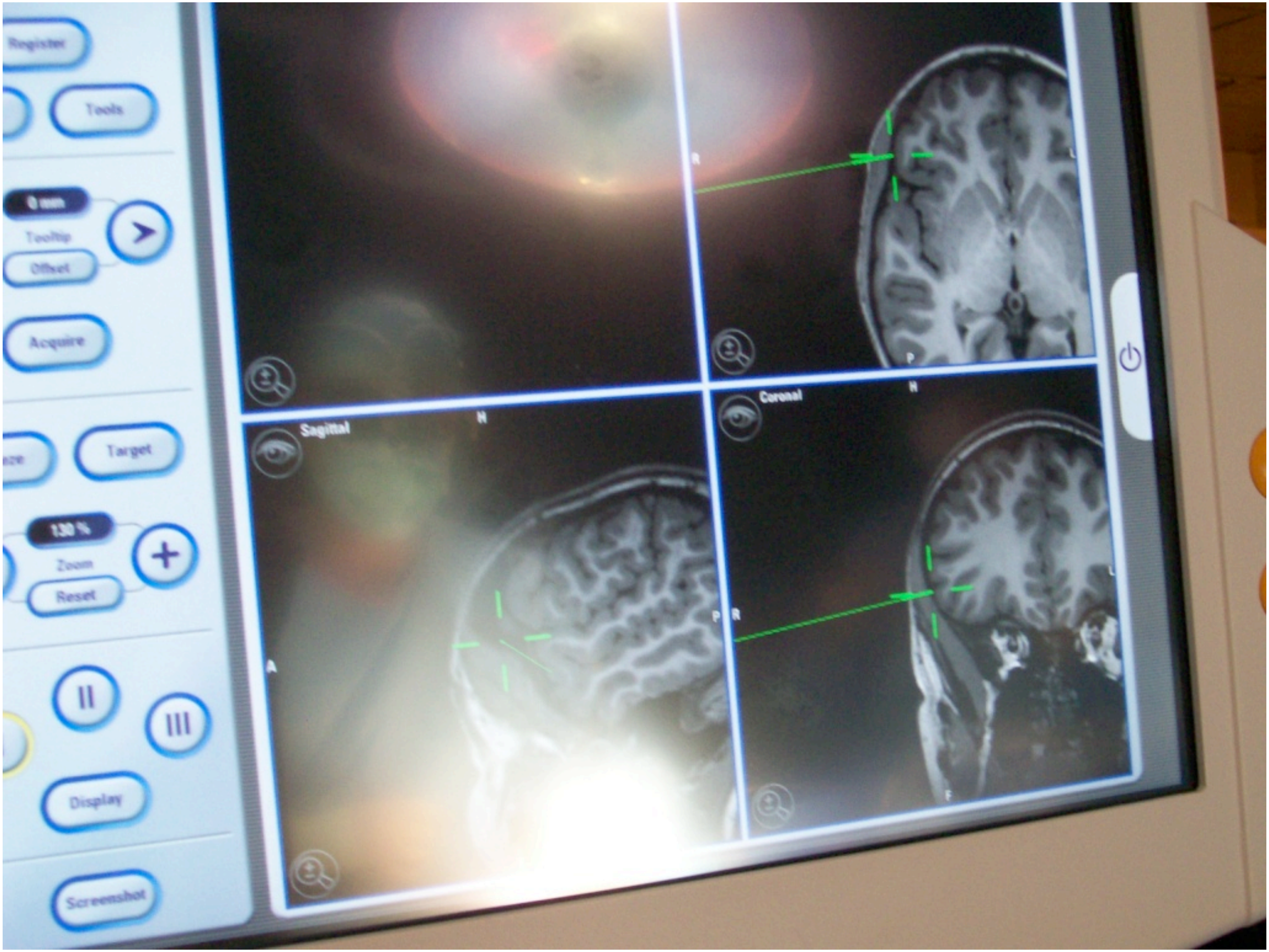
Register
Tools
0 mm
Tooltip
Offset
Acquire
Target
130 %
Zoom
Reset
II
III
Display
Screenshot
Sagittal
Coronal

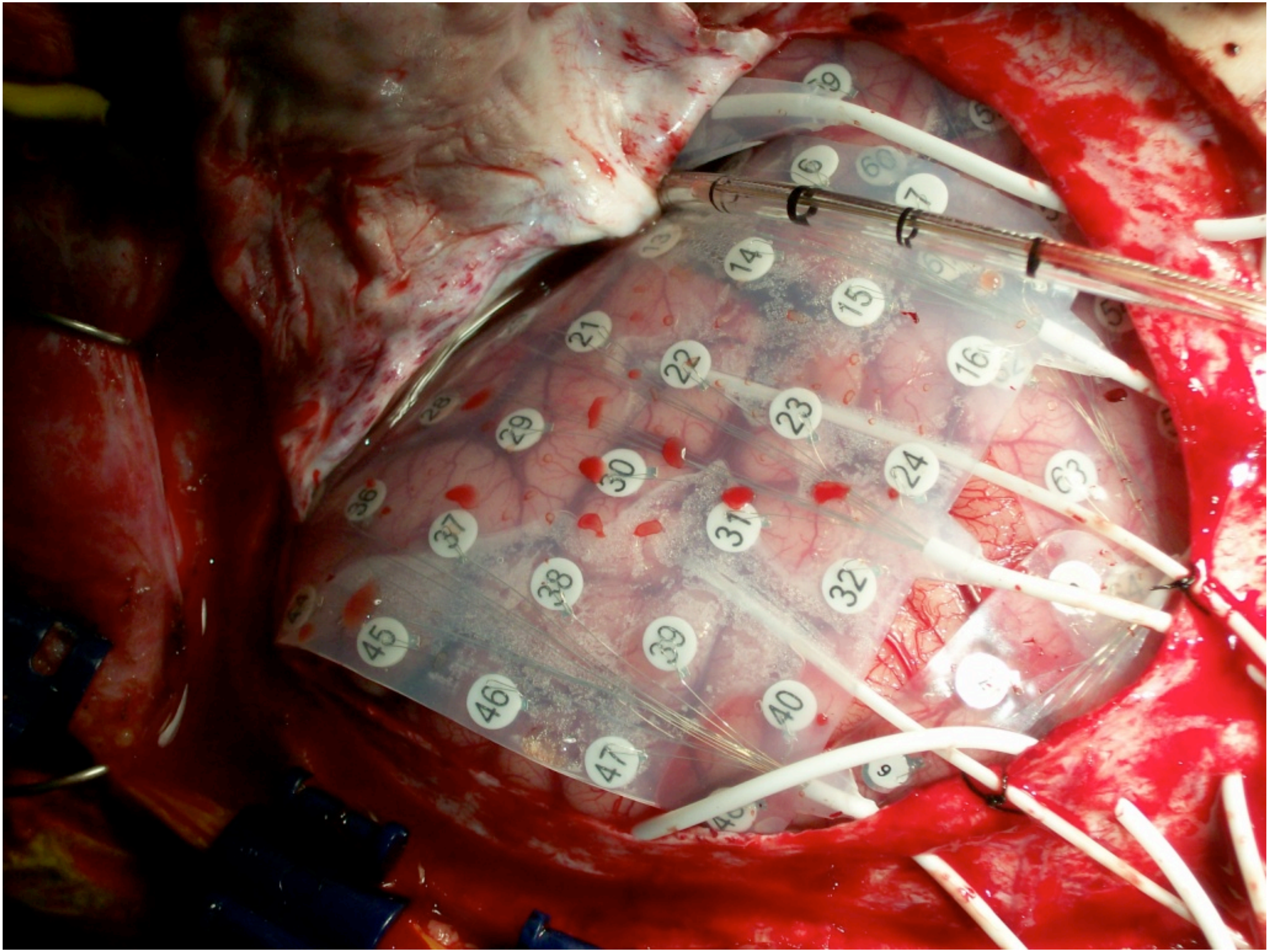
14
15
21
22
16
23
28
29
24
63
30
36
37
31
38
32
45
39
46
40
47
60

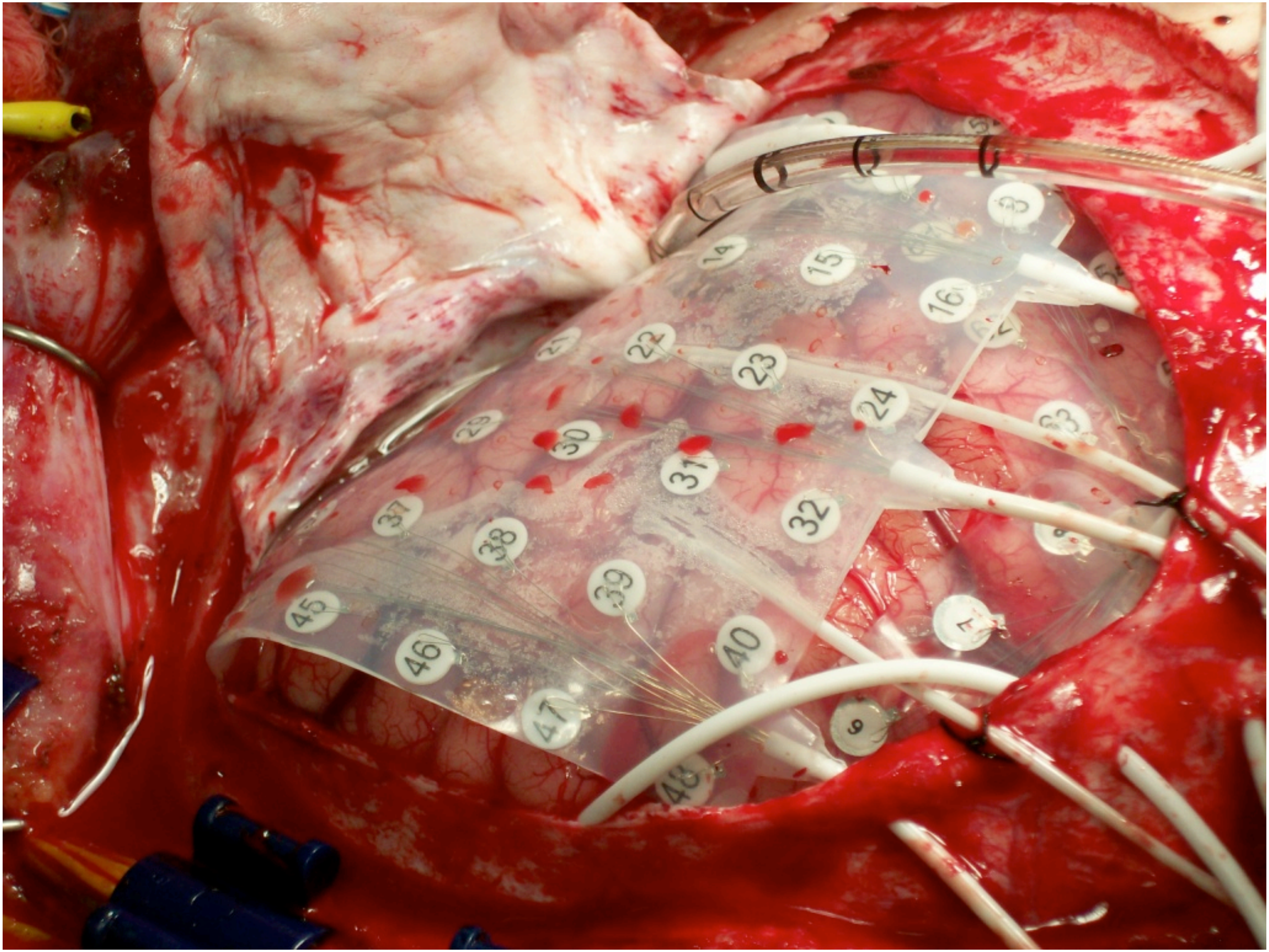
14
15
16
21
22
23
24
29
30
31
32
37
38
39
40
45
46
47
48

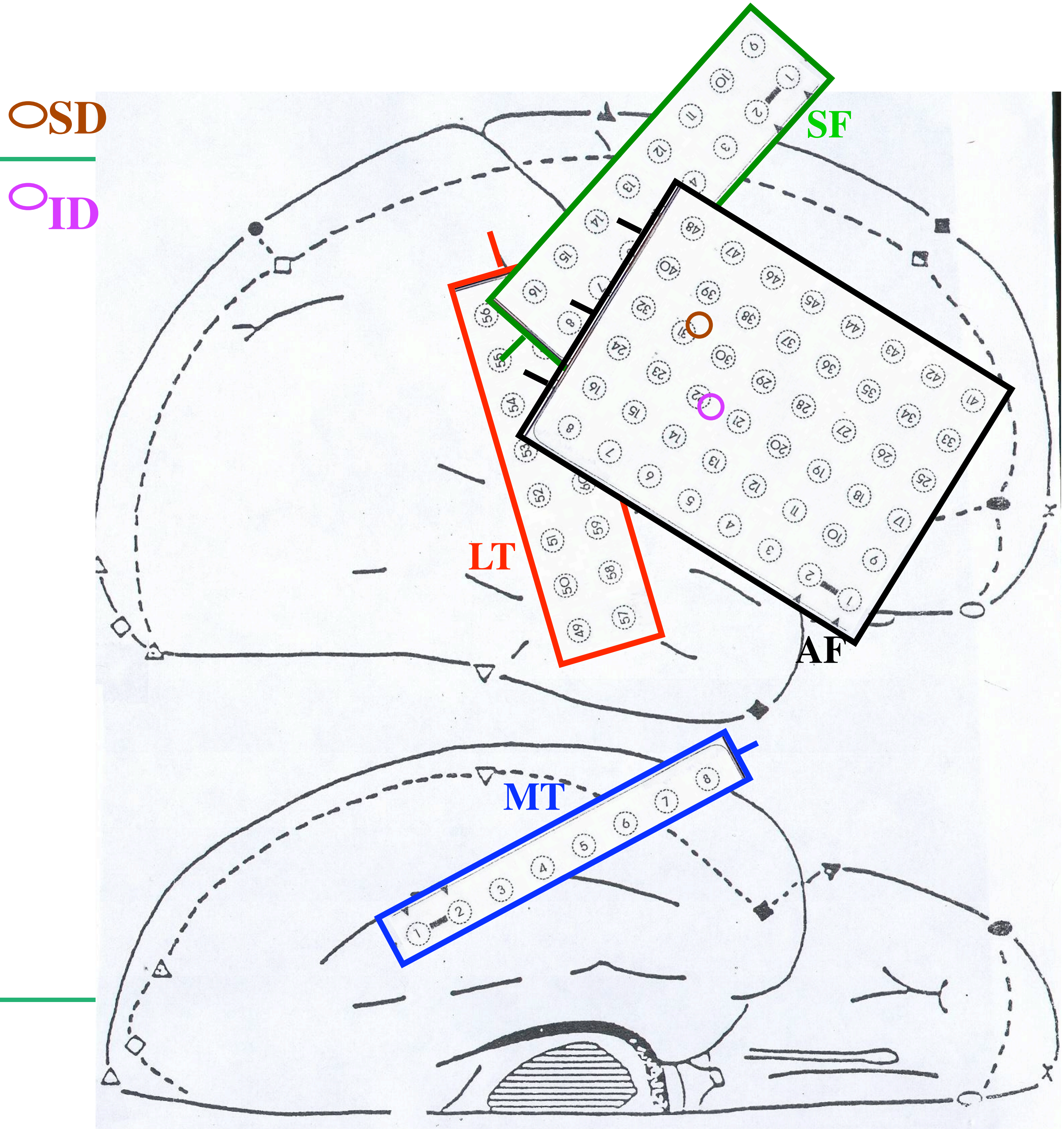
SD
ID
SF
LT
AF
MT

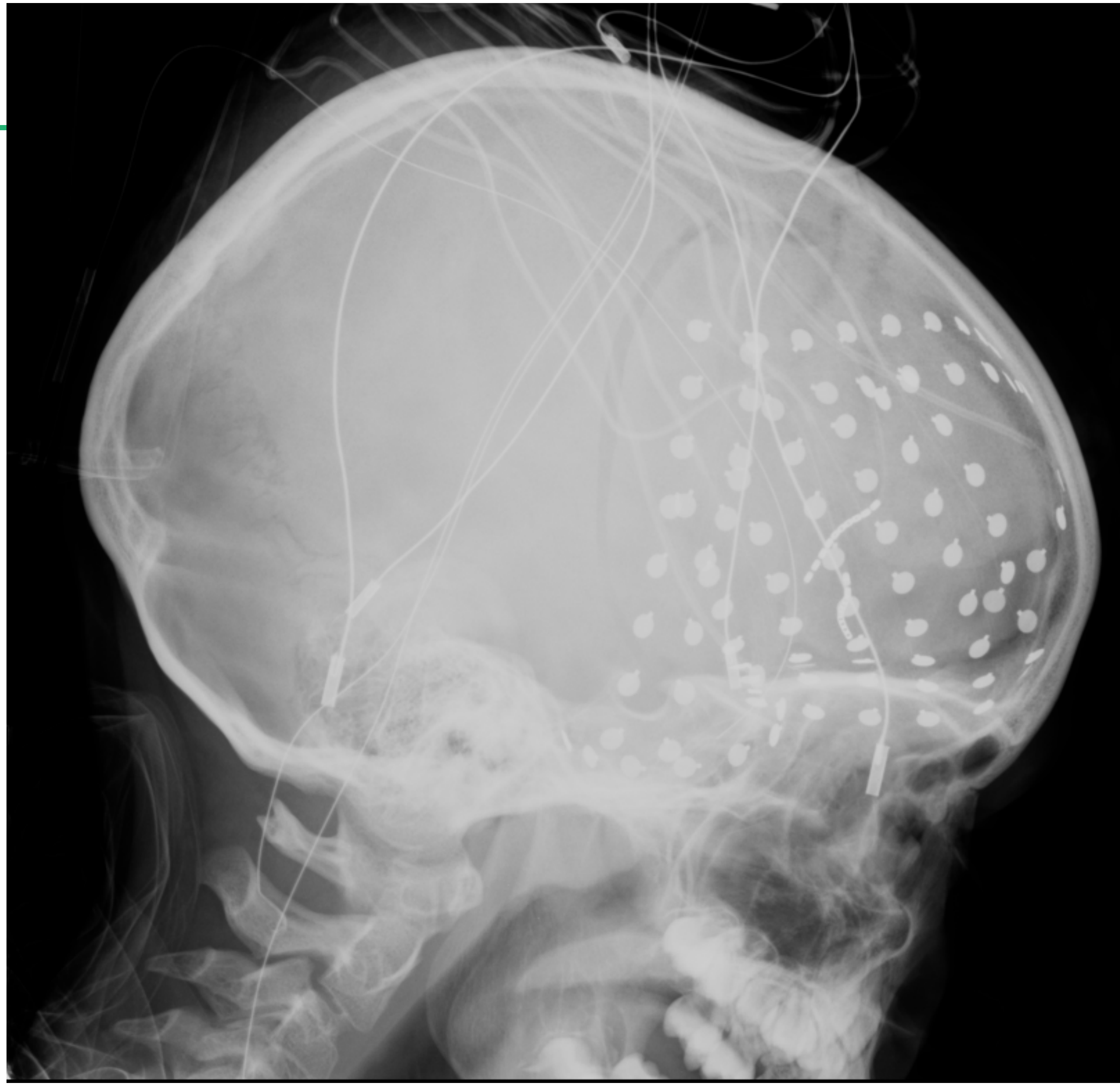

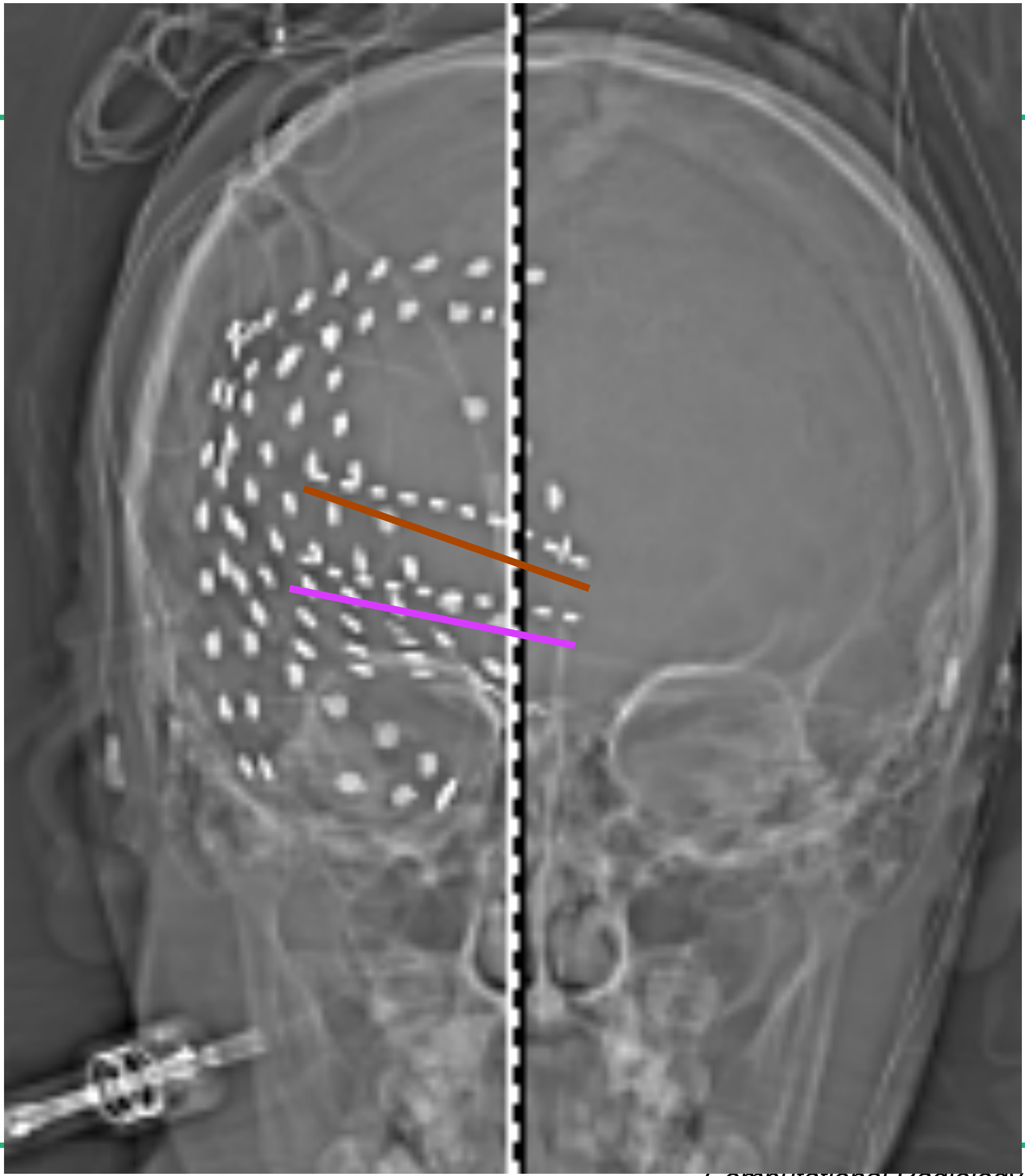

CT with strip/grid/depth electrodes

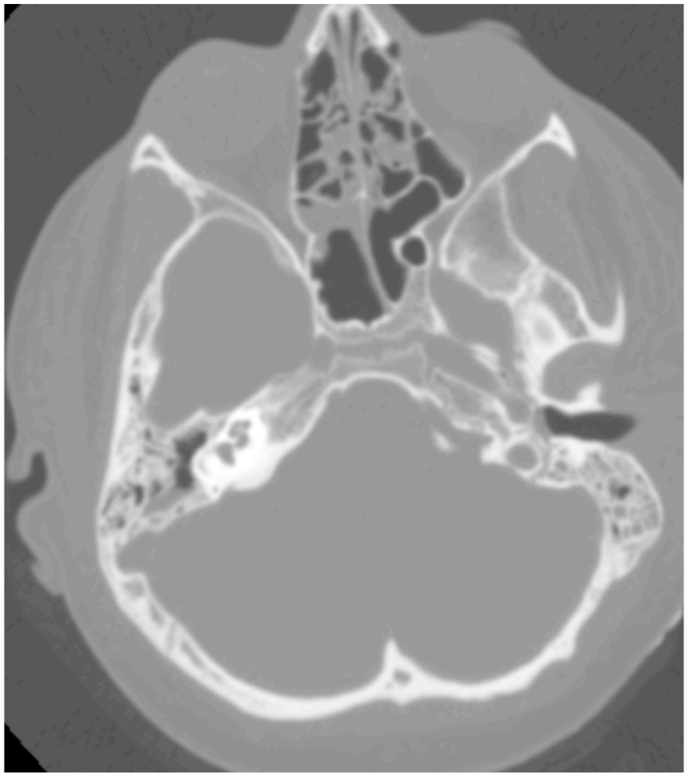

CT and preop MRI fusion

3D visualization of electrodes

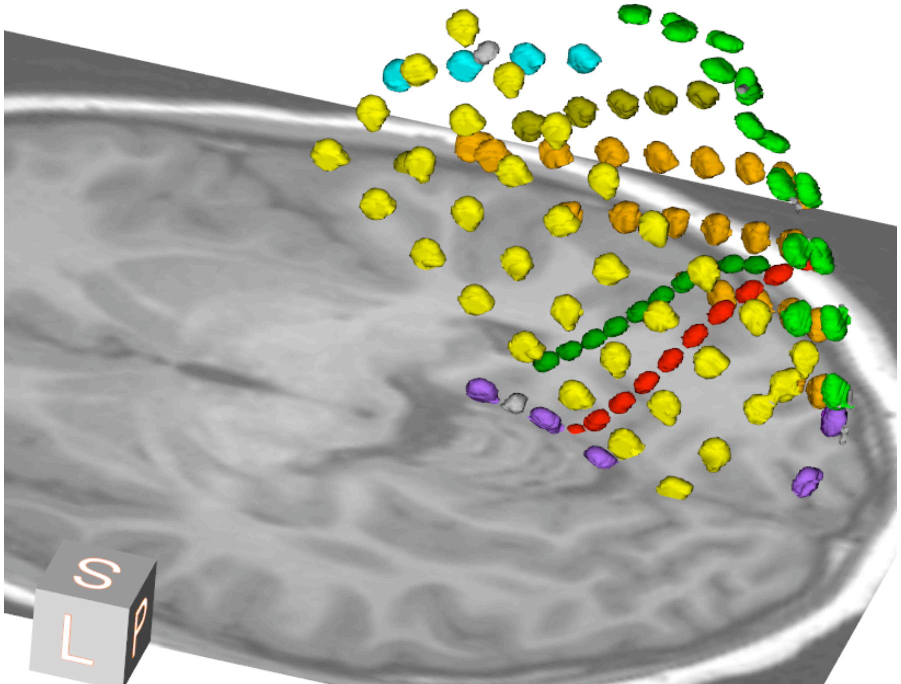

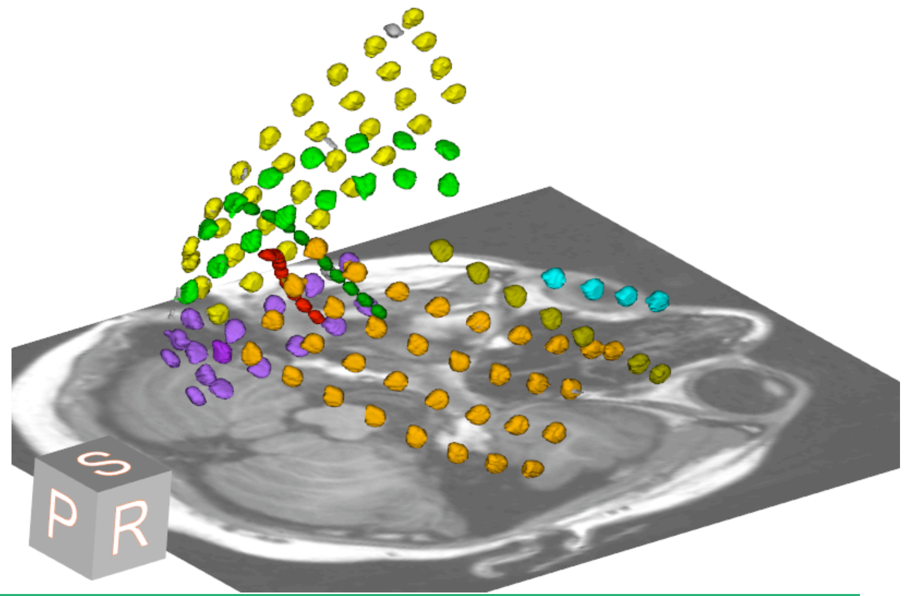

EEG/MEG Source Imaging

- Noninvasive measurements

128 channel EEG

MEG

EEG/MEG Source Reconstruction

Measure EEG and/or MEG.

Reconstruct the current distribution.

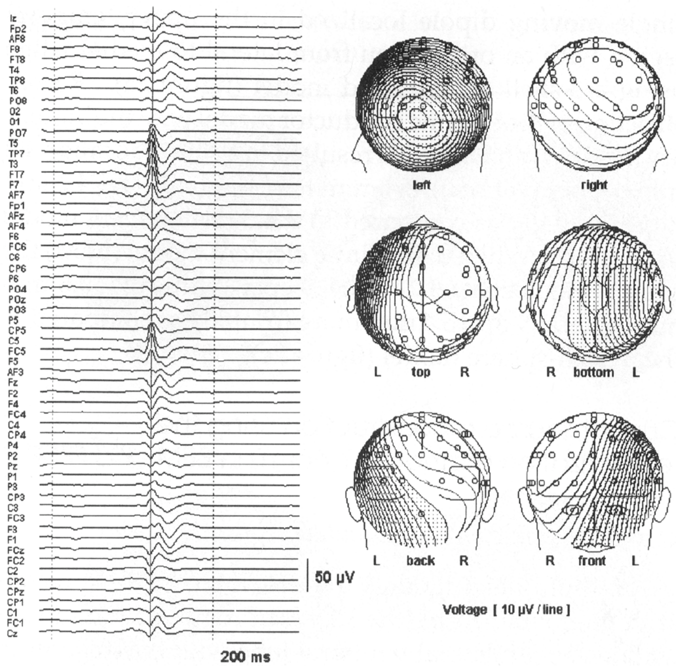

EEG/MEG inverse problem

The source model

Microscopic current flow (~5×10^{-5} nAm)

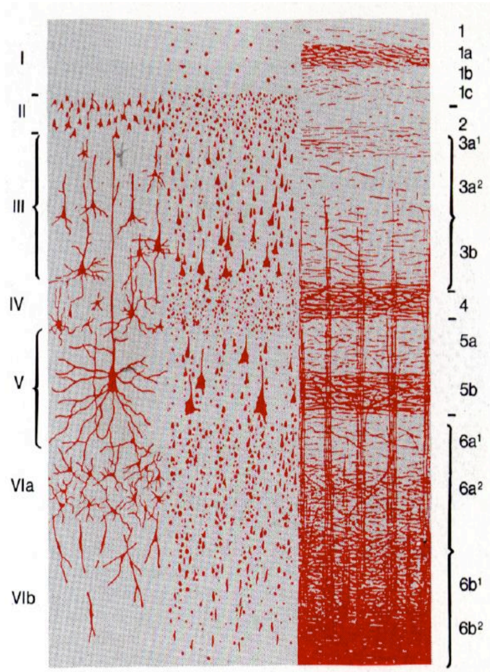

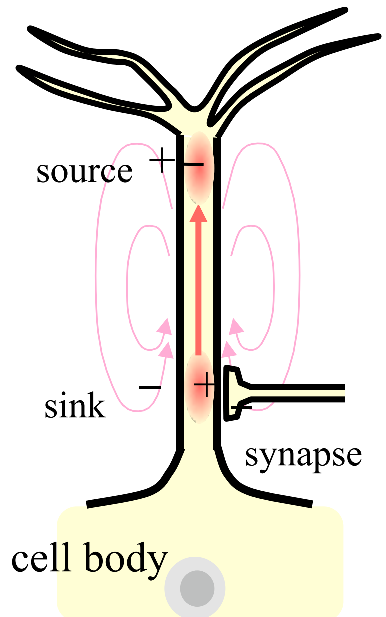

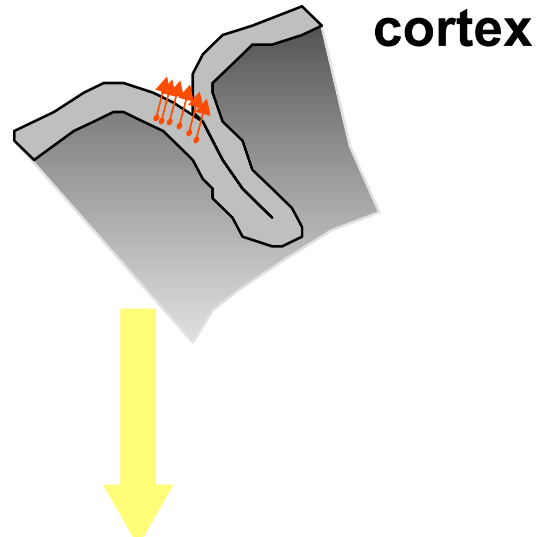

Equivalent Current Dipole (Primary current) (~50 nAm)

parameters:

position : x, y, z
direction : θ, ϕ
magnitude : μ

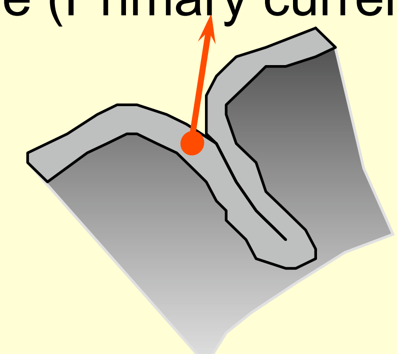

Size of Macroscopic Neural Activity

~30 mm^2 = **5.5×5.5 mm^2**

Bioelectromagnetic field simulation

Place a dipole

Compute the EEG

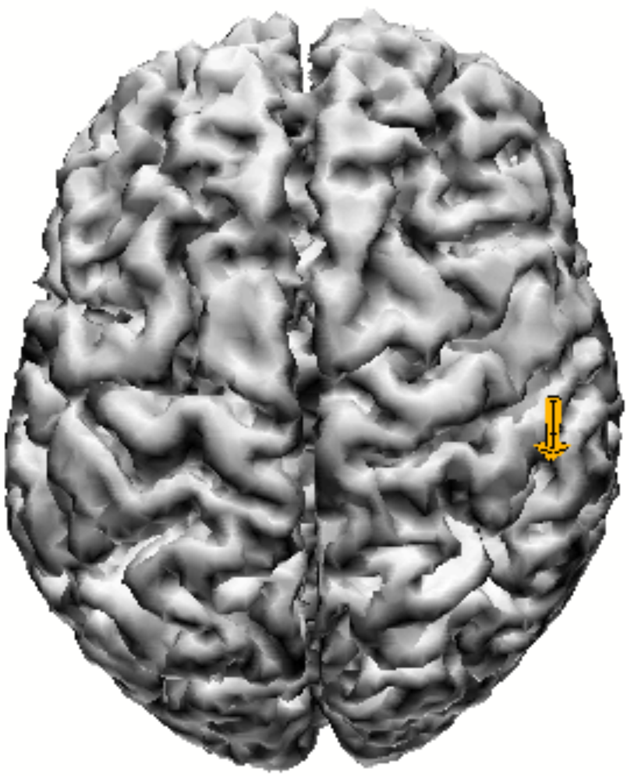

Simulate quasistatic Maxwell equations.

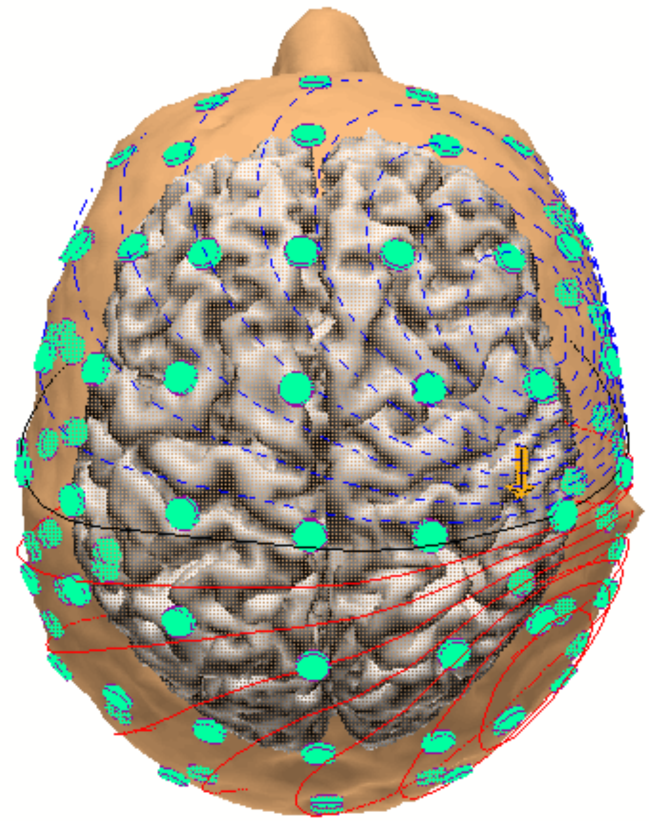

EEG forward problem

Bioelectromagnetic field simulation

Place a dipole

Compute the MEG

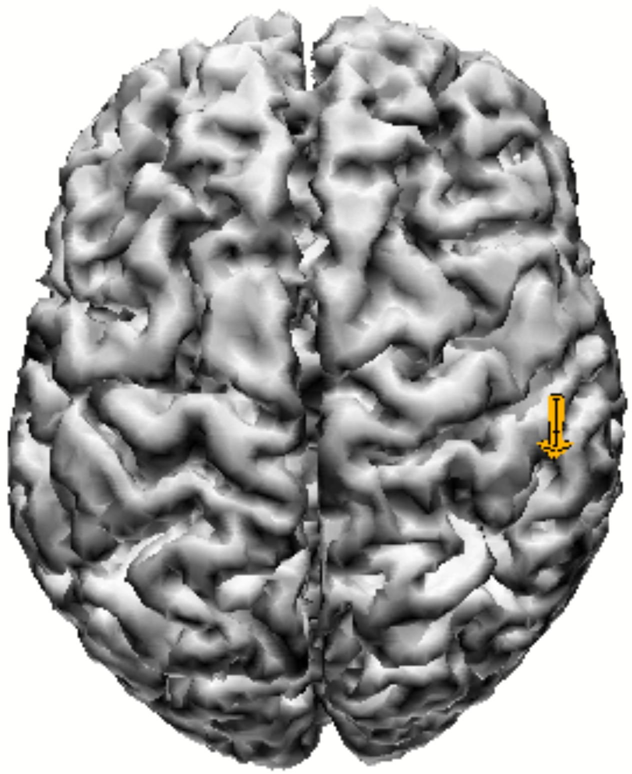

Simulate quasistatic

Maxwell equations.

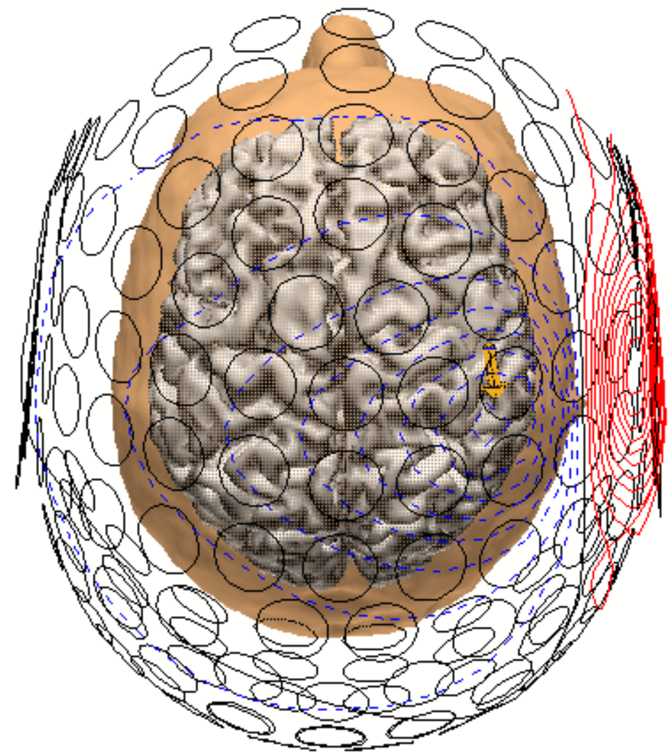

MEG forward problem

The forward problem:
Volume conductor modeling

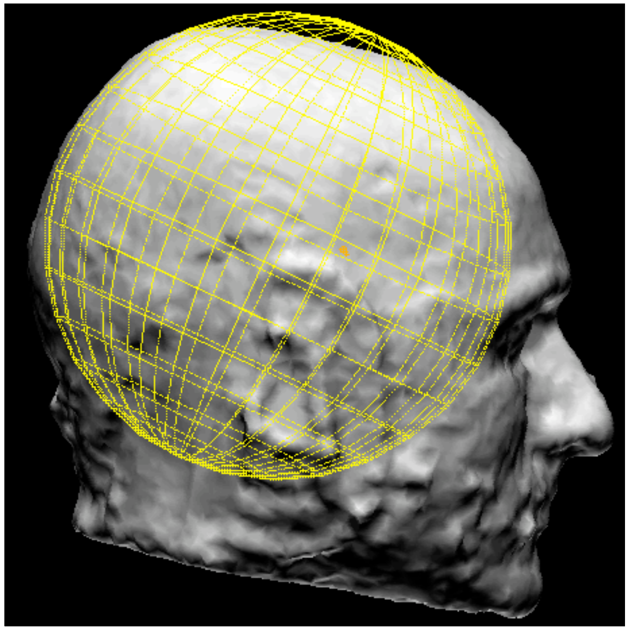

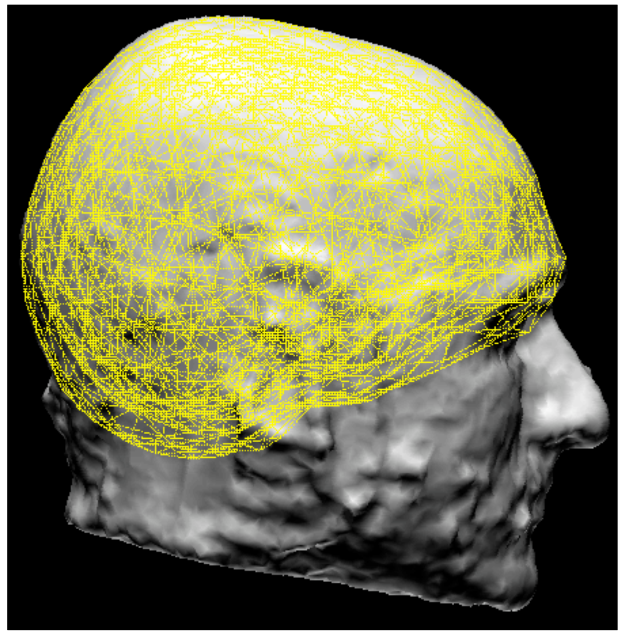

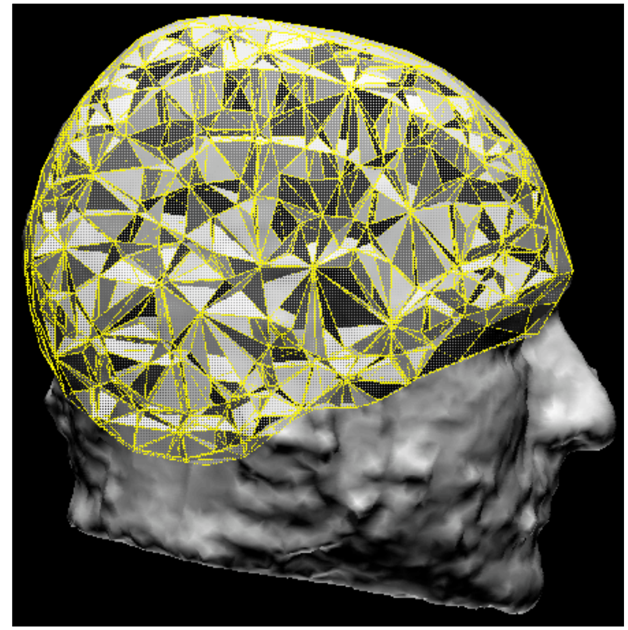

3 Shell

	Geometry	Conductivity
Skin	unrealistic	unreal.
Skull	unreal.	unreal.
CSF	unreal.	unreal.
GM	unreal.	unreal.
WM	unreal.	unreal.

Boundary Element (BE)

	Geometry	Conductivity
Skin	realistic	realistic
Skull	realistic	unrealistic
CSF	unrealistic (1 isotropic value)	
GM		
WM		

Finite Element (FE)

	Geometry	Conductivity
Skin	realistic	realistic
Skull	realistic	realistic
CSF	realistic	realistic
GM	realistic	realistic
WM	realistic	realistic

EEG Source Imaging Solution

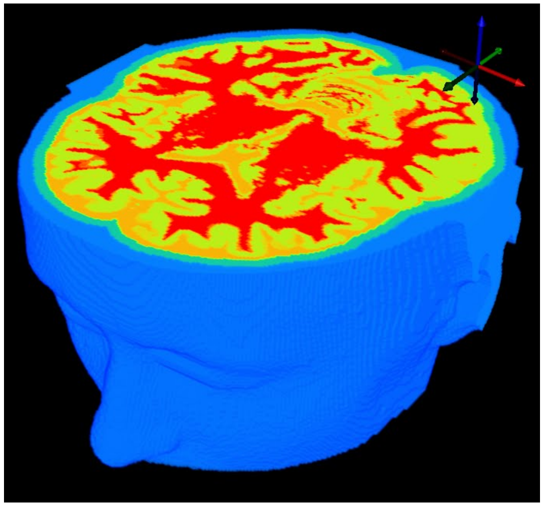

Patient-Specific Segmentation

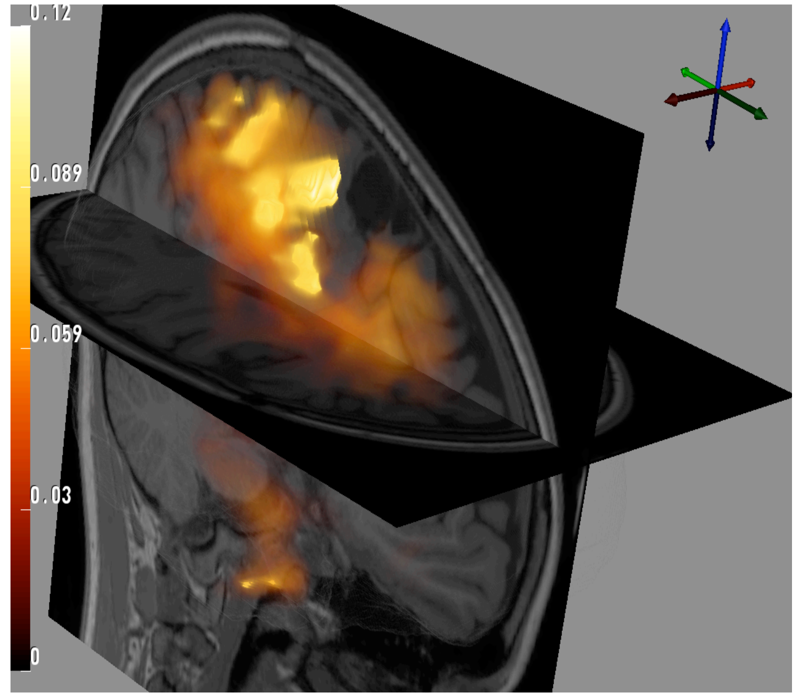

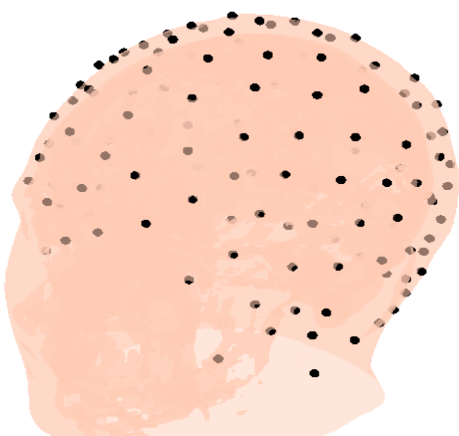

Electrode to MRI Registration

Imaging Enables Guidance in Surgery

- Patient specific modeling with:
  - Advanced image acquisition.
  - Automated image analysis.
    - Segmentation.
    - Registration.
  - Increased computational capacity and efficient algorithms to simulate electromagnetic propagation.
- Expanding accuracy and robustness.

Fetal Brain Volumetry through MRI Volumetric Reconstruction and Segmentation

Ali Gholipour, Judy A. Estroff, Carol E. Barnewolt, Susan A Connolly, Simon K. Warfield

Computational Radiology Laboratory (CRL) and

Advanced Fetal Care Center (AFCC)

Department of Radiology, Children's Hospital Boston

and Harvard Medical School

CARS 2010 June 26, 2010

Computational Radiology Laboratory

How is fetal imaging performed?

- Ultrasonography
- Magnetic Resonance Imaging (MRI)
- Biometry based on 2D measurements
- Volumetry based on several 2D sections

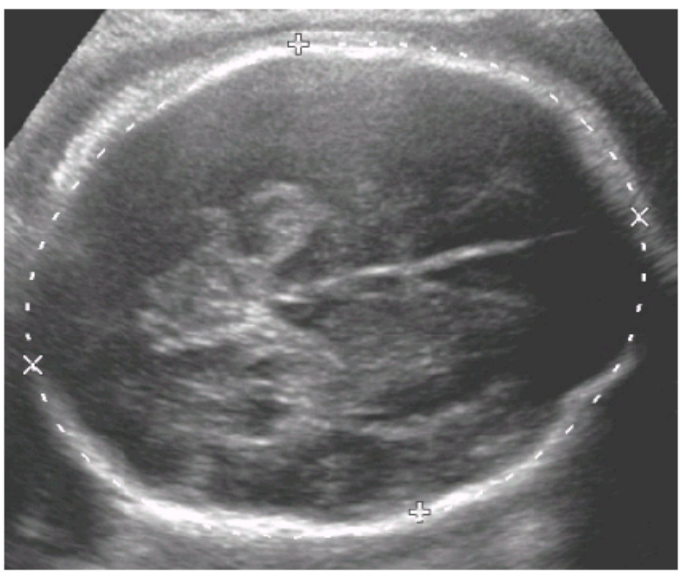

Fetal Brain Volumetry

- Fetal brain volumetry is crucial for the quantitative evaluation of fetal development.
- But it is limited by
  - dependency on motion-free scans,
  - tedious manual segmentation, and
  - spatial inaccuracy due to thick-slice acquisitions.

- We present an image processing pipeline to address these limitations. This involves fetal brain MRI volumetric reconstruction and segmentation.

What is current fetal MRI practice?

- Single-shot fast spin echo (SSFSE) MRI for fast snapshot imaging in the presence of intermittent fetal motion.

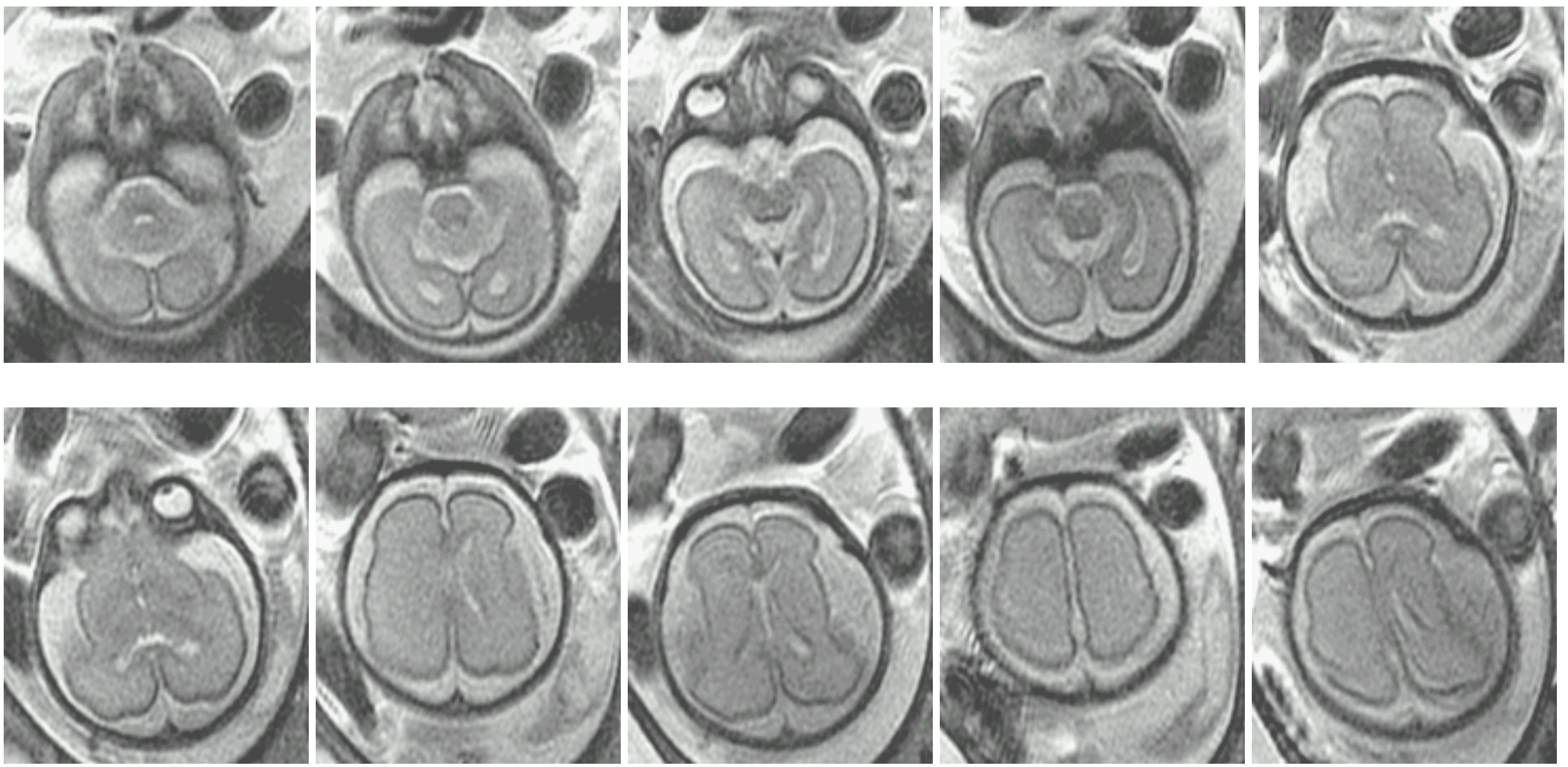

What do the images look like?

Multiple ssFSE images are acquired in fetal orthogonal planes (**axial**, coronal, sagittal).

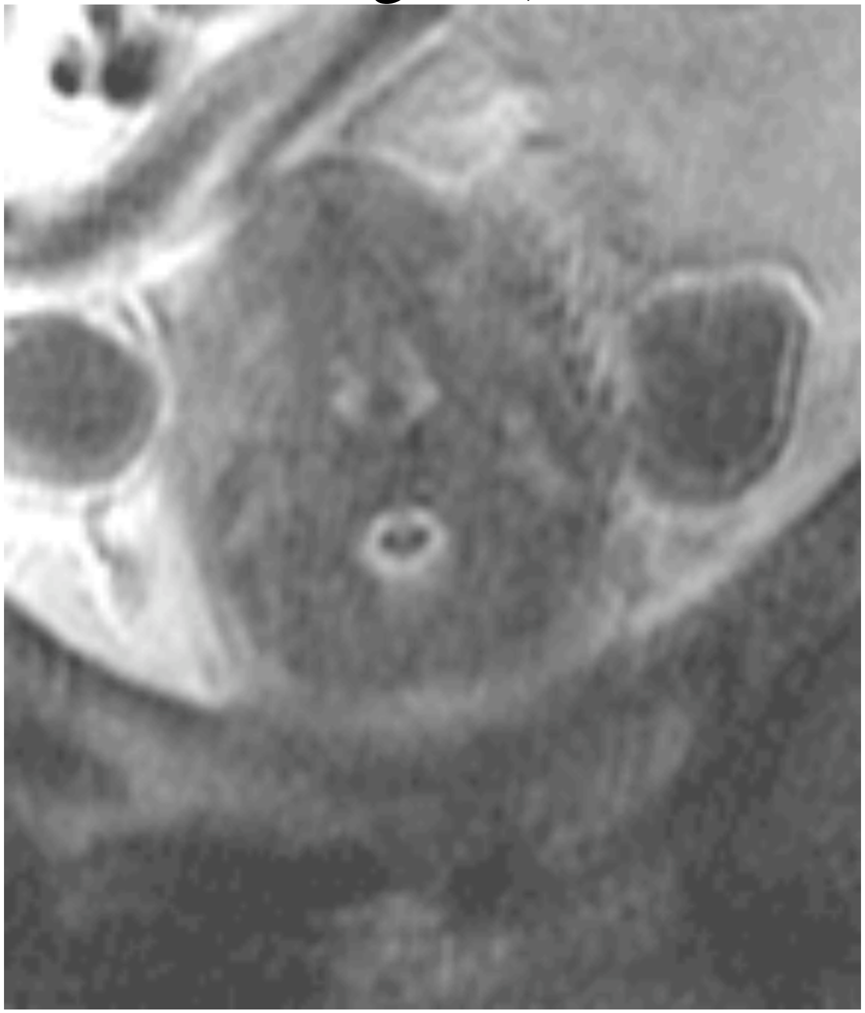

What do the images look like?

Multiple ssFSE images are acquired in fetal orthogonal planes (axial, **coronal**, sagittal).

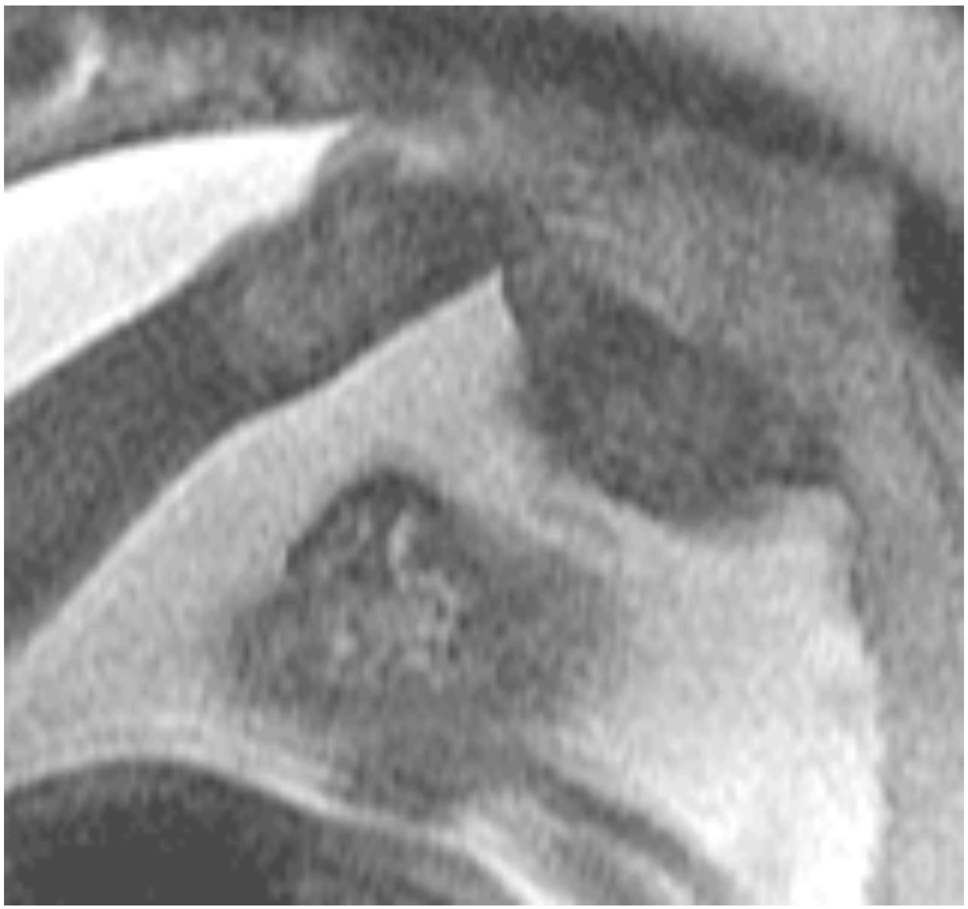

What do the images look like?

Multiple ssFSE images are acquired in fetal orthogonal planes (axial, coronal, **sagittal**).

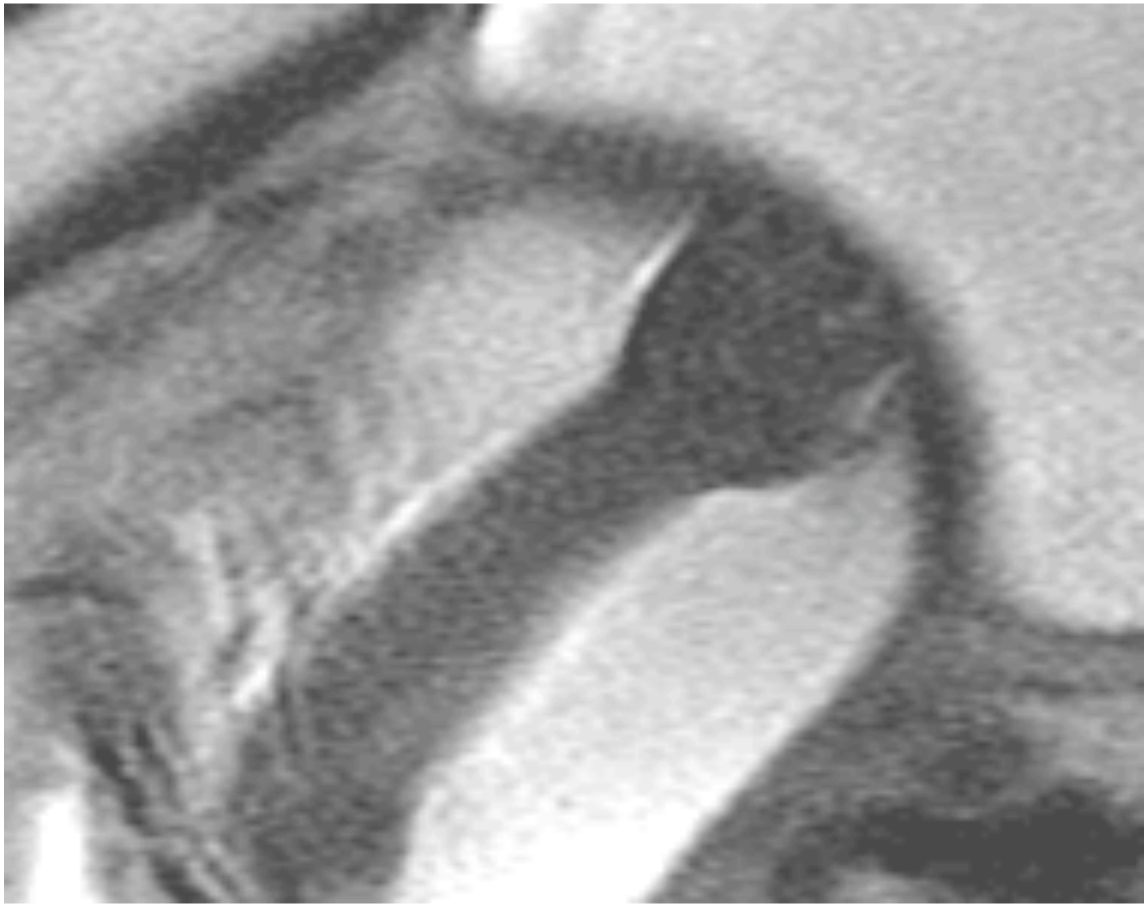

What do the images look like?

- Due to motion and thick slice acquisitions the out-of-plane views do not reflect the 3D anatomy and coherent tissue boundaries.

Axial view

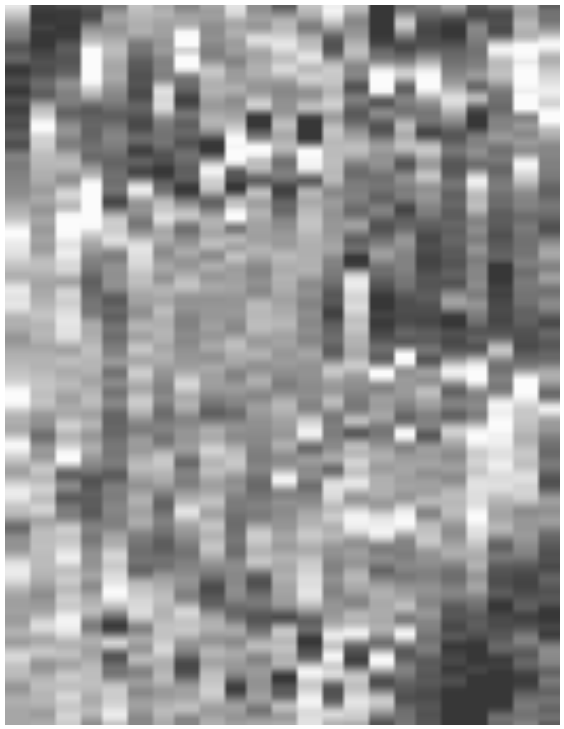

Sagittal view

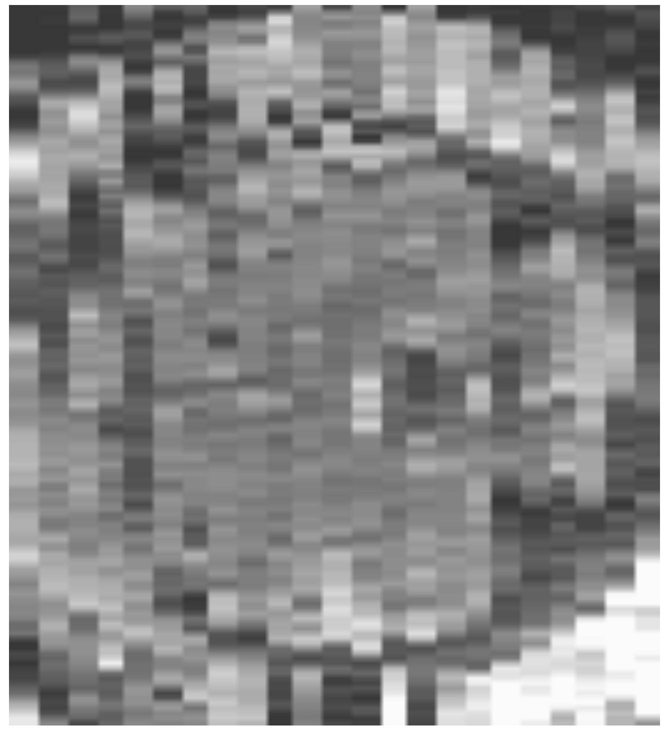

Coronal view

Limitations and objective

- Thick slice acquisitions are necessary to maintain high signal-to-noise ratio.
- Inter-slice motion artifacts are typically observed.
- 3D fetal brain MRI is desired for improved evaluation and automated segmentation and analysis.

How to reconstruct 3D fetal MRI?

- A first simple idea: define the high-resolution 3D image space, resample the SSFSE scans, and average the resampled scans.

Axial view

Coronal view

Sagittal view

Not effective! Motion correction is needed.

Correction for Motion

- Slice-to-volume registration
  - 3D Rigid registration to an estimated reconstructed volume.
  - The first estimation is obtained by averaging the SSFSE scans.

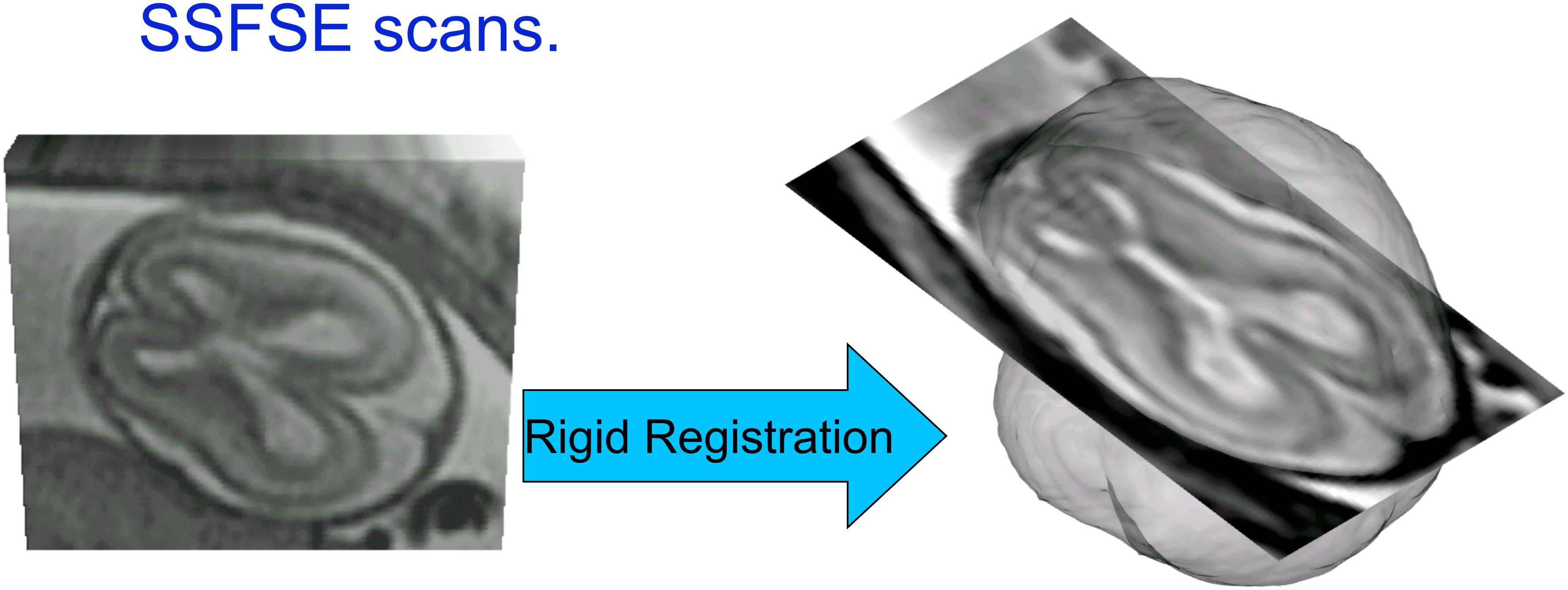

Scattered data interpolation (SDI)

- After motion correction, the voxels from slices will be scattered data in the 3D volumetric image space.

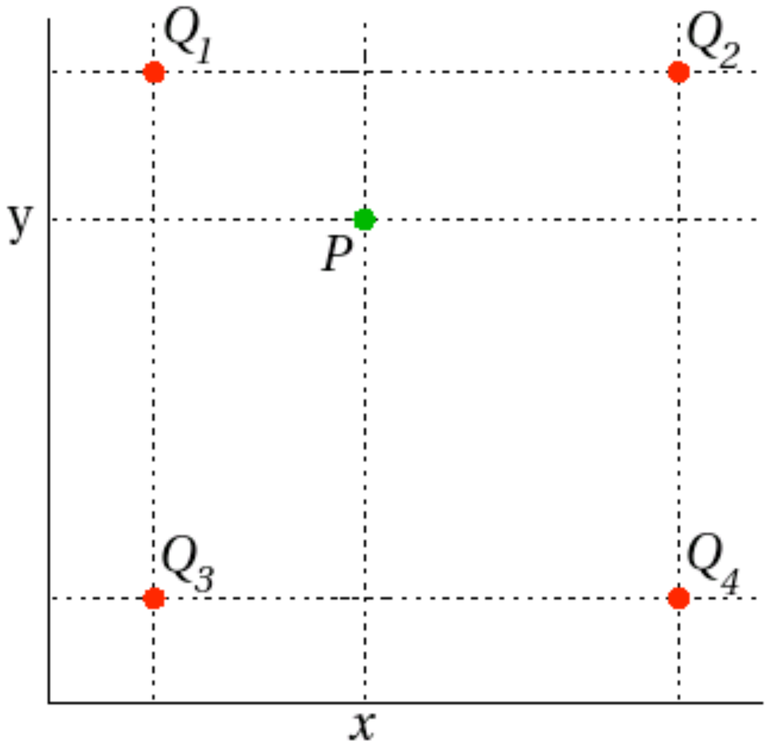

Regular grid interpolation

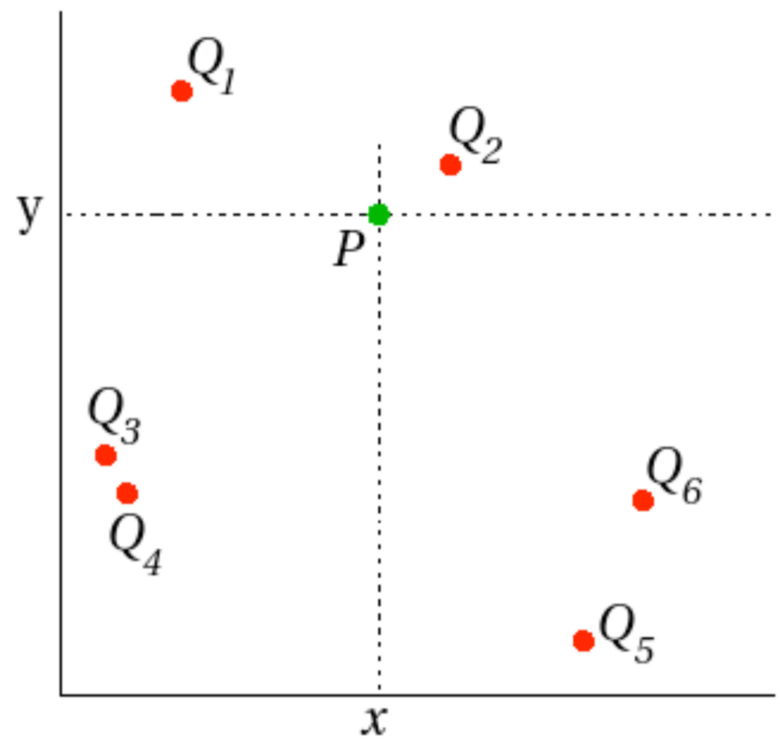

Scattered data interpolation

Scattered data interpolation (SDI)

- Scattered data interpolation is performed using sample weighting through kernels.

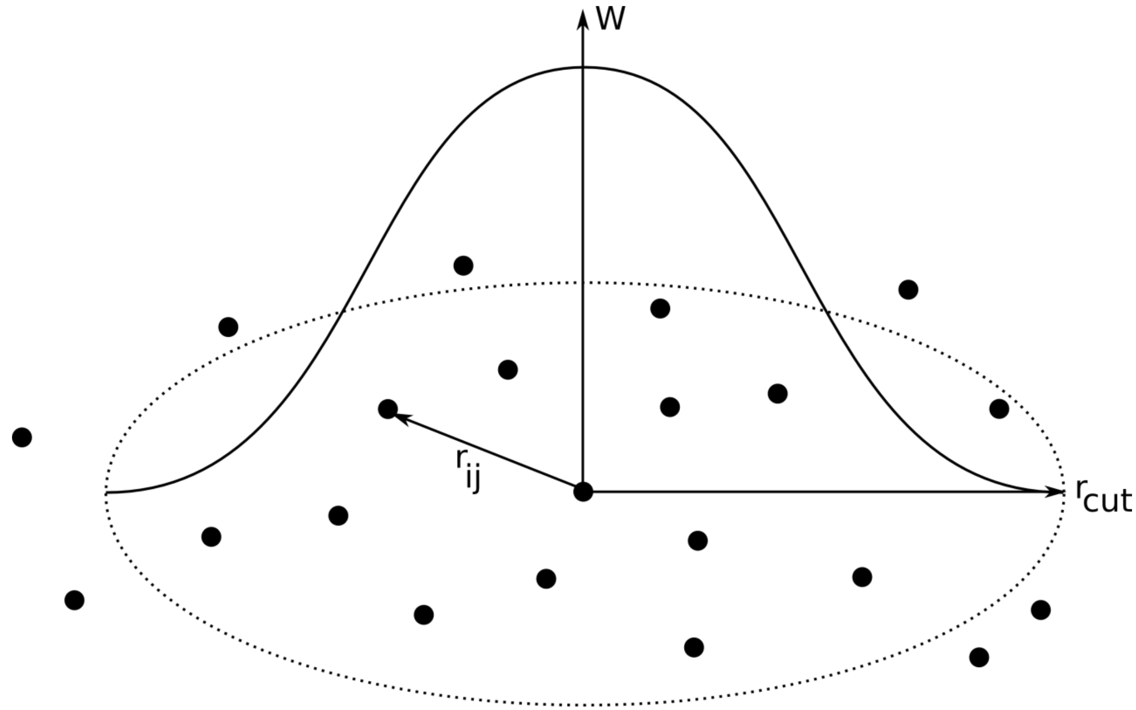

[1] Rousseau et al. Acad. Radiol. 2006; [2] Jiang et al. IEEE Tran Med. Imag. 2007

Limitations of SDI

- SDI result depends on the choice of the interpolation kernel and the kernel size.
- Thick-slice voxels are heterogeneous and involve signal averaging in the slice select direction, thus they should not be approximated as points.

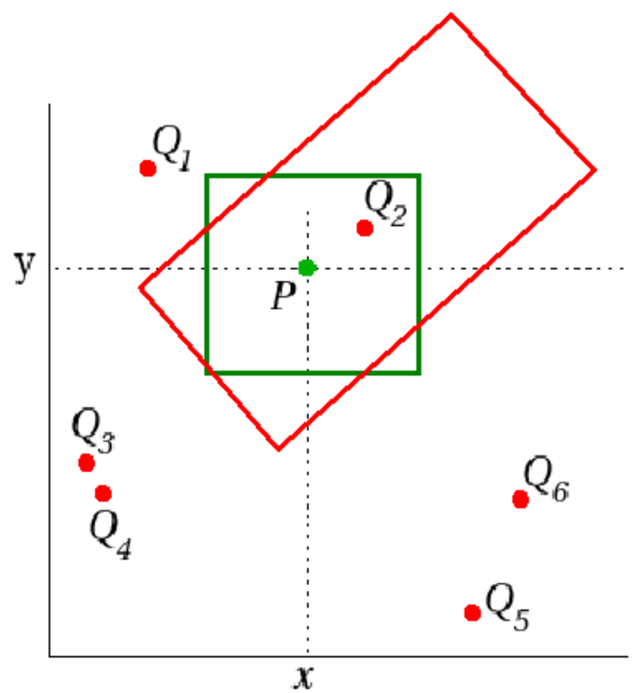

1mm x 1mm x 4mm

Our approach: Slice acquisition model

Imaged object

noise

number of slices

k^{th} 2D slice

$$\underline{Y}_k = \mathbf{D}_k \mathbf{B}_k \mathbf{S}_k \mathbf{M}_k \underline{X} + \underline{V}_k \quad , \quad k = 1, \ldots, n$$

Motion (3D)

Down-sampling

PSF blur

Slice selection profile (3D)

$$\left| \vec{\mu}_{sk} . \vec{r} - s_{0k} \right| < \Delta s_k / 2$$

[4] Gholipour & Warfield MICCAI'09; [5] Gholipour et al. IEEE Tran Med. Imag. 2010

Image reconstruction

- Find the high-resolution image (*X*)
  - Maximum likelihood estimation to minimize an error function between the reconstructed volume and the acquired slices.

$$\underline{\hat{X}} = \underset{\underline{X}}{ArgMin}\left[\sum_{k=1}^{N} d\left(\underline{Y}_k, \mathbf{D}_k\mathbf{B}_k\mathbf{S}_k\mathbf{M}_k\underline{X}\right)\right]$$

$$\underline{\hat{X}} = \underset{\underline{X}}{ArgMin}\left[\sum_{k=1}^{N} \left\|\mathbf{D}_k\mathbf{B}_k\mathbf{S}_k\mathbf{M}_k\underline{X} - \underline{Y}_k\right\|_2^2 + \lambda\left\|\mathbf{C}\underline{X}\right\|_2^2\right]$$

Super-resolution reconstruction

- Iterations of slice-to-volume registration, scattered data interpolation, and maximum likelihood super-resolution reconstruction.

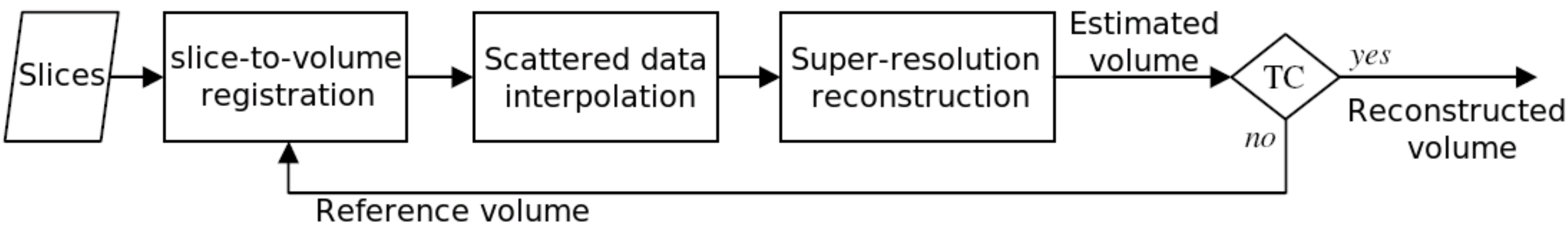

Super-resolution reconstruction through iterative maximum likelihood error minimization:

$$\underline{\hat{X}}^{n+1} = \underline{\hat{X}}^{n} + \alpha\left[\sum_{k=1}^{N} \mathbf{M}_k^{\mathbf{T}}\mathbf{S}_k^{\mathbf{T}}\mathbf{B}_k^{\mathbf{T}}\mathbf{D}_k^{\mathbf{T}}\left(\underline{Y}_k - \mathbf{D}_k\mathbf{B}_k\mathbf{S}_k\mathbf{M}_k\underline{\hat{X}}^{n}\right) - \lambda\mathbf{C}^{\mathbf{T}}\mathbf{C}\underline{\hat{X}}^{n}\right]$$

Data and experiments

- 22 Fetal MRI cases
  - 1.5-T TwinSpeed Signa system (GE Healthcare) with an 8-channel phased-array cardiac coil.
  - without maternal sedation or breath-hold.
  - Multiple SSFSE MRI with in-plane resolution of 0.7 to 0.8 mm and slice thickness of 3 or 4 mm.
  - The gestational age (GA) range of 19.28 to 38.43 weeks (mean 27.892, stdev 6.876).

Results – 19 week fetus

Axial SSFSE 4 mm slices

3D recon. Volume 0.8 mm

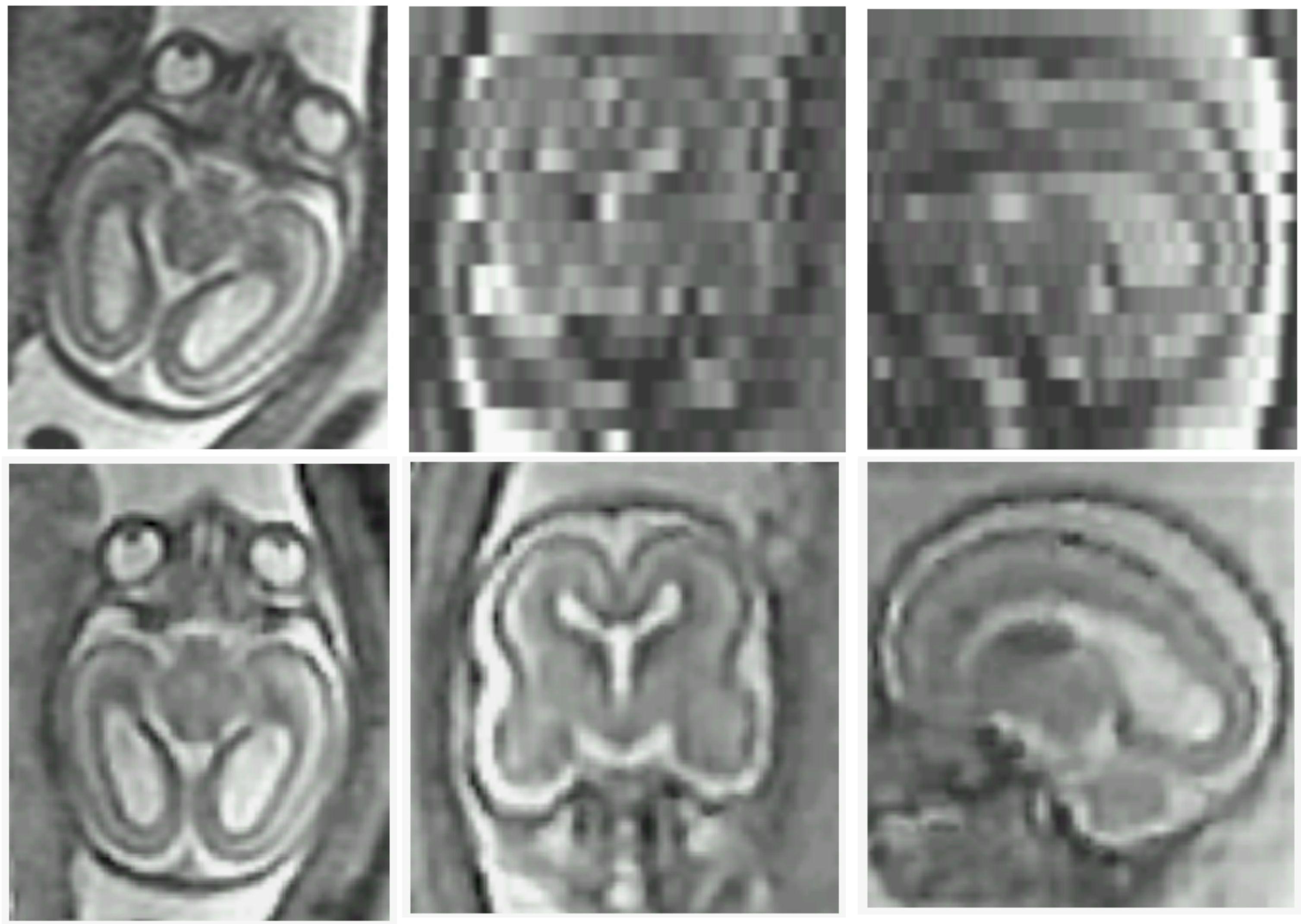

axial plane | coronal plane | sagittal plane

Results – 36 week fetus

Axial
SSFSE
6 mm
slices

3D
recon.
Volume
0.8 mm

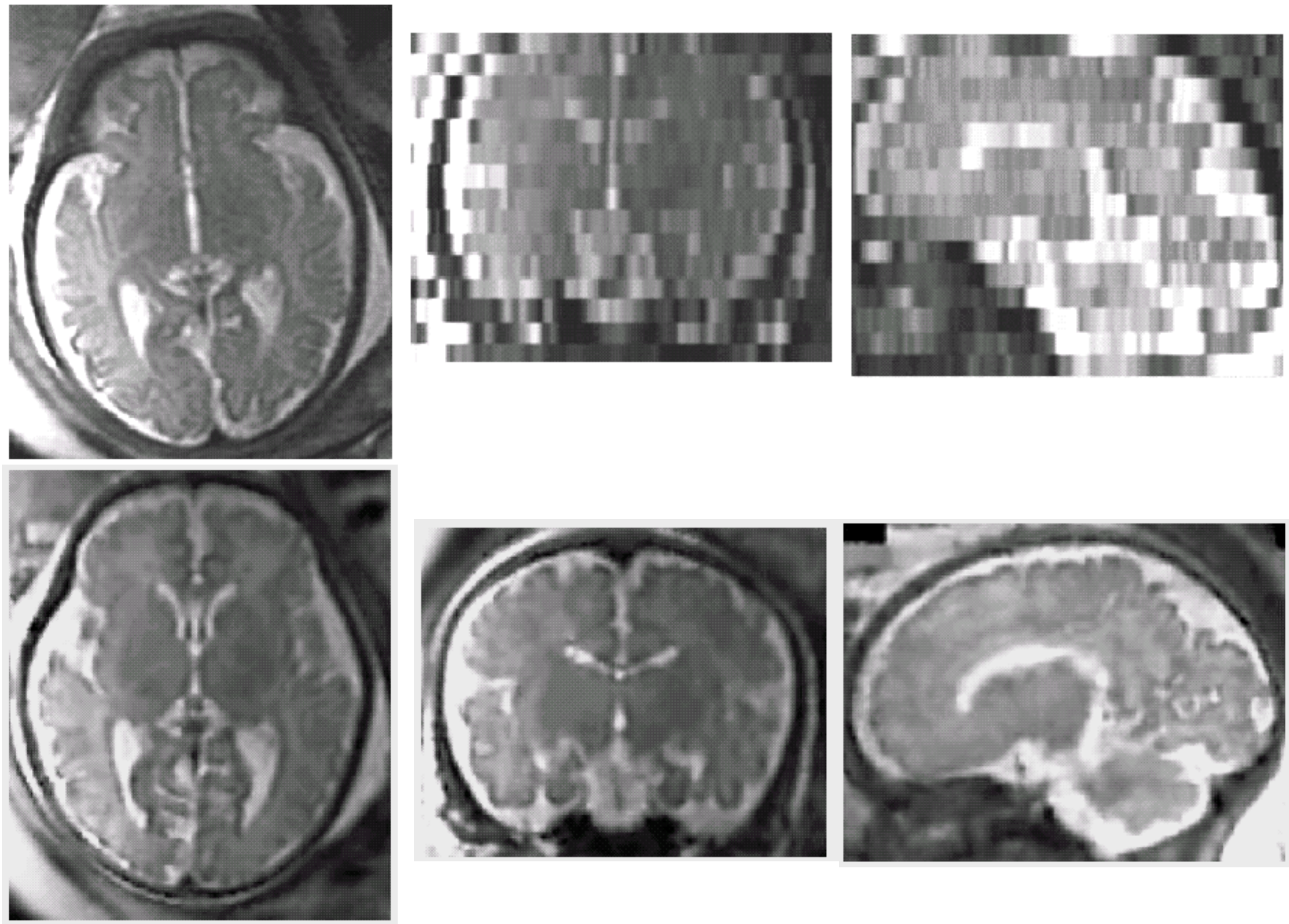

axial plane | coronal plane | sagittal plane

Results – 2mm slice acquisitions

SagittalS
SFSE
2 mm
slices

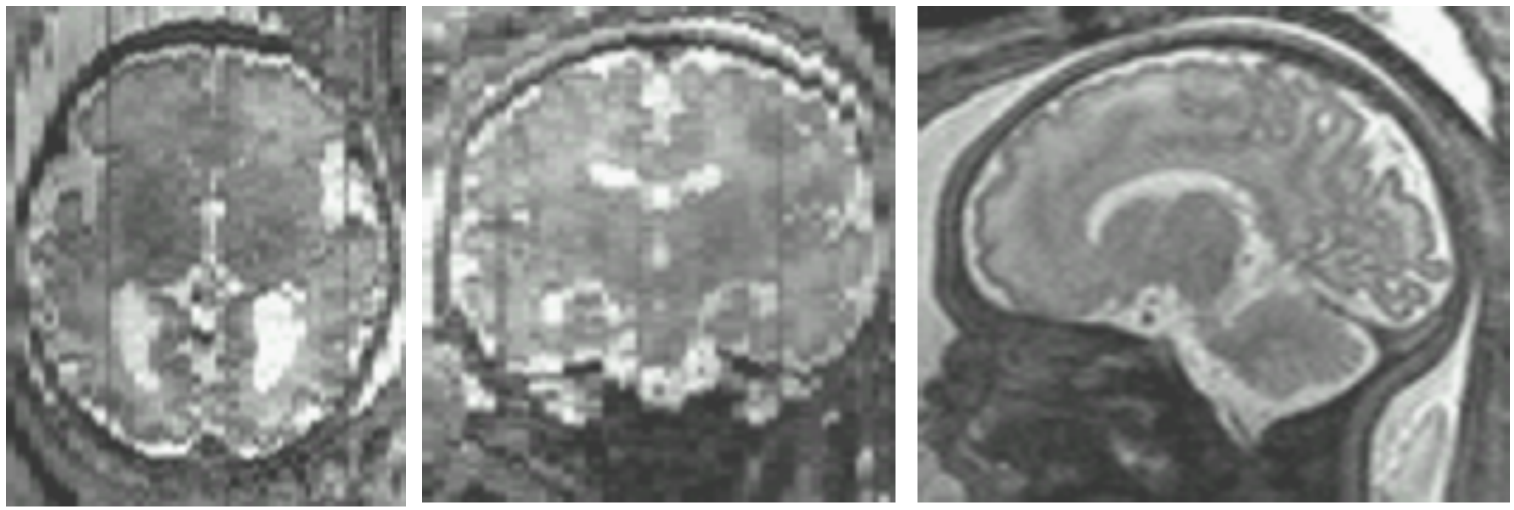

3D
recon.
Volume
0.8 mm

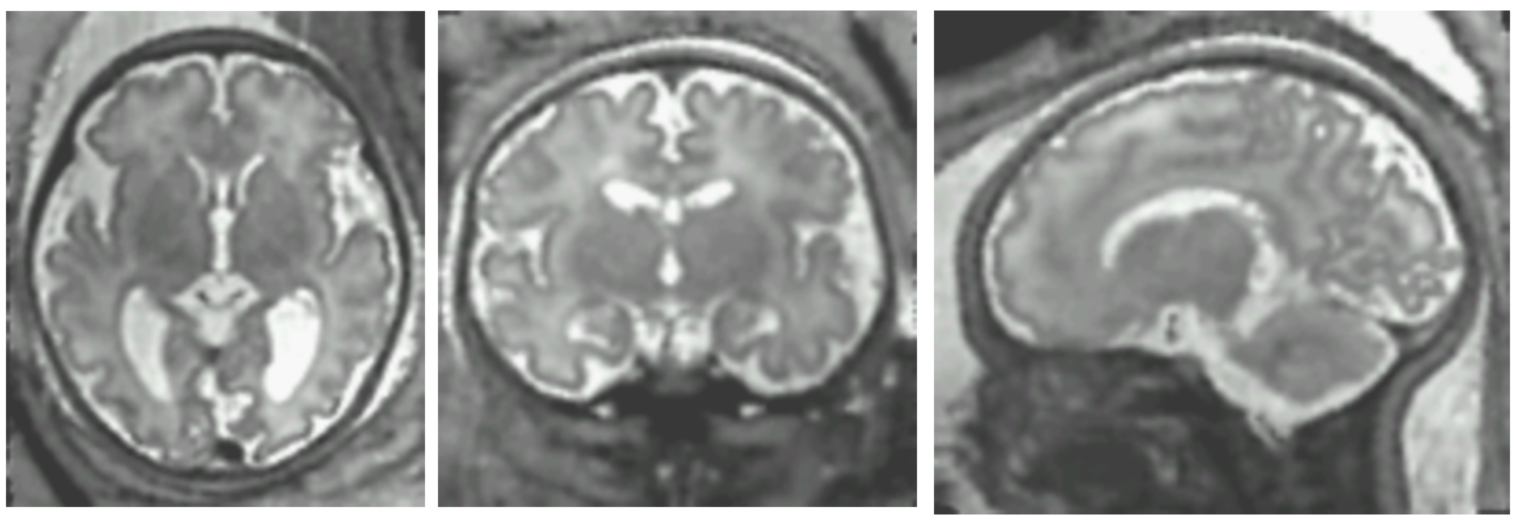

Supervised automated segmentation

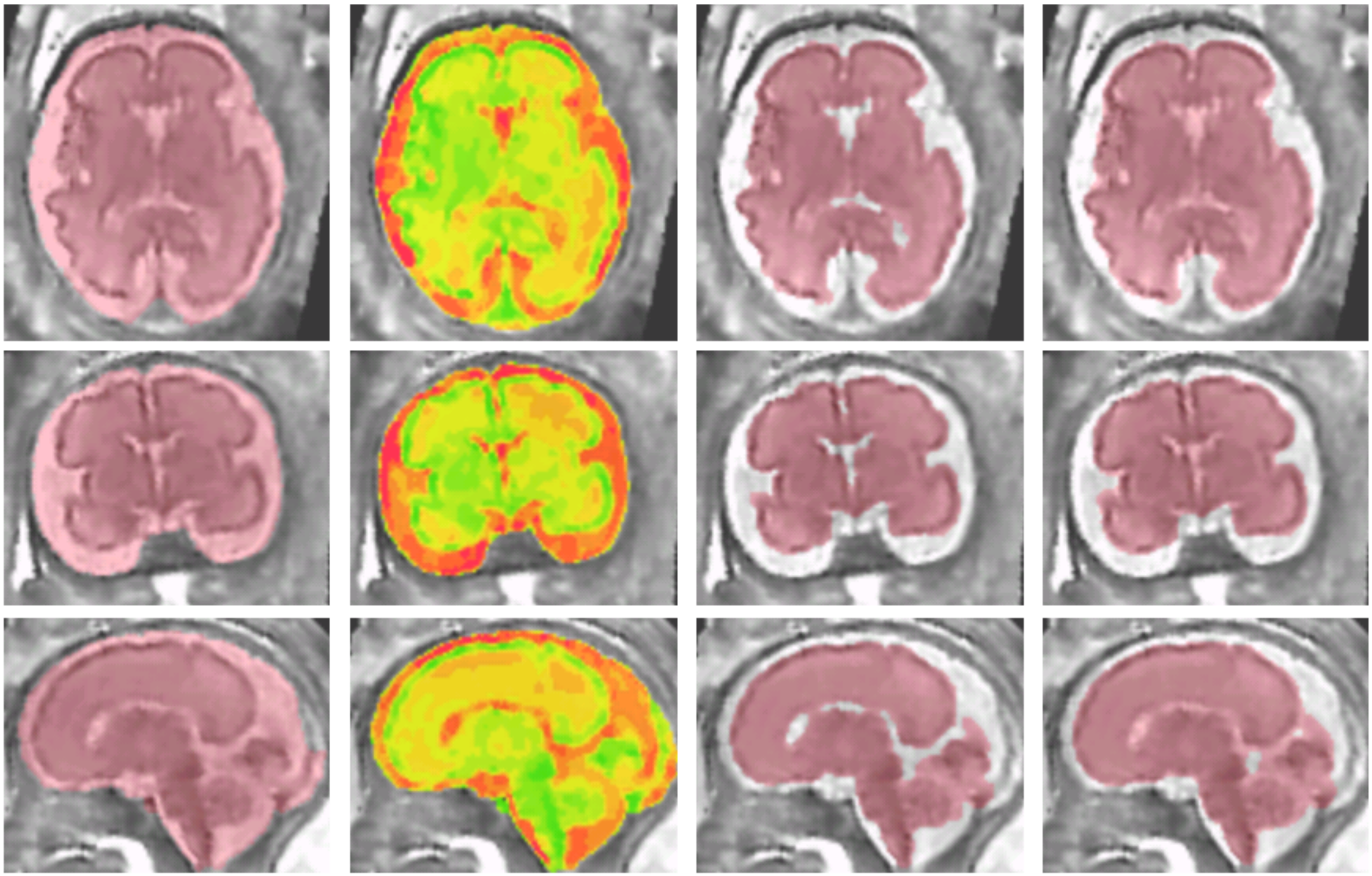

intracranial volume | tissue types | parenchyma | brain volume

Fetal brain MRI segmentation

- Evaluation of brain segmentation
  - Comparison to manual segmentation for 5 randomly chosen cases
  - Dice overlap measure, and
  - specificity and sensitivity measures

	C3	C6	C11	C13	C16
Dice index	0.9330	0.9206	0.9480	0.9575	0.9700
Specificity	0.9977	0.9948	0.9984	0.9953	0.9978
Sensitivity	0.9498	0.9444	0.9205	0.9594	0.9943

Intracranial and brain volumetry

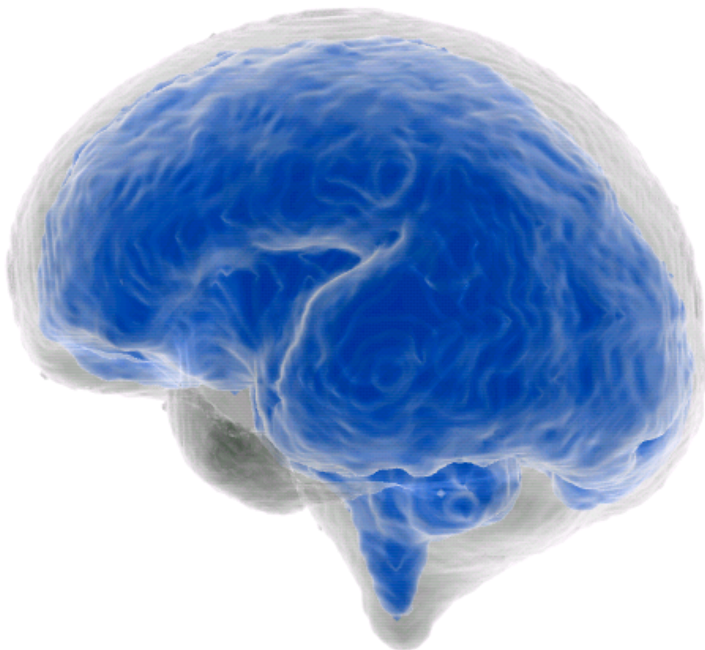

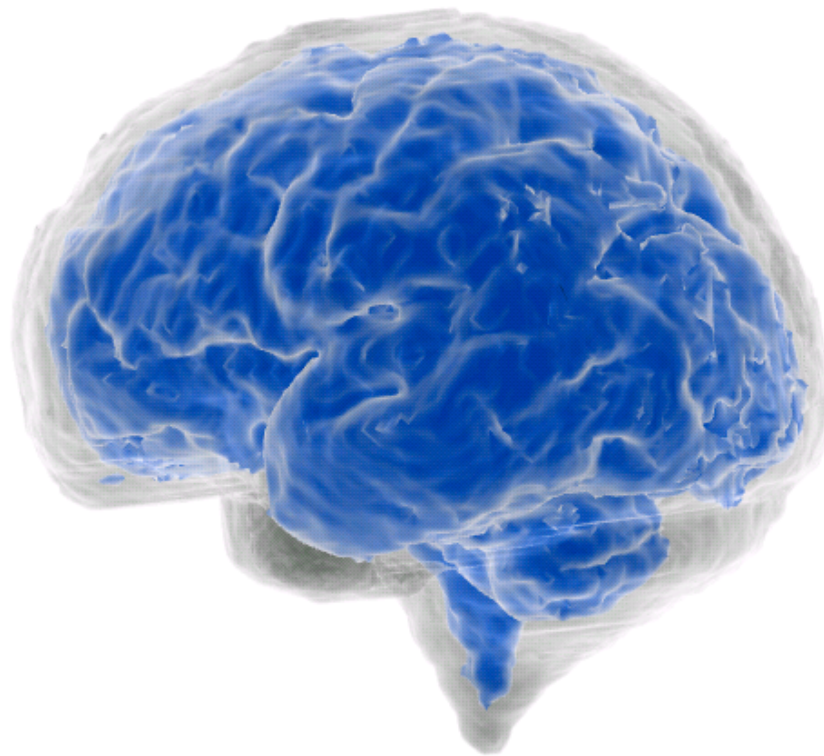

27.86 week fetus
Intracranial volume 210.13 mL
Brain volume 160.13 mL

31.43 week fetus
Intracranial volume 308.57 mL
Brain volume 202.52mL

Automated brain volumetry

- Comparison of Brain Volumes (BV) (in milliliters) using our volume reconstruction and supervised automated segmentation algorithm vs. using manual segmentation on high-resolution volumetric images.

	C3	C6	C11	C13	C16
BV (estimated)	79.01	39.14	416.96	137.96	325.50
BV (manual)	77.17	38.45	416.00	133.49	313.17
BV (% error)	2.33 %	1.76 %	0.23 %	3.25 %	3.79 %

Brain volumetry Analysis

- Brain volume vs. gestational age (22 fetuses)

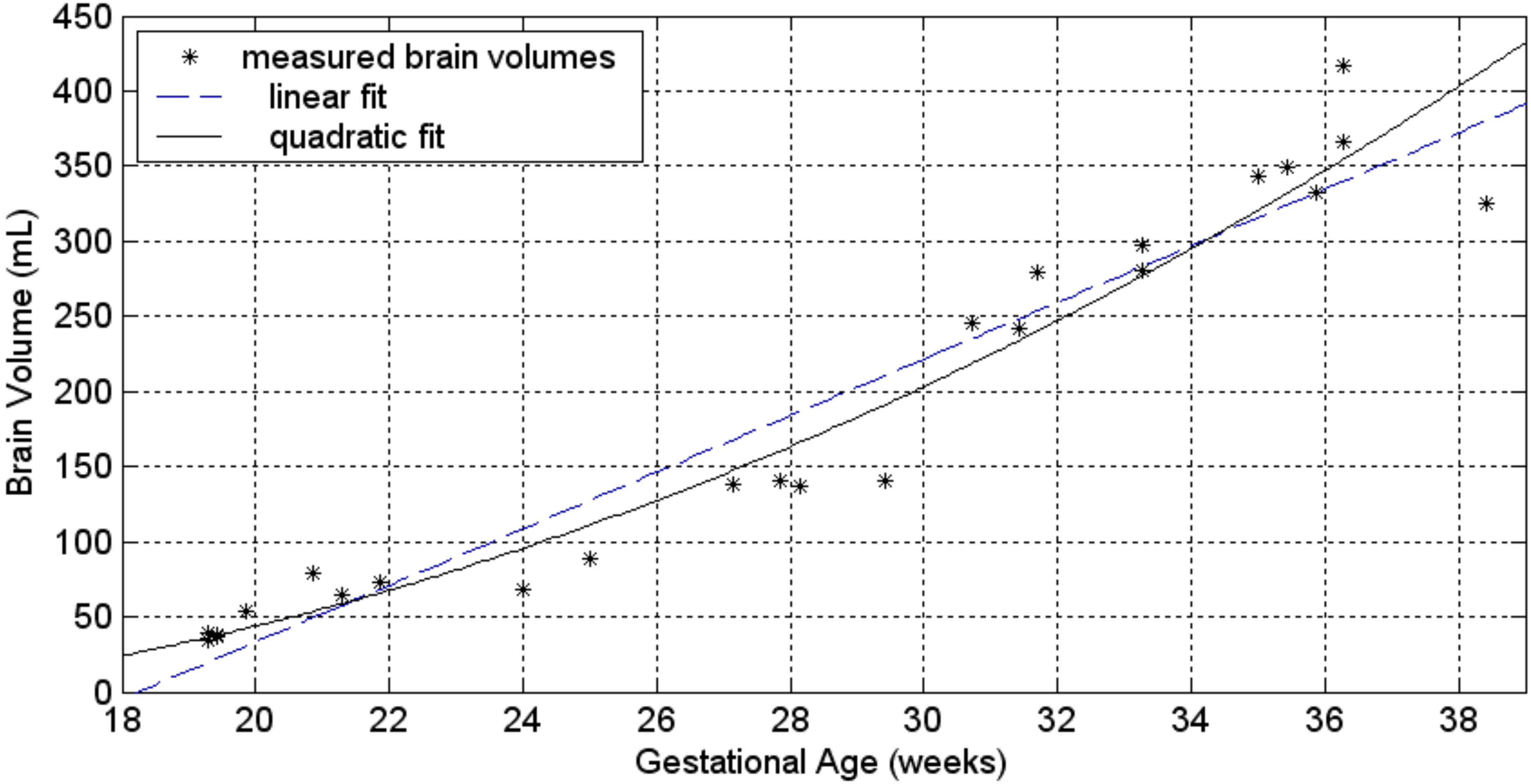

Brain volumetry analysis

- The coefficient of determination (r^2) goodness-of-fit measures for linear, quadratic, and exponential model fittings to the volumetry data
  – suggests that a quadratic model best describes the BV, ICV, and PV changes vs. GA.

	r^2 (ICV)	r^2 (BV)	r^2 (PV)
Linear fit	0.912	0.925	0.937
Quadratic fit	0.916	0.940	0.949
Exponential fit	0.810	0.850	0.829

3D segmentation and visualization

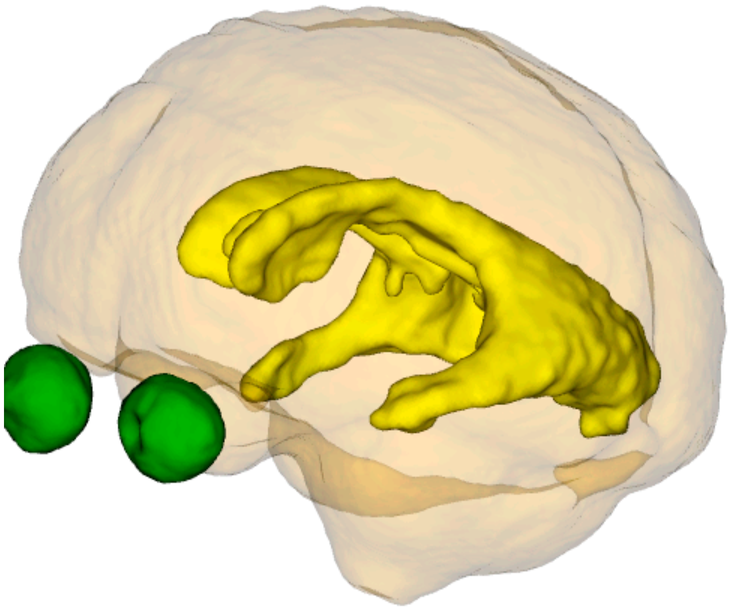

31.71 week normal fetus

Normal shape and morphology of the ventricles is appropriately visualized in 3D

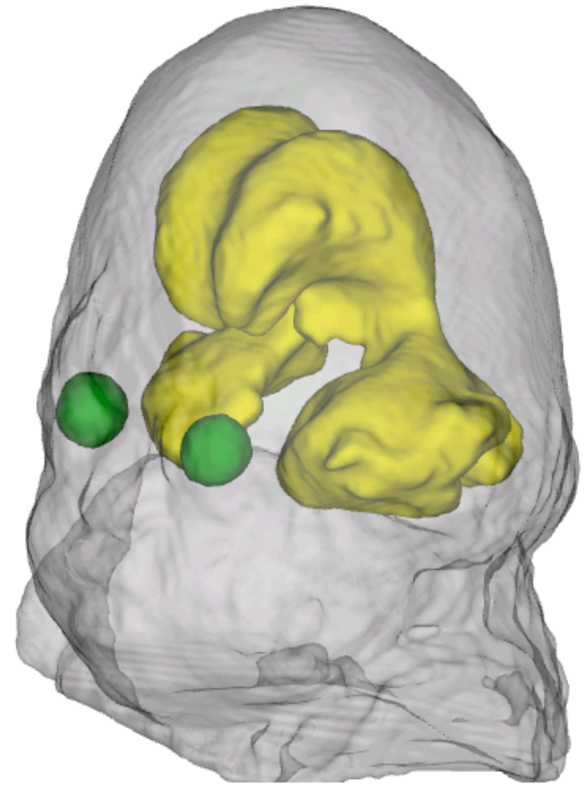

37.14 week fetus with Craniosynostosis

Abnormal head shape and the enlarged and abnormal morphology of ventricles in 3D

3D segmentation and visualization

- Surface model rendering of a fetus (33.28 week)
  - Body
  - Face
  - Cerebrospinal fluid
  - Orbits
  - Airways
  - Lungs

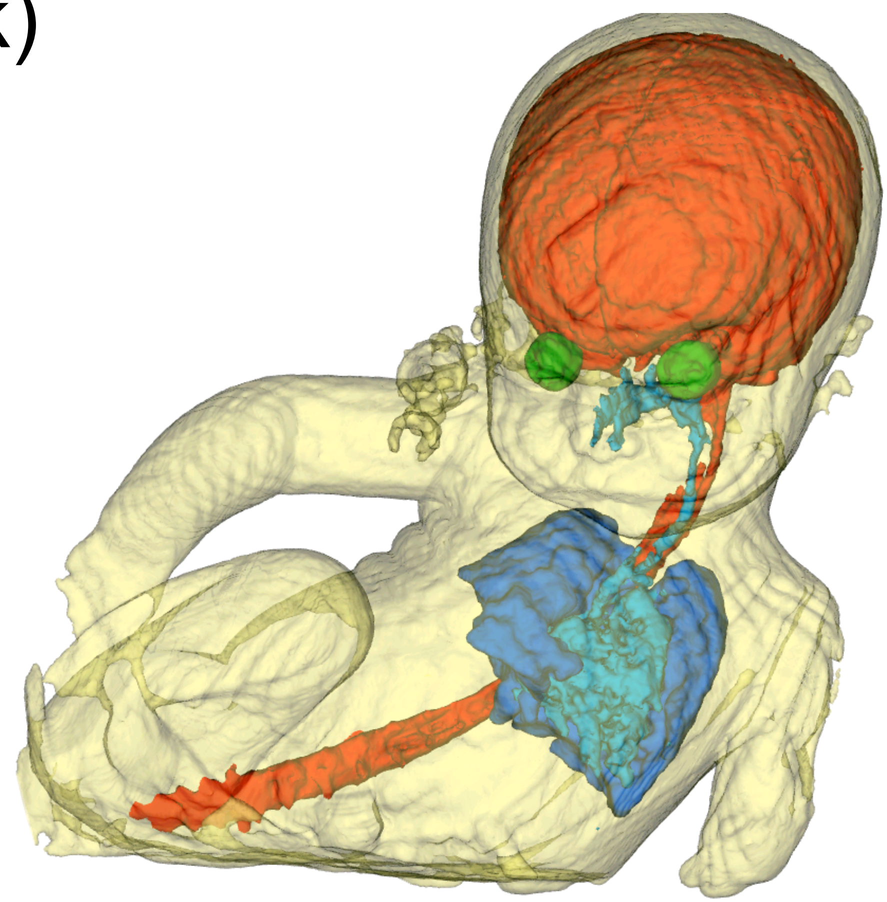

Conclusion

- We demonstrated an image processing pipeline that resolves the limitations of current fetal brain volumetry techniques by avoiding:
  - dependence on motion-free scans
  - tedious manual segmentation, and
  - thick slice interpolation.
- The algorithm utilizes motion correction, volumetric reconstruction, and segmentation techniques.
- The reconstructed volumetric images reflect anatomic details and coherent structural boundaries in 3D, which are not apparent in the original SSFSE scans.

References

- Jiang et al., IEEE Trans Med Imag. 2007, 26(7): 967-980
- Rousseau et al., Acad Radiol. 2006; 13(9):1072-81
- Kim et al., IEEE Trans Med Imag. 2010
- Gholipour et al., MICCAI 2009
- Gholipour et al., IEEE Trans Med Imag 2010

Computational Radiology Laboratory
Harvard Medical School
www.crl.med.harvard.edu

Children's Hospital
Department of Radiology
Boston Massachusetts

Image Segmentation for Pediatric Brain MRI

Simon K. Warfield, Ph.D.
Associate Professor of Radiology
Harvard Medical School

Children's Hospital Boston
The Hospital for Children

MRI of Newborn Infants

Feed and wrap infant

3T MRI of infant

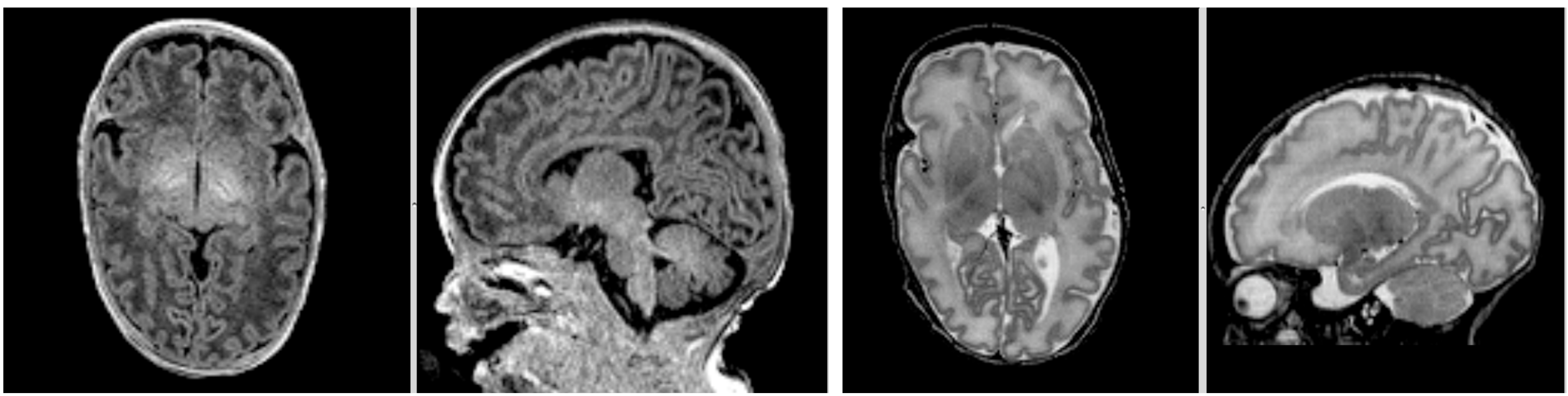

Motivation

- Increasing prevalence of surviving very low birth weight premature infants
- Very low birth weight infants have high rates of adverse neurodevelopmental outcomes:
  - 10-15% develop cerebral palsy
  - 50% develop significant neurobehavioral problems including
    - Lowered IQ
    - ADHD
    - Anxiety disorders
    - Learning difficulties
- Considerable educational burden with significant economic and social implications.

Newborn Brain: Structural MRI

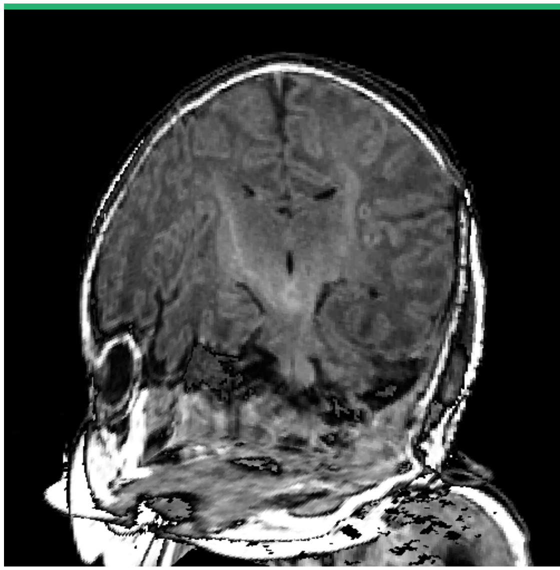

Healthy fullterm infant.

SPGR (T1w) of infant with PVL.

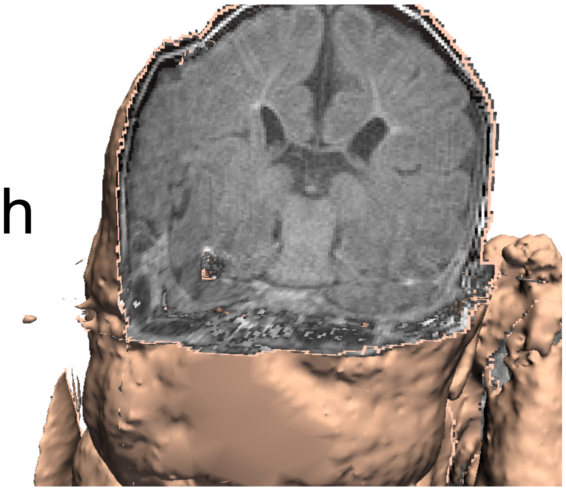

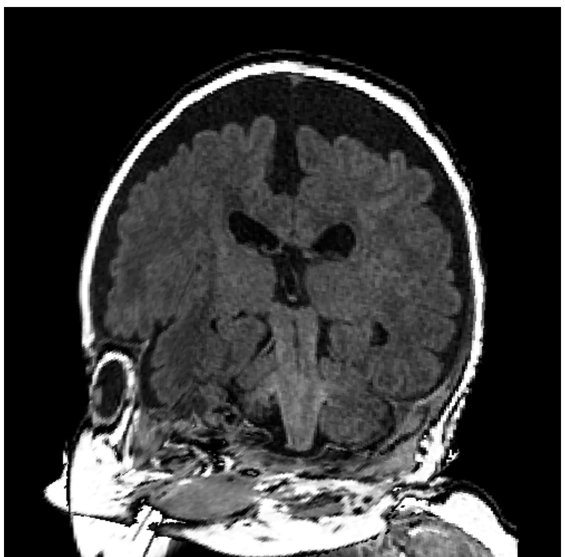

CSE (T2w) of infant with PVL.

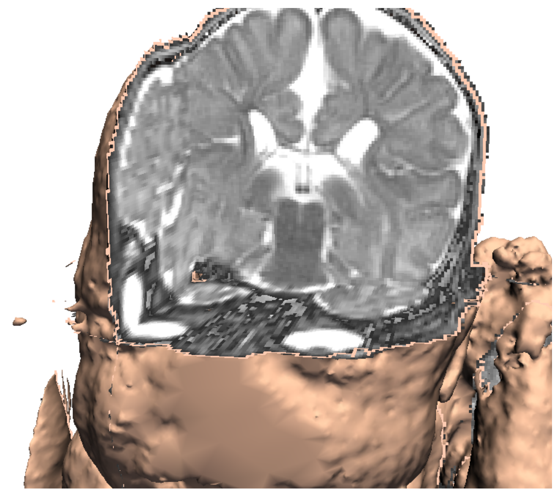

Fullterm infant with delayed development.

Skin shown in pink.

Studying Brain Development

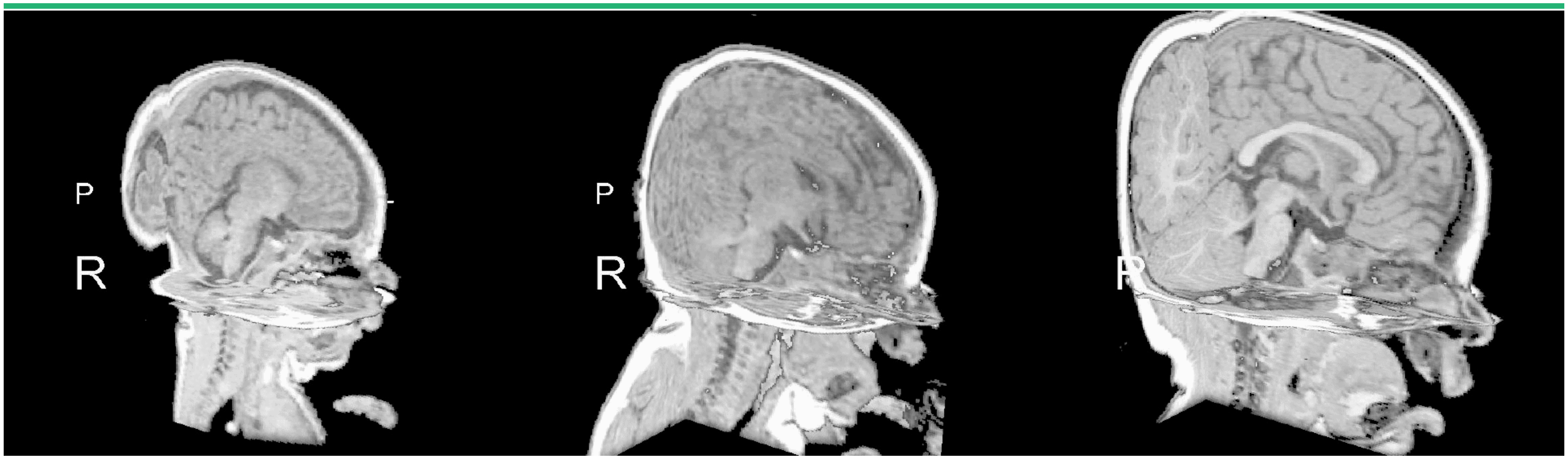

10 weeks premature

Term equivalent age

9 months

A sequence of MRI of the same infant: shortly after premature birth, at term equivalent age, and at nine months. The sequence of growth of the brain and development of myelination in the white matter can be best followed by quantitative 3D assessment.

MRI predicts later outcomes

- Quantitative analysis of tissue volume from MRI at term equivalent age has been shown to predict:
  - Impaired visual function in VLBW infants at age 2 (Shah et al. 2006)
  - Object working memory deficits at age 2 (Woodward et al. 2005)
  - PDI and MDI at age 2 (Thompson et al. 2008)

Tissue Class Training Data

- Our previous work has utilized interactive selection of per-subject training data:
  - Time consuming,
  - Subject to intra-rater and inter-rater variability,
  - Enabled identification of subtle contrast between different tissue types.
- We sought to develop an algorithm that avoids per-subject interaction, while maintaining excellent performance.
  - Weisenfeld and Warfield, NeuroImage, 2009.

Template to Target Registration

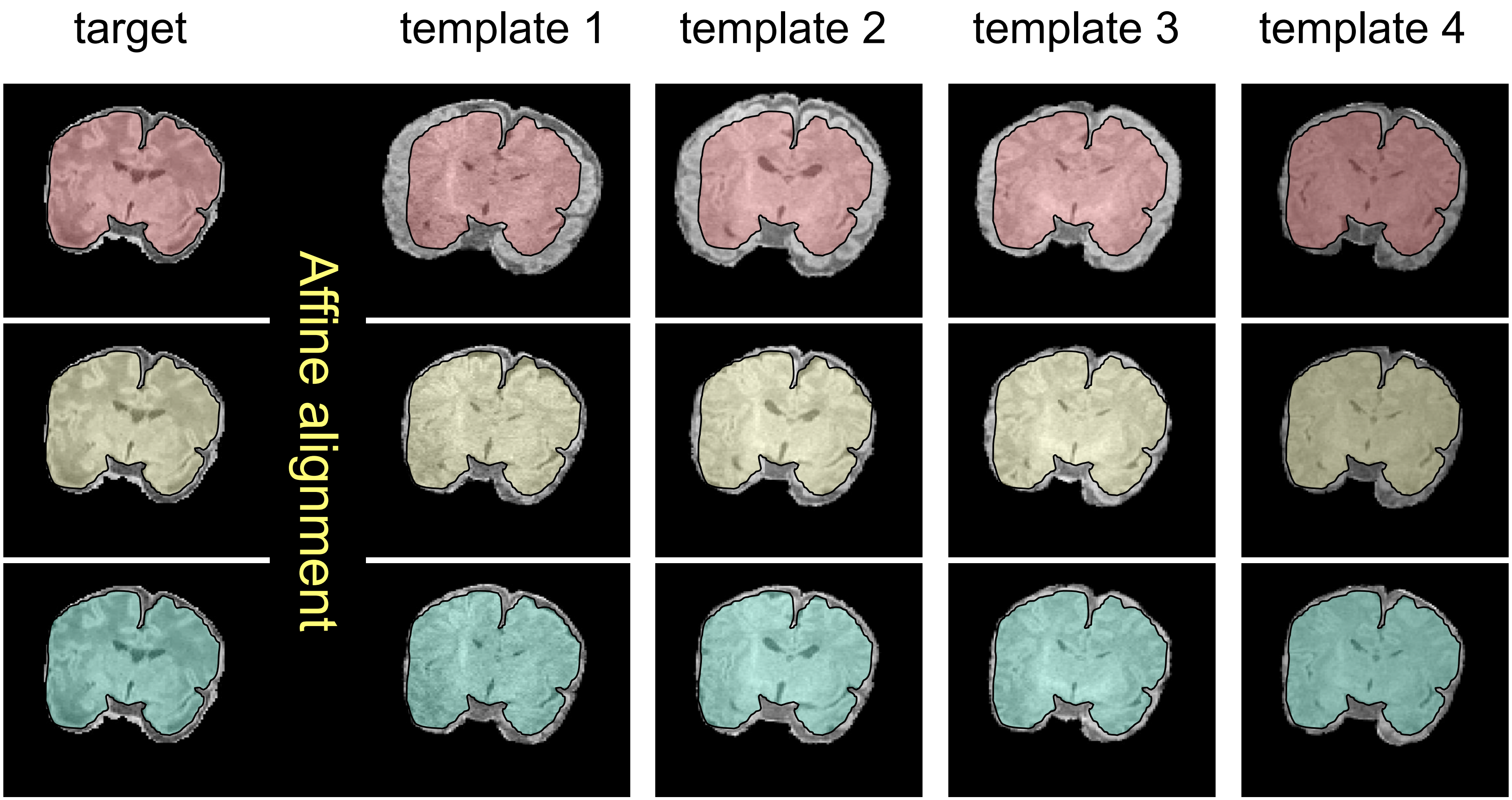

Tissue prototypes manually identified

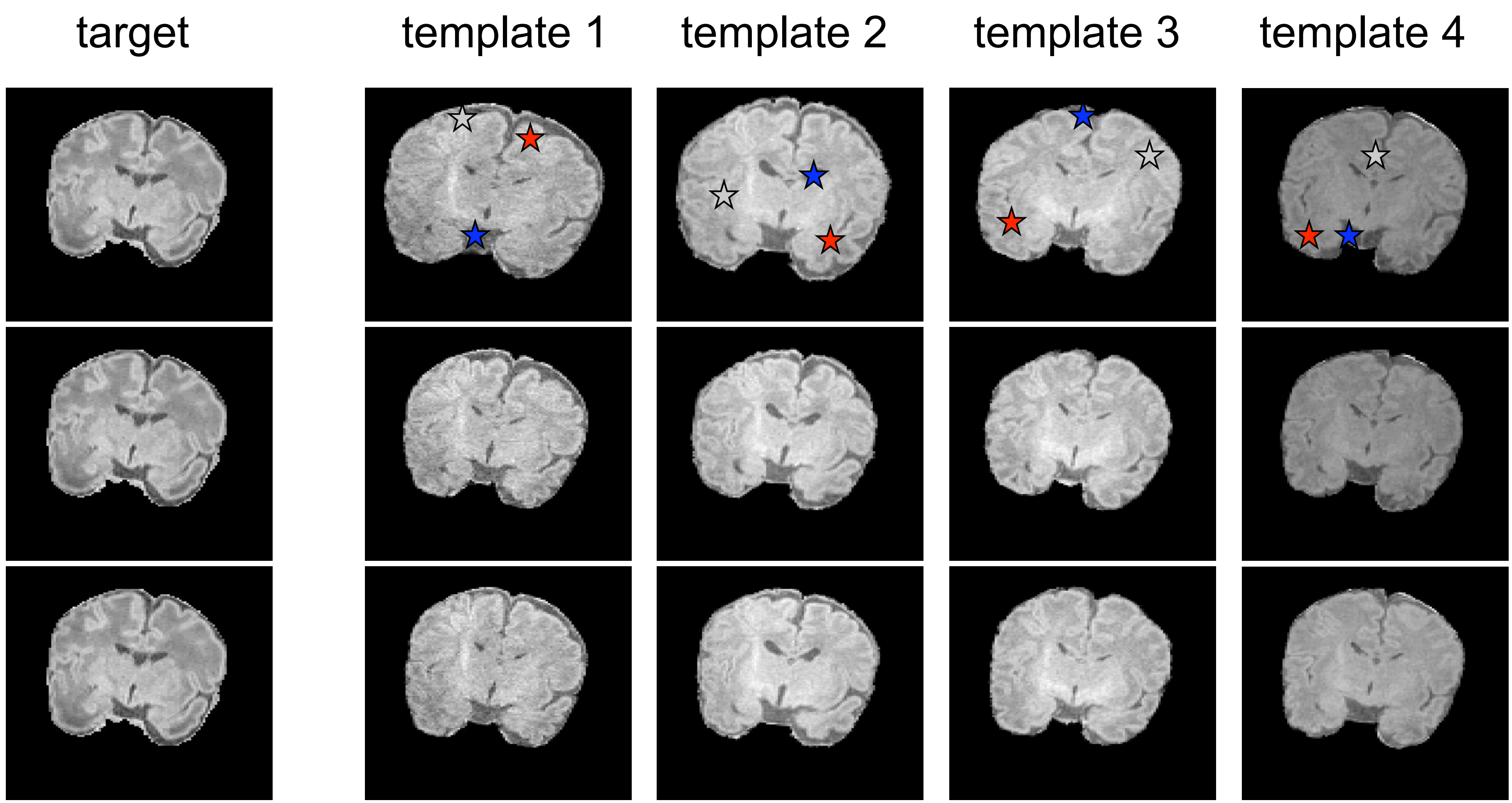

tissue class samples selected once on the original template images.

Tissue prototypes transferred

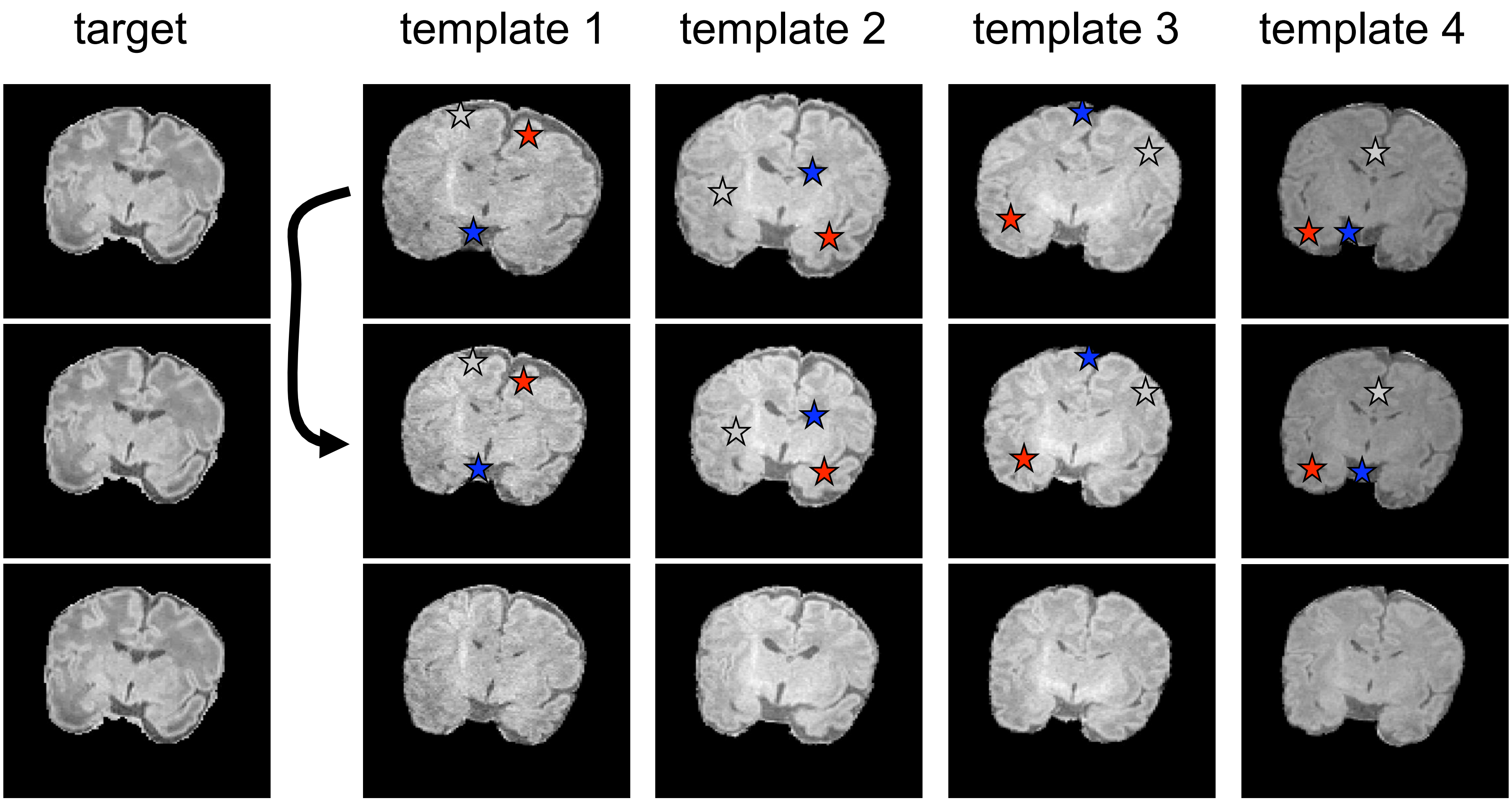

and then projected through the affine transform…

Tissue prototypes transferred

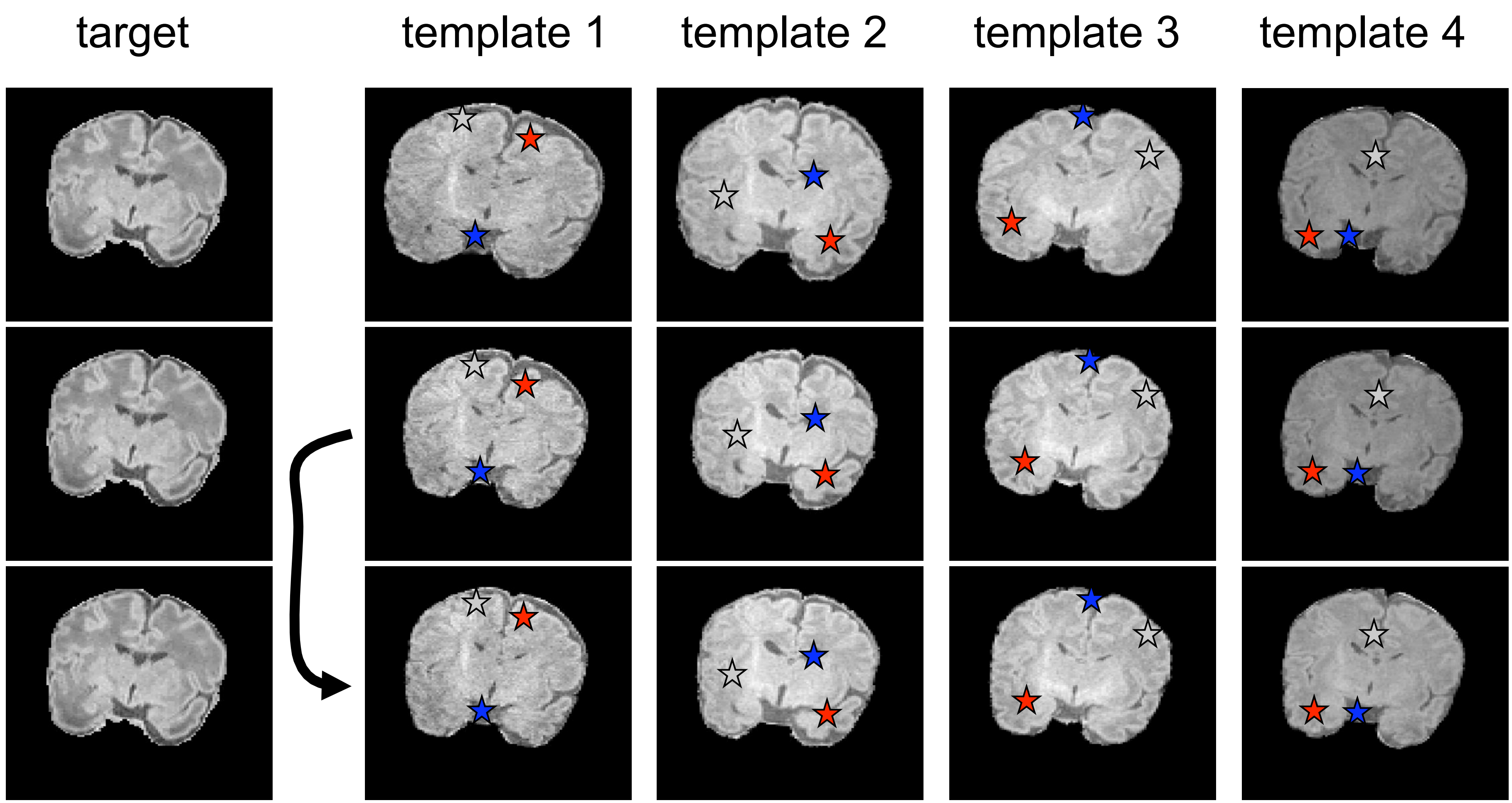

and then projected through the b-spline *non-linear* transform…

Tissue prototypes transferred

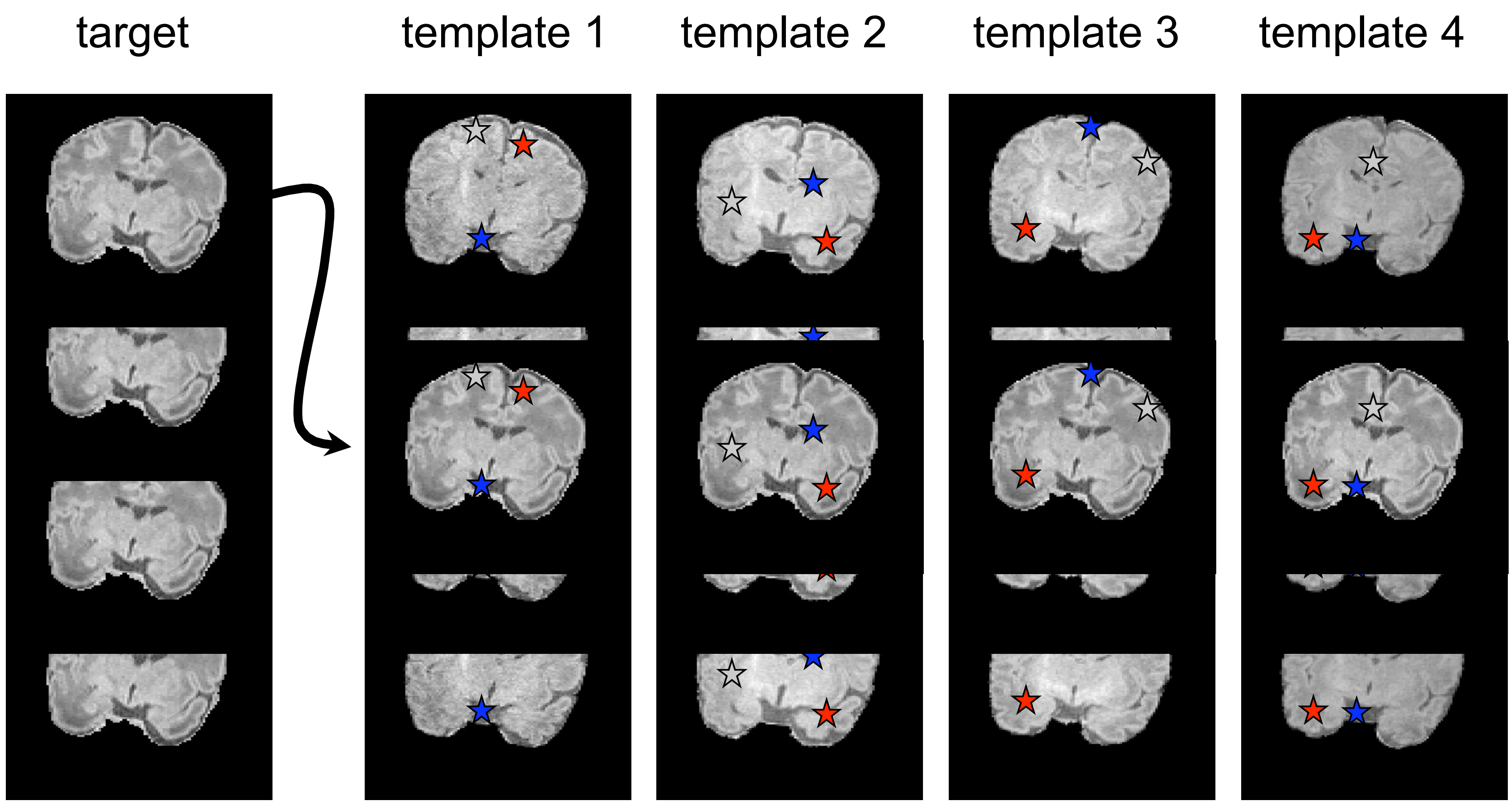

Different prototype configurations are projected onto the target subject

Multiple Configurations on the Target

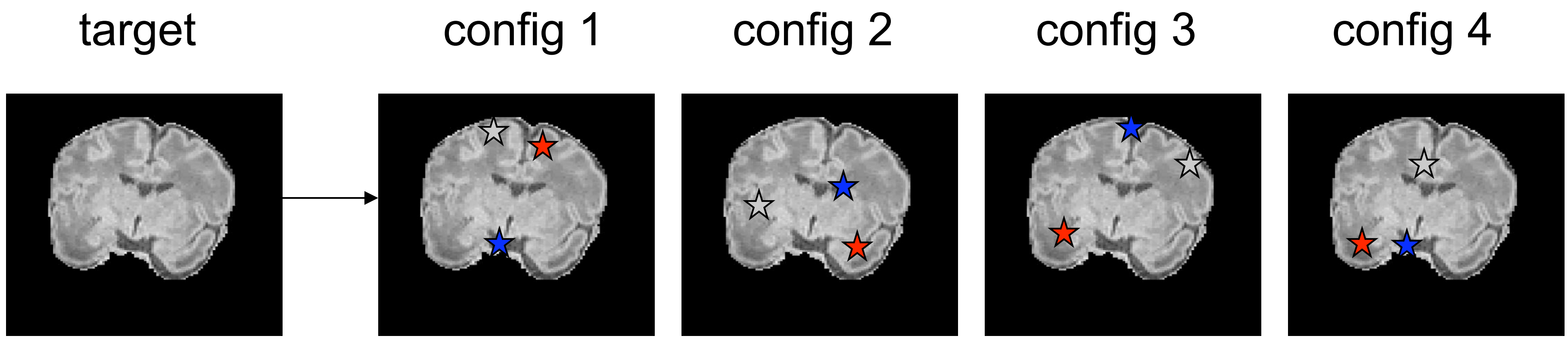

The different prototype configurations represent the physical variation among the template subjects. By adding template subjects, and choosing prototypes by hand *only once*, a wider range of physical variation can be accommodated. Once a template subject is added, it is re-used without further human intervention.

The image *intensity* data used is *only* from the individual under study (the target).

Multiple Configurations on the Target

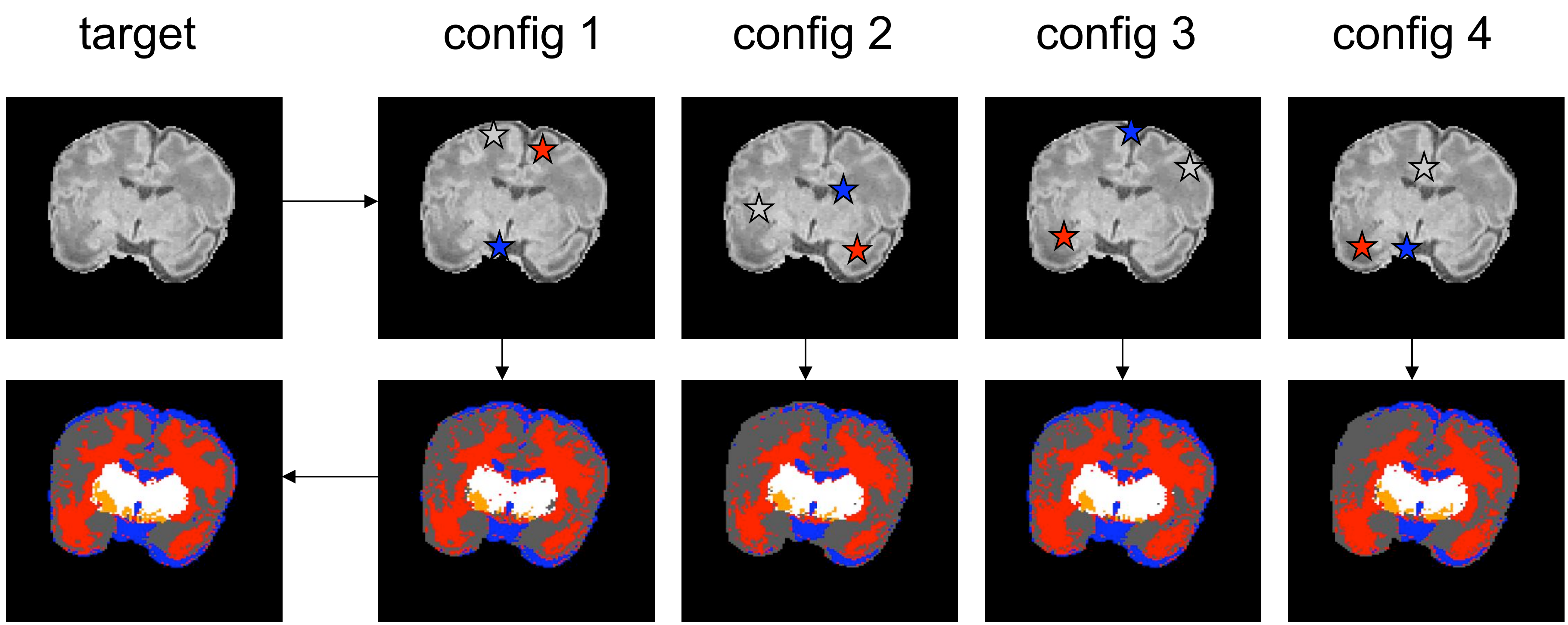

Each configuration of sample coordinates leads to a different candidate segmentation of the target subject.

STAPLE is used to combined candidate segmentations.

Configurations are Edited

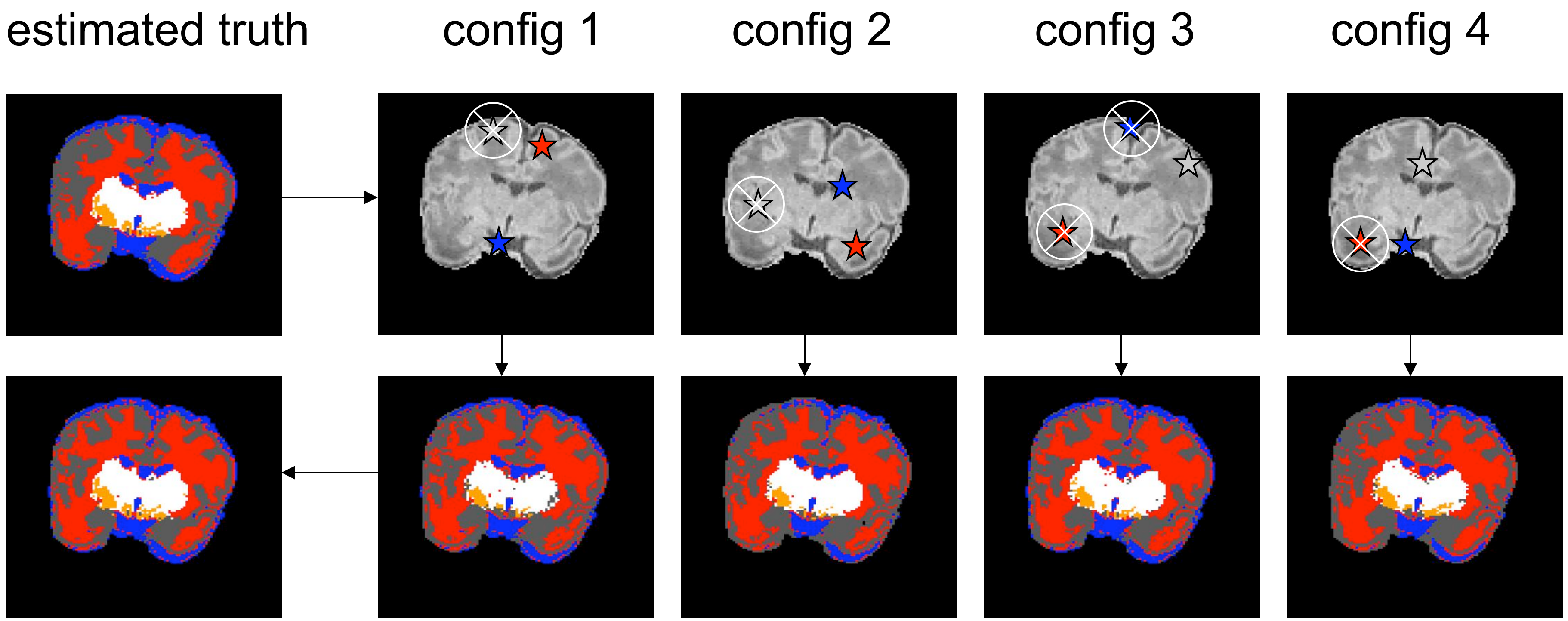

The previous iteration's STAPLE output (top left) is used to identify and eliminate prototypes which are inconsistent with the data.

Adaptation of training data

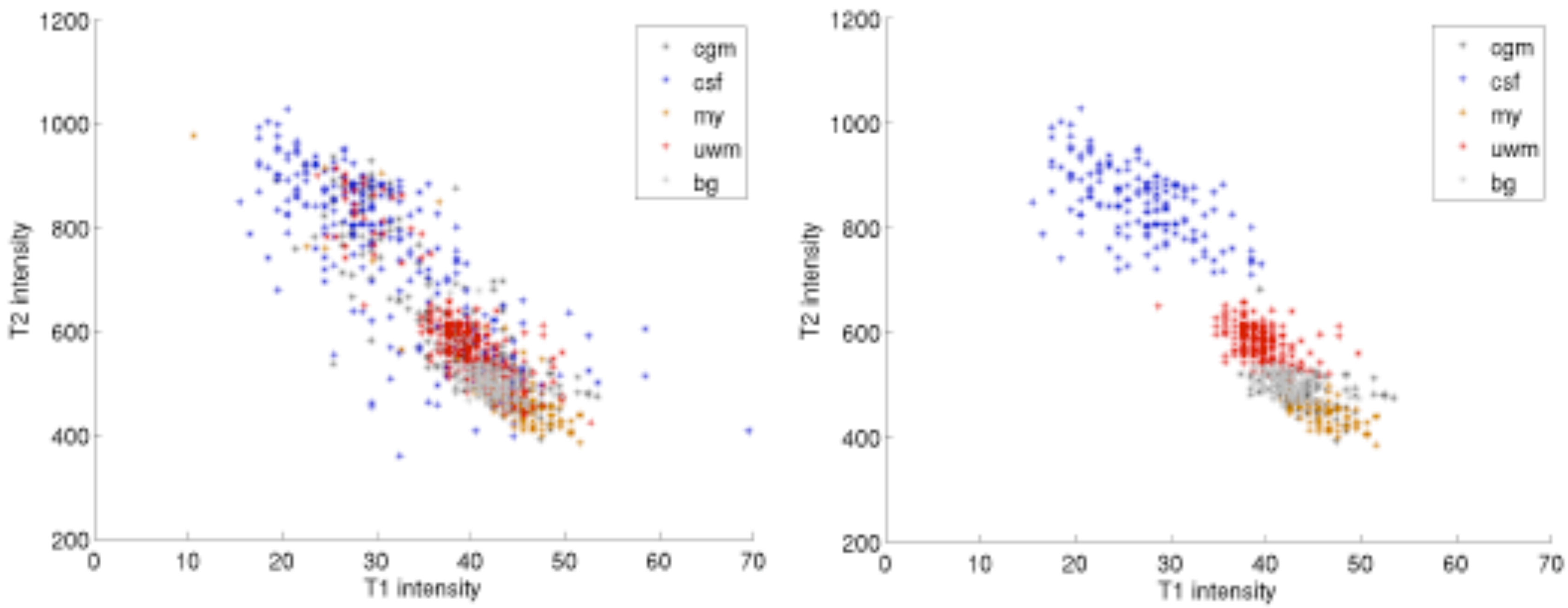

Evolution of feature space of training data through the automated projection and editing process.

Tissue class boundaries in feature space are identified.

Evaluation of training data

		train	
		$\mathcal{M}$	$\mathcal{A}$
test	$\mathcal{M}$	0.95 ± 0.02	0.93 ± 0.02
	$\mathcal{A}$	0.95 ± 0.01	0.97 ± 0.01

Posterior probability of correct classification with manually and automatically generated training data.

	test					
Subject	$\mathcal{M}$	$\mathcal{A}^0$	$\mathcal{A}^1$	$\mathcal{A}^2$	$\mathcal{A}^3$	$\mathcal{A}^{\mathrm{FINAL}}$
1	0.98	0.66	0.77	0.86	0.91	0.93
2	0.96	0.65	0.77	0.87	0.92	0.94
3	0.96	0.66	0.79	0.89	0.94	0.95
4	0.96	0.65	0.78	0.87	0.92	0.94
5	0.94	0.66	0.78	0.87	0.93	0.95
6	0.94	0.67	0.80	0.90	0.94	0.95
7	0.94	0.66	0.79	0.89	0.94	0.96
8	0.94	0.70	0.82	0.91	0.96	0.97
9	0.94	0.67	0.79	0.89	0.93	0.95
10	0.96	0.69	0.80	0.89	0.94	0.96
mean±sd	0.95 ± 0.02	0.67 ± 0.02	0.79 ± 0.02	0.88 ± 0.02	0.93 ± 0.01	0.95 ± 0.01

Improved consistency of GM, UWM and CSF over iterations of editing of training data.

Segmentation comparison

Subject	CGM	CSF	myelin	UMWM	SCGM
1	0.95	0.82	0.63	0.95	0.92
2	0.89	0.94	0.80	0.89	0.86
3	0.89	0.93	0.71	0.91	0.89
4	0.84	0.95	0.70	0.85	0.81
5	0.92	0.93	0.77	0.93	0.88
6	0.89	0.98	0.77	0.93	0.85
7	0.93	0.96	0.70	0.96	0.89
8	0.91	0.97	0.79	0.93	0.87
9	0.87	0.94	0.66	0.91	0.80
10	0.94	0.80	0.67	0.95	0.88
mean±sd	0.90 ± 0.03	0.92 ± 0.06	0.72 ± 0.06	0.92 ± 0.03	0.86 ± 0.04

Dice coefficient comparing interactive to automated tissue classification.

Segmentation comparison

Subject		CGM	CSF	myelin	UMWM	SCGM
1	experts	0.86 ± 0.06	0.89 ± 0.05	0.81 ± 0.11	0.85 ± 0.05	0.86 ± 0.08
	automatic	0.75	0.96	0.86	0.79	0.96
2	experts	0.87 ± 0.06	0.93 ± 0.02	0.96 ± 0.05	0.87 ± 0.06	0.90 ± 0.12
	automatic	0.77	0.98	0.96	0.72	0.74
3	experts	0.90 ± 0.04	0.91 ± 0.02	0.77 ± 0.06	0.88 ± 0.03	0.91 ± 0.03
	automatic	0.77	0.97	0.81	0.78	0.95
4	expert	0.87 ± 0.08	0.91 ± 0.02	0.81 ± 0.06	0.87 ± 0.04	0.94 ± 0.04
	automatic	0.84	0.95	0.69	0.70	0.94

Comparison of predictive values of tissue segmentations obtained by interactive drawing and by automated tissue classification.

Newborn brain segmentation

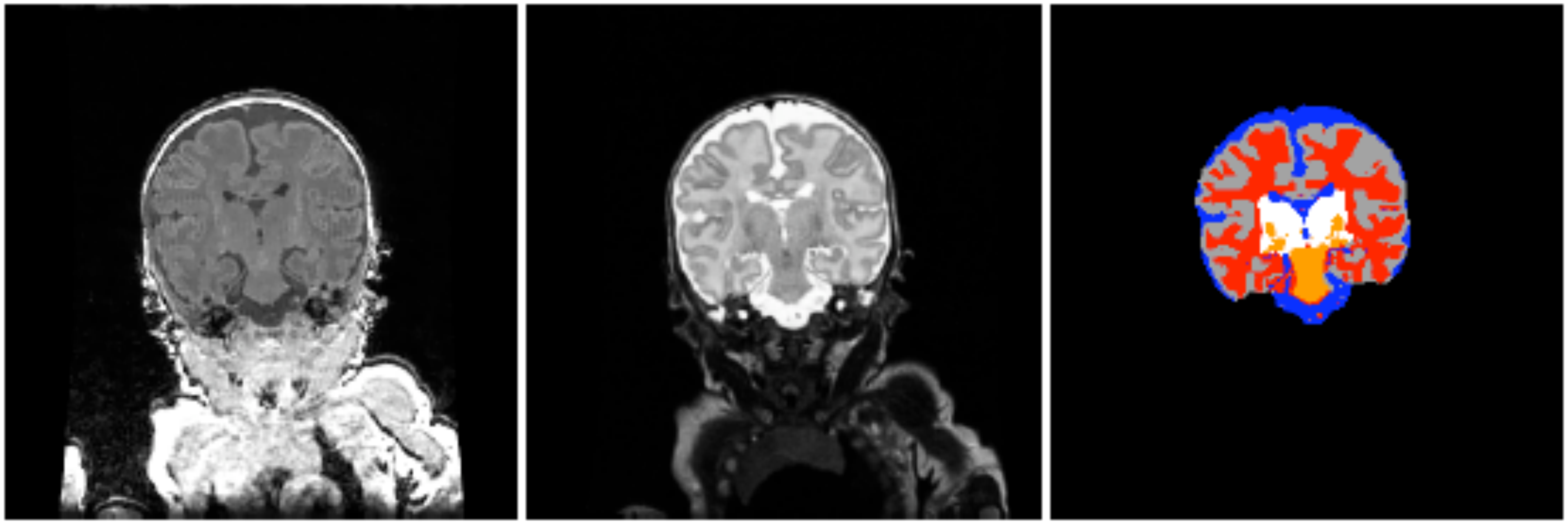

Segmentation Algorithm

- Weisenfeld and Warfield, NeuroImage 2009
- Automatic estimation of training data is comparable to interactive selection by an expert.
- Automated segmentation compares well to hand-drawn segmentations.
- Software for pediatric MRI analysis, CRKit, supported by NIH.

Acknowledgments

- This research was supported in part by NIH grants R01 RR021885, R01 GM074068 and R01 EB008015.

- The clinical fetal MRI data were collected at the Advanced Fetal Care Center (AFCC) at Children's Hospital Boston.

Acknowledgements

- Benoit Scherrer
- Ali Gholipour
- Mustafa Sahin
- Ralph Suarez
- Damon Hyde
- Olivier Commowick
- Ann Poduri
- Tobias Loddenkemper
- Arne Hans
- Heidelise Als
- Neil Weisenfeld
- Xavier Tomas-Fernandez
- Ayelet Akselrod-Ballin
- Steve Whalen
- Joe Madsen
- Sanjay Prabhu
- Anne Bergin

This study was supported by:

Center for the Integration of Medicine and Innovative Technology

R01 RR021885, R01 EB008015, R03 EB008680

Acknowledgements

Colleagues contributing to this work:

- Neil Weisenfeld.
- Andrea Mewes.
- Petra Huppi.
- Olivier Clatz.
- Terrie Inder.
- Olivier Commowick.
- Arne Hans.
- Heidelise Als.
- Lianne Woodward.
- Frank Duffy.
- Arne Hans.
- Deanne Thompson.

This study was supported by:

Center for the Integration of Medicine and Innovative Technology

R01 RR021885, R01 GM074068 and R01 HD046855.

Bottom Line: Improved Patient Care

- Provide new capabilities that transcend human limitations in intervention
- Increase consistency and quality of interventional treatments